

1 **Secondary Organic Aerosol Production from Local Emissions Dominates the**
2 **Organic Aerosol Budget over Seoul, South Korea, during KORUS-AQ**

3 Benjamin A. Nault^{1,2}, Pedro Campuzano-Jost^{1,2}, Douglas A. Day^{1,2}, Jason C. Schroder^{1,2}, Bruce
4 Anderson³, Andreas J. Beyersdorf^{3,*}, Donald R. Blake⁴, William H. Brune⁵, , Yonghoon Choi^{3,6},
5 Chelsea A. Corr^{3,**}, Joost A. de Gouw^{1,2}, Jack Dibb⁷, Joshua P. DiGangi³, Glenn S. Diskin³, Alan
6 Fried⁸, L. Gregory Huey⁹, Michelle J. Kim¹⁰, Christoph J. Knote¹¹, Kara D. Lamb^{2,12}, Taehyoung
7 Lee¹³, Taehyun Park¹³, Sally E. Pusede¹⁴, Eric Scheuer⁷, Kenneth L. Thornhill^{3,6}, Jung-Hun Woo¹⁵,
8 and Jose L. Jimenez^{1,2}

9

10 *Affiliations*

11 1. Department of Chemistry, University of Colorado, Boulder, CO, USA

12 2. Cooperative Institute for Research in Environmental Sciences, University of Colorado, Boulder, CO,
13 USA

14 3. NASA Langley Research Center, Hampton, Virginia, USA

15 4. Department of Chemistry, University of California, Irvine, Irvine, CA, USA

16 5. Department of Meteorology and Atmospheric Science, Pennsylvania State University, University Park,
17 Pennsylvania, USA

18 6. Science Systems and Applications, Inc., Hampton, Virginia, USA

19 7. Earth Systems Research Center, Institute for the Study of Earth, Oceans, and Space, University of New
20 Hampshire, Durham, New Hampshire, USA

21 8. Institute of Arctic and Alpine Research, University of Colorado, Boulder, CO, USA

22 9. School of Earth and Atmospheric Sciences, Georgia Institute of Technology, Atlanta, Georgia, USA

23 10. Division of Geological and Planetary Sciences, California Institute of Technology, Pasadena, CA, USA

24 11. Meteorologisches Institut, Ludwig-Maximilians-Universität München, München, Germany

25 12. Chemical Sciences Division, Earth System Research Laboratory, National Oceanic and Atmospheric
26 Administration, Boulder, CO, USA

27 13. Department of Environmental Science, Hankuk University of Foreign Studies, Republic of Korea

28 14. Department of Environmental Sciences, University of Virginia, Charlottesville, VA, USA

29 15. Department of Advanced Technology Fusion, Konkuk University, Seoul, Republic of Korea

30 * Now at: Department of Chemistry and Biochemistry, California State University, San Bernardino,
31 California

32 ** Now at: USDA UV-B Monitoring and Research Program, Natural Resource Ecology
33 Laboratory, Colorado State University, Fort Collins, CO, USA

34

35 *Correspondence to:* J. L. Jimenez (jose.jimenez@colorado.edu)

36

37 **Abstract**

38 Organic aerosol (OA) is an important fraction of submicron aerosols. However, it is challenging
39 to predict and attribute the specific organic compounds and sources that lead to observed OA
40 loadings, largely due to contributions from secondary production. This is especially true for
41 megacities surrounded by numerous regional sources that create an OA background. Here, we
42 utilize *in-situ* gas and aerosol observations collected on-board the NASA DC-8 during the
43 NASA/NIER KORUS-AQ (KORea United States-Air Quality) campaign to investigate the
44 sources and hydrocarbon precursors that led to the secondary OA (SOA) production observed over
45 Seoul. First, we investigate the contribution of transported OA to total loadings observed over
46 Seoul, by using observations over the West Sea coupled to FLEXPART Lagrangian simulations.
47 During KORUS-AQ, the average OA loading advected into Seoul was $\sim 1 - 3 \mu\text{g sm}^{-3}$. Second,
48 taking this background into account, the dilution-corrected SOA concentration observed over
49 Seoul was $\sim 140 \mu\text{g sm}^{-3} \text{ppmv}^{-1}$ at 0.5 equivalent photochemical days. This value is at the high
50 end of what has been observed in other megacities around the world ($20-70 \mu\text{g sm}^{-3} \text{ppmv}^{-1}$ at 0.5
51 equivalent days). For the average OA concentration observed over Seoul ($13 \mu\text{g sm}^{-3}$), it is clear
52 that production of SOA from locally emitted precursors is the major source in the region. The
53 importance of local SOA production was supported by the following observations: (1)
54 FLEXPART source contribution calculations indicate any hydrocarbons with a lifetime less than
55 1 day, which are shown to dominate the observed SOA production, mainly originate from South
56 Korea. (2) SOA correlated strongly with other secondary photochemical species, including short-
57 lived species (formaldehyde, peroxy acetyl nitrate, sum of acyl peroxy nitrates, dihydroxy toluene,
58 and nitrate aerosol). (3) Results from an airborne oxidation flow reactor (OFR), flown for the first
59 time, show a factor of 4.5 increase in potential SOA concentrations over Seoul versus over the
60 West Sea, a region where background air masses that are advected into Seoul can be measured. (4)
61 Box model simulations reproduce SOA observed over Seoul within 15% on average, and suggest
62 that short-lived hydrocarbons (i.e., xylenes, trimethylbenzenes, semi- and intermediate volatility
63 compounds) were the main SOA precursors over Seoul. Toluene, alone, contributes 9% of the
64 modeled SOA over Seoul. Finally, along with these results, we use the metric $\Delta\text{OA}/\Delta\text{CO}_2$ to
65 examine the amount of OA produced per fuel consumed in a megacity, which shows less variability
66 across the world than $\Delta\text{OA}/\Delta\text{CO}$.

67 **1. Introduction**

68 Prior to 1950, 30% of the human population resided in urban areas (UNDESA, 2015). In
69 2007, the human population living in urban areas had increased to over 50% (making it the first
70 time in human history that more people reside in urban than rural areas), and it is predicted that
71 nearly 2/3 of the human population will be living in urban areas by 2050 (Monks et al., 2009;
72 UNDESA, 2015; Baklanov et al., 2016). Urban areas are large sources of anthropogenic emissions
73 to the atmosphere (from sources including transportation, industry, cooking, personal care
74 products, and power produced from fossil fuels), and these emissions have important impacts on
75 local, regional, and global air pollution, climate, and human and ecological health (Hallquist et al.,
76 2009; Monks et al., 2009; Myhre et al., 2013; Baklanov et al., 2016; WHO, 2016; Cohen et al.,
77 2017; Landrigan et al., 2018; McDonald et al., 2018). Effects from urban emissions are strongly
78 modulated by the chemical evolution of the primary emissions (e.g., nitrogen oxides,
79 hydrocarbons, and primary organic aerosols) to secondary pollutants, including secondary organic
80 aerosols (SOA, produced from atmospheric reactions) and other aerosol (Monks et al., 2009).
81 These emissions and their chemical by-products significantly influence hemispheric climate and
82 air quality. They increase mortality in polluted urban areas, leading to over 3 million premature
83 deaths annually (Lelieveld et al., 2015; Baklanov et al., 2016; WHO, 2016). Finally, the emissions
84 and production of anthropogenic aerosol may strongly regulate cloud nucleation (Peng et al.,
85 2014), which impacts the aerosols' direct and indirect effects on climate (Myhre et al., 2013).

86 Production of SOA is poorly understood (Hallquist et al., 2009; Shrivastava et al., 2017;
87 Tsimpidi et al., 2017), including in large urban environments (Volkamer et al., 2006; de Gouw et
88 al., 2008, 2009; Hayes et al., 2015; Woody et al., 2016; Janssen et al., 2017; Ma et al., 2017). It
89 has been shown that a large fraction (35 – 85%) of urban fine aerosol is composed of OA (Zhang

90 et al., 2007; Jimenez et al., 2009), and a substantial fraction of this OA is typically SOA produced
91 through the chemical processing of urban hydrocarbon emissions (Kleinman et al., 2016, 2007,
92 2008, 2009, Dzepina et al., 2009, 2011; DeCarlo et al., 2010; Hodzic et al., 2010; Hersey et al.,
93 2013; Zhao et al., 2014, 2016; Freney et al., 2014; Hayes et al., 2015; Ma et al., 2017). Also,
94 observations indicate the majority of urban SOA production is rapid and is nearly completed within
95 24 equivalent photochemical hours (a measure of OH exposure, assuming interactions in a volume
96 with 1.5×10^6 molecules/cm³ OH throughout a 24 h period; equivalent age enables comparison of
97 chemistry rates across different events or studies) (DeCarlo et al., 2010; Hayes et al., 2013; Freney
98 et al., 2014; Hu et al., 2016; Ortega et al., 2016; Ma et al., 2017), even during winter (Schroder et
99 al., 2018). This consistently rapid SOA production over urban areas around the world may be due
100 to the short lifetime (less than one day) of urban semi- and intermediate-volatile organic
101 compounds (S/IVOCs), that numerous studies suggest to be major SOA precursors, along with
102 aromatics (Robinson et al., 2007; Zhao et al., 2014, 2016; Hayes et al., 2015; Ma et al., 2017;
103 McDonald et al., 2018). S/IVOCs and low volatility organic compounds (LVOCs—compounds
104 produced from the photooxidation of hydrocarbons (Robinson et al., 2007; Kroll and Seinfeld,
105 2008; Murphy et al., 2011; Palm et al., 2016)) are challenging to measure due to strong interaction
106 with inlet and instrument surfaces (e.g., Pagonis et al., 2017), limiting our knowledge of the
107 emission rates and concentrations of these species in the atmosphere (Zhao et al., 2014; Hunter et
108 al., 2017). It has also been recently shown that historical chamber SOA yields are biased low due
109 to unaccounted-for partitioning of S/IVOCs to walls (Matsunaga and Ziemann, 2010; Zhang et al.,
110 2014; Krechmer et al., 2016, 2017). These missing or under-represented compounds and low-
111 biased yields, along with uncertain emission inventories for SOA precursors (Shrivastava et al.,
112 2008; Woody et al., 2016; Murphy et al., 2017), led SOA modeling efforts over urban areas using

113 pre-2007 models to under-predict observed SOA concentrations (de Gouw et al., 2005, 2009;
114 Volkamer et al., 2006; Dzepina et al., 2009; Freney et al., 2014; Woody et al., 2016). More recent
115 modeling efforts have achieved closure (and sometimes over-prediction) of the observed SOA, but
116 with some controversy about the real causes of the increased modeled SOA (Dzepina et al., 2009;
117 Hodzic et al., 2010; Tsimpidi et al., 2010; Hayes et al., 2015; Cappa et al., 2016; Ma et al., 2017;
118 McDonald et al., 2018).

119 Another complexity in understanding SOA production over urban areas is addressing the
120 contributions of transport of SOA and its gas-phase precursors. Airborne observations of SOA and
121 SOA precursors upwind, over, and downwind of megacities around the world (Kleinman et al.,
122 2007, 2008, 2009, 2016, DeCarlo et al., 2008, 2010; Bahreini et al., 2009; McMeeking et al., 2012;
123 Craven et al., 2013; Freney et al., 2014; Schroder et al., 2018) have constrained the role of regional
124 transport versus megacity emissions. In general, these studies show that there is often regional
125 background SOA, often due to biogenic compounds and regional pollution, transported into
126 megacities, but that rapid SOA production is always observed and is generally dominated by the
127 anthropogenic emissions from the urban area being studied.

128 The Seoul Metropolitan Area (SMA), as considered here, is a densely populated megacity,
129 extending beyond Seoul proper into the large Incheon and Gyeonggi cities. SMA has ~24 million
130 people, or ~50% of the South Korean population, living on ~12,000 km² of land (Park et al., 2017).
131 SMA has large anthropogenic emissions but is also often downwind of China, presenting the
132 challenge of separating local emissions and production of SOA versus transport of SOA and its
133 precursors from regions upwind (H. S. Kim et al., 2007; Heo et al., 2009; Kim et al., 2009, 2016;
134 Jeong et al., 2017; H. Kim et al., 2017; H. C. Kim et al., 2017; Lee et al., 2017; Seo et al., 2017;
135 Kim et al., 2018). Most of the studies in this region have used ground-based observations and/or

136 3D models to characterize the amount of aerosol, and aerosol precursors, transported to SMA and
137 South Korea, finding 50 to 80% of the aerosol load is due to international transport in the seasons
138 with favorable synoptic conditions (winter and spring). Though satellites are starting to be used to
139 investigate transport of aerosols into SMA and South Korea (Lee et al., 2013; Park et al., 2014;
140 Jeong et al., 2017), retrievals typically do not provide any chemical characterization or vertical
141 location of the aerosol (boundary layer versus free troposphere), and are typically strongly
142 influenced by larger aerosols (e.g., mineral dust). Airborne observations of the upwind transport
143 and local production of aerosol and aerosol precursors have the potential to directly assess the
144 impact of transport versus local emissions in this region.

145 In this study, we use observations collected on board the NASA DC-8 research aircraft
146 during the NASA/NIER (South Korean National Institute of Environmental Research) KOREan
147 United States Air Quality (KORUS-AQ) field campaign. These data provided the opportunity to
148 investigate SOA production; as well as, the role of OA and SOA precursor transport on the OA
149 concentration and SOA production over Seoul during the campaign. We evaluate the observed
150 SOA production over the SMA with source analysis models, correlation of secondary gas-phase
151 species with SOA, an oxidation flow reactor, and box modeling to constrain local versus transport
152 contributions. These results are discussed and placed into context of improving our knowledge
153 about SOA production and sources in urban environments.

154 **2. Methods**

155 Here, we introduce the KORUS-AQ campaign (Sect. 2.1), the key instruments for this
156 study (2.2), additional measurements used in the analyses (2.3), and the airborne oxidation flow
157 reactor (2.4). All linear fits, unless otherwise noted, use the least orthogonal distance regression
158 fitting method (ODR).

159 **2.1 KORUS-AQ brief overview**

160 KORUS-AQ was conducted over South Korea and the West Sea during May – June, 2016.
161 This study focuses on the NASA DC-8 (Aknan and Chen, 2018) observations; however, there were
162 numerous other measurement platforms in operation (Al-Saadi et al., 2015). The DC-8 was
163 stationed in the Songtan area of Pyeongtaek, South Korea, approximately 60 km south of Seoul.
164 The DC-8 flew 20 research flights (RF) (Figure 1; Table S1). For each RF, the DC-8 would take-
165 off from near Seoul, typically at 8:00 local time (LT), which is Korean Standard Time, and perform
166 a missed approach over Seoul Air Base, which is less than 15 km from the Seoul city center. This
167 pattern was typically conducted 2 more times during each flight, around 12:00 LT and prior to
168 landing (~15:00 LT), leading to 55 missed approaches over Seoul during the campaign. Each
169 missed approach involved flying near Seoul below 1000 m (above ground) for 15 – 45 minutes,
170 providing a large number of observations of the Seoul boundary layer. The observations collected
171 during this pattern, along with any other flights conducted within the coordinates defined as Seoul
172 (Table S2, Fig. S1) are referred to as “Seoul” below.

173 Briefly, the SMA is bordered by the West Sea (i.e., the Yellow Sea) and Gyeonggi Bay to
174 the west and forests and mountainous regions to the north, south, and east (Park et al., 2017).
175 Within this region, nearly 30% of the land is used for human activities, ~21% is used for cropland,
176 pasture, and grassland, and ~36% is forested (Park et al., 2017). During the time period of KORUS-
177 AQ, the wind was typically from the west to northwest, meaning that observations over the West
178 Sea represent typical background (inflow) air mass observations for Seoul (H. C. Kim et al., 2017).
179 May and June are typically characterized by low precipitation and rising temperatures prior to the
180 summer monsoon (Hong and Hong, 2016; H. C. Kim et al., 2017).

181 Besides the Seoul missed approaches, the DC-8 would fly either over the West Sea, the
182 Jeju jetway, or the Busan jetway at four different altitudes (nominally ~300 m, ~1000 m, ~1500
183 m, and ~7500 m above ground, depending on the height of the boundary layer, clouds, and
184 chemical forecasts). Many of the 3 lower elevation sampling legs around South Korea encountered
185 significant pollution, similar to the flight segments over Seoul. Similar to Seoul, the approximate
186 coordinates defining these regions are also included in Table S2. For this study, the observations
187 over the West Sea have been split into 2 categories: “clean,” referring to the typical conditions
188 observed during KORUS-AQ, and “transport/polluted,” referring to one RF (RF12, 24/May/2016)
189 that had direct transport of pollution from the Shanghai region over the West Sea. Also, RF11
190 (21/May/2016) is not included in the West Sea category, as this flight was sampling outflow from
191 the SMA (prevailing winds from the east).

192 **2.2 CU-AMS sampling and analysis**

193 A highly customized, high-resolution time-of-flight aerosol mass spectrometer (HR-ToF-
194 AMS, Aerodyne Research, Inc.) was flown on the NASA DC-8 during KORUS-AQ. Hereafter,
195 this instrument will be referred to as CU-AMS since there were two high-resolution AMSs on the
196 DC-8 during KORUS-AQ (see Sect. 2.4). Both AMSs measured non-refractory composition of
197 PM₁ (particulate matter with aerodynamic diameters less than 1 μm) (DeCarlo et al., 2006;
198 Canagaratna et al., 2007). The key differences between the two AMSs was the type of vaporizer
199 (standard for CU-AMS versus capture for the other AMS), which has been described in prior
200 publications (Jayne and Worsnop, 2015; Hu et al., 2017a, 2017b, 2018a, 2018b; Xu et al., 2017)
201 and below and in Sect. 2.4. The basic concept, and operation, of the CU-AMS for aircraft sampling
202 has been described elsewhere (DeCarlo et al., 2006, 2008, 2010; Dunlea et al., 2009; Cubison et
203 al., 2011; Kimmel et al., 2011; Schroder et al., 2018), and a brief description of other important

204 details follow. For detailed information on field AMS calibrations, positive matrix factorization,
205 photochemical clock calculations, and model setups, see Supplemental Sect. S2 – S7.

206 Ambient particles were drawn into the airplane through an NCAR High-Performance
207 Instrumented Airborne Platform for Environmental Research Modular Inlet (HIMIL; Stith et al.,
208 2009) at a constant standard ($T = 273 \text{ K}$ and $P = 1013 \text{ hPa}$) flow rate of 9 L min^{-1} . The RAM
209 heating of the inlet dried the aerosol prior to entering the airplane, and the temperature of the cabin
210 (typically $\sim 10^\circ\text{C}$ higher than ambient) maintained the sampling line RH to less than 40%, ensuring
211 the aerosol remained dry prior to entering the AMS. The sample was introduced into the AMS
212 aerodynamic focusing lens (Zhang et al., 2002, 2004), operated at 1.5 Torr, through a pressure-
213 controlled inlet, which was operated at 433 hPa (325 Torr) (Bahreini et al., 2008). The lens
214 transmission calibrations (SI Sect. 2 and Fig. S4) was conducted through the entire plumbing,
215 including the pressure-controlled inlet. There were minimal losses of ammonium nitrate and
216 sulfate through the pressure-controlled inlet during these calibrations. The focused particles were
217 then introduced after several differential pumping stages into a detection chamber, where they
218 impacted on an inverted cone porous tungsten vaporizer (“standard” vaporizer) held at 600°C . The
219 non-refractory species were flash-vaporized and the vapors were ionized by 70 eV electron
220 ionization. Finally, the ions were extracted, and analyzed by a high-resolution time-of-flight mass
221 spectrometer (HTOF, ToFwerk AG). The residence time from outside the inlet to the vaporizer was
222 $\sim 0.4 \text{ s}$ in the boundary layer and $\sim 1.0 \text{ s}$ at 7500 m during KORUS-AQ. Unless otherwise noted,
223 all aerosol data reported here is at standard temperature (273 K) and pressure (1013 hPa) (STP),
224 leading to the notation $\mu\text{g sm}^{-3}$ (sm^{-3} is the standard volume, in m^3 , at STP). Notation in scm^{-3} is
225 also at STP.

226 For KORUS-AQ, the CU-AMS was operated in the Fast Mass Spectrum (FMS) mode
227 (Kimmel et al., 2011), in order to obtain high-time resolution measurements (1 Hz) continuously.
228 Each FMS 1 s “run” is either collected as chopper closed (background with particle beam blocked)
229 or chopper open (background plus ambient particles and air) position. For KORUS-AQ, the CU-
230 AMS sampled with chopper closed for 6 s and chopper open for 46 s. For the remaining 8 s of the
231 1 min cycle, it sampled with the efficient particle time-of-flight (ePToF) mode which provides
232 particle sizing but with reduced sensitivity (Fig. S2). Also, once every 20 – 30 min, rapid sampling
233 (20 s) of outside air through a particle filter was used to ensure quality control of the instrument
234 background and detection limits. The filters provide data quality checks throughout the flight by
235 checking for leaks as the cabin changes pressure, to determine the response time of the different
236 species (typically less than 2 seconds), and to validate the real-time continuous detection limits
237 calculated by the Drewnick et al. (2009) method. The average of the two background signal periods
238 (chopper closed) before and after the open signal was subtracted from each 1 s open measurement.
239 In addition to the 1 s data, we reported a 1 min data product, in which we averaged raw mass
240 spectra prior to fitting the high-resolution ions, leading to improved signal-to-noise (SNR) from
241 reduced nonlinear fitting noise (beyond the expected increased SNR from averaging in an ion-
242 counting noise regime). For this study, the 1 min data product is used since the additional spatial
243 resolution provided by the 1 s product was not required for the analysis of regional plumes. The
244 software packages Squirrel V1.60 and PIKA V1.20 within Igor Pro 7 (Wavemetrics) (DeCarlo et
245 al., 2006; Sueper, 2018) were used to analyze all AMS data.

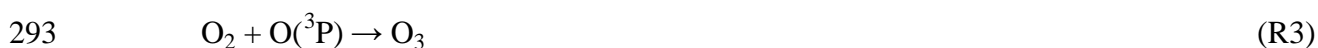
246 The CU-AMS always used the “V-mode” ion path (DeCarlo et al., 2006), with a spectral
247 resolution ($m/\Delta m$) of 2500 at m/z 44 and 2800 at m/z 184. The collection efficiency (CE) for the
248 CU-AMS was estimated per Middlebrook et al. (2012), and ranged from 0.5 – 1 (Fig. S28), with

249 most of the values occurring around 0.5. Calibrations of the CU-AMS are discussed in the
250 supplement (Sect. S2), and detection limits for the 1 min data were 26, 12, 4, 10, and 115 ng sm⁻³
251 for SO₄ (sulfate), NO₃ (nitrate), NH₄ (ammonium), Chl (chloride), and OA, respectively (Note that
252 the charge symbol is not included for the nominally inorganic species, as organic compounds may
253 make (typically small) contributions to these species (e.g., organonitrates, organosulfates, and
254 reduced organic nitrogen species) (Huffman et al., 2009; Farmer et al., 2010). On average, during
255 the campaign, organic nitrates were ~8% of the total CU-AMS NO₃ signal, and were only an
256 important contribution to the NO₃ signal when NO₃ was less than 0.50 μg sm⁻³ (Fig. S38). pNO₃
257 will be used throughout the rest of the paper to represent aerosol NO₃ and to ensure it is not
258 confused with radical NO₃. These detection limits are estimated for every data point per Drewnick
259 et al. (2009) and remained nearly constant during each flight and throughout the campaign. The
260 detection limits were scaled by ~×0.8, based on comparison with periodic filter blanks
261 (Campuzano-Jost et al., 2016), since the Drewnick et al. (2009) method only uses some ions to
262 determine the detection limits, while filters take all ions into account, and thus the latter provide a
263 more accurate estimate. It was found that the scaling with the periodic blanks from the filters were
264 not impacted by the length of sampling outside air through the filter. The low limit of detection for
265 these species remained nearly constant during the flight by using a cryogenic pump that lowered
266 the temperature of a surface surrounding the vaporizer region to 90 K. This freezes out most
267 background gases, and provided consistently low detection limits during the flight, when other
268 AMSs may suffer from increased detection limits after several hours into a flight due to pumping
269 out of large initial backgrounds. The cryogenic pump is necessary since the airplane had power
270 only 3 hours prior to take-off until 2 hours after landing; therefore, the CU-AMS was not constantly
271 being pumped. This leads to high backgrounds each time the instrument is started. The 2σ accuracy

272 for the CU-AMS of inorganic and organic species is estimated to be 35% and 38%, respectively
273 (Bahreini et al., 2009). The O/C and H/C ratios were determined using the improved-ambient
274 method (Canagaratna et al., 2015). The CU-AMS was fully operational during KORUS-AQ,
275 except for 2 hours in RF01, leading to nearly 99% data collection coverage. Additional information
276 on AMS data interpretation can be found in Jimenez et al. (2018) as well as the datafile headers
277 for the KORUS-AQ AMS data (Aknan and Chen, 2018).

278 **2.3 Oxidation flow reactor sampling and analysis**

279 The Potential Aerosol Mass (PAM) oxidation flow reactor (OFR) measures the aerosol
280 mass that can be formed from the precursors that are present in ambient or laboratory air (Kang et
281 al., 2007; Lambe et al., 2011). The OFR has been successfully deployed in multiple urban and
282 forested locations to quantify potential SOA (Ortega et al., 2016; Palm et al., 2016, 2017, 2018;
283 Kang et al., 2018). The chemical regimes and comparability to ambient results of the OFR have
284 been characterized extensively by modeling, which indicate that SOA formation proceeds by
285 chemistry similar to the atmosphere, dominated by OH oxidation under low-NO conditions (Li et
286 al., 2015; Peng et al., 2015, 2016). The sampling schematic of the OFR during KORUS-AQ is
287 shown in Fig. S12. Briefly, it is a 13 L (45.7 cm length OD × 19.7 cm ID) cylindrical aluminum
288 tubular vessel that uses two low-pressure mercury 185 and 254 nm lamps (BHK, Inc., model no.
289 82-904-03) to produce OH radical through the photolysis of ambient H₂O, O₂, and O₃ (R1 – R5).
290 This mode of operation is referred to as “OFR185.”





296 The KORUS-AQ study represents the first airborne operation of an OFR to our knowledge.
297 Unlike prior ground-based field studies (Ortega et al., 2016; Palm et al., 2016, 2017, 2018), the
298 UV lamps were typically maintained at one constant light setting since the OFR was sampling
299 more rapidly varying air masses. Since external OH reactivity (OHR) and water vapor
300 concentrations changed with air mass, a range of OH exposures (OH_{exp}) were reached inside the
301 OFR despite the constant photolytic flux (Peng et al., 2015). The OFR OH_{exp} was calibrated using
302 two different methods: (1) Using the removal of ambient CO in the OFR during flight (on-line
303 calibration in Fig. S14a). (2) While on the ground, injecting known amounts of humidified
304 (multichannel Nafion drier) CO from a zero air cylinder spiked with ~2 ppmv of CO (Scott
305 Marrin), and varying the light intensity to produce different amounts of OH (off-line calibration in
306 Fig. S14b) and thus CO reactive removal. Both the off- and on-line approach yielded a calibration
307 factor of $\times 0.4$ for the OH_{exp} , calculated using the parameterization of Peng et al. (2015), similar to
308 Palm et al. (2016). The OH_{exp} calculated with the calibrated equation is used for periods in which
309 the Picarro was not sampling the OFR output. A histogram of the other key parameters used to
310 calculate OH_{exp} with the Peng et al. (2015) equation— $H_2O(g)$ (measured by DLH) and ambient
311 OH reactivity (measured by ATHOS)—are shown in Fig. S15. The OFR operating conditions were
312 in the “Safe” zone (Peng et al., 2015, 2016), meaning that they were consistent with tropospheric
313 chemistry.

314 A key difference between the operation of this OFR during KORUS-AQ and previous field
315 studies (which did not use any inlet (Ortega et al., 2016; Palm et al., 2016, 2017, 2018)) was that
316 the gas and aerosol passed through ~1.8 m of ~4.6 mm ID stainless steel tubing at 5 vlp
317 (residence time ~1.4 s through tubing). The residence time in the OFR was ~150 s. The gas and

318 aerosol sample entered the OFR through a 1/2" press fitted stainless steel inlet that was coated in
319 SilcoNert (SilcoTek Co, Bellefonte, PA) and had 18 evenly spaced holes (Fig. S13), to promote
320 more even injection of the sample into the OFR flow cross-section (Ortega et al., 2016; Palm et
321 al., 2017; Mitroo et al., 2018). The gas-phase output of the OFR was sampled by an 8.25 cm
322 diameter Teflon ring inside the OFR connected to 1/8" Teflon tubing, and sampled by two gas
323 analyzers for O₃ (Model 205, 2B Technologies, Boulder, CO, USA) and CO (Picarro, see above).
324 The aerosol was sampled by a 2 mm ID stainless steel tube. A constant flow through the OFR at
325 all times was maintained with a bypass flow (when the CU-AMS or CO instrument were not
326 sampling from the OFR) to always maintain a constant residence time in the OFR. The CU-AMS
327 sampled from the OFR for 12 – 15 seconds every three minutes (Fig. S2). This sampling scheme
328 was chosen to ensure the CU-AMS had a high sampling frequency for ambient aerosol, while also
329 sampling the OFR once each time the air inside it was replaced (given its residence time of ~150
330 s).

331 In prior ground-based studies the OFR was placed outside, leading to the ambient and OFR
332 temperature being within 1 – 2°C (Ortega et al., 2016; Palm et al., 2016, 2017, 2018). During
333 KORUS-AQ the OFR was housed inside the DC-8 cabin, which was typically ~10°C (range 0 –
334 20°C) warmer than ambient air (Fig. S16). Since (NH₄)₂SO₄ is nonvolatile, there was little impact
335 on the amount of SO₄ entering and exiting the OFR (as confirmed when the UV lights were off
336 and OH_{exp} was zero) (Fig. S17). For OA, which is typically a mixture of semivolatile and
337 nonvolatile compounds, and for pNO₃, which can be quite semivolatile (Huffman et al., 2009;
338 Cappa and Jimenez, 2010), the mass concentration exiting the OFR was significantly lower than
339 when entering, with lights off. This is due to evaporation of OA and pNO₃ at the warmer cabin
340 temperatures and longer residence times (~150 s). However, for ambient measurements, the

341 residence time was less than 1 s (Sect 2.2), which is rapid enough to prevent volatilization of OA
342 and pNO₃, as discussed in prior work (Guo et al., 2016, 2017; Shingler et al., 2016). Thus, the
343 average ratio of OA transmitted through the OFR versus bypassing the OFR with lights off is used
344 (slope in Fig. S17) as an approximate correction for the amount of OA that should have exited the
345 OFR without chemistry when the OFR was in oxidation mode. These values were highly correlated
346 ($R^2 = 0.94$) and did not vary for the entire campaign, leading to confidence in the correction. This
347 corrects for the semi-volatile nature of ambient OA, but it does not correct for any temperature
348 dependence of SOA formation.

349 The average aerosol condensation sink (CS) inside the OFR is needed for the LVOC fate
350 model described in Palm et al. (2016) to compute the amount of condensable vapors that do not
351 form SOA in the OFR (due to residence-time limitations and surface losses), but that would be
352 expected to form SOA in the atmosphere. Since there were no particle sizers available to estimate
353 the changes in the aerosol surface area after the OFR (Palm et al., 2016), we used Eq. (1) to estimate
354 the average aerosol surface area in the OFR and estimated condensational sink (CS_{est}).

$$355 \quad CS_{est} = CS_{amb} \times \left(\frac{AMS \text{ Tot Mass Out} + AMS \text{ Tot Mass In}}{2 \times AMS \text{ Tot Mass In}} \right)^{2/3} \times 2 \quad (1)$$

356 The CS_{amb} (ambient condensational sink) is calculated using the LAS and SMPS measurements.
357 The second term is a scaling factor to account for the observed increase in mass in OFR (with a
358 power of 2/3 for approximate conversion to relative surface area). The third term is a scaling factor
359 for relative increase in surface area due to strong nanoparticle formation in the OFR, as observed
360 in Los Angeles during CalNex (Ortega et al., 2016). A hygroscopic growth factor is not included
361 in the CS_{est} (Palm et al., 2016) as the aerosol in the OFR was dry (Sect. 2.1).

362 One simple way to confirm the validity of the OH exposures derived from the in-field
363 calibrations and measurements, is to compare the observed versus modeled sulfate enhancements

364 in the OFR while traversing SO₂ plumes (Palm et al., 2016) (Fig. S18 and S19). Albeit the point-
365 to-point comparison is noisy as expected, we find good agreement on average between the modeled
366 and measured SO₄ enhancement (slope = 0.94), validating the quantification of the OFR for this
367 study. We obtained results from the OFR for all flights except RF12 (24/May/2016), when a valve
368 malfunction prevented measurements of O₃ and thus the ability to quantify OFR OH_{exp}. During
369 this flight, the Picarro was also not sampling from the OFR.

370 **2.4 Co-located supporting measurements used in this study**

371 In addition, the CU-AMS measurements, this study utilizes several co-located gas- and
372 aerosol-phase measurements collected on-board the DC-8.

373 **2.4.1 Gas-phase measurements**

374 NO, NO₂, NO_y, and O₃ were measured by the NCAR chemiluminescence instrument
375 (Weinheimer et al., 1994). For CO, the ambient measurements were made with the NASA Langley
376 tunable diode laser absorption spectroscopy (DACOM) (Sachse et al., 1987) while the
377 measurements for CO exiting the oxidation flow reactor (Sect. 2.3) were made with a Picarro
378 G2401-m. The Picarro was calibrated in flight with a WMO traceable gas standard. Gas-phase
379 H₂O was measured with the NASA Langley open-path tunable diode laser hygrometer (DLH)
380 (Diskin et al., 2002). The Pennsylvania State University Airborne Tropospheric Hydrogen Oxides
381 Sensor (ATHOS), based on laser-induced fluorescence, measured OH, HO₂, and OH reactivity
382 (Faloona et al., 2004; Mao et al., 2009). Hydrocarbons were measured by the University of
383 California-Irvine whole air sampler (WAS), followed by analysis with a gas-chromatography
384 followed by either a flame ionization detector or mass spectrometer (Blake et al., 2003), and also
385 by the University of Oslo proton transfer reaction time-of-flight mass spectrometer (PTR-MS)
386 (Wisthaler et al., 2002; Müller et al., 2014). SO₂ and speciated acyl peroxy nitrates (e.g., PAN and

387 PPN) were measured by the Georgia Institute of Technology chemical ionization mass
388 spectrometer (GT-CIMS) (Huey et al., 2004; Slusher et al., 2004; S. Kim et al., 2007) The sum of
389 the total peroxy nitrates (ΣROONO_2) and total alkyl and multifunctional nitrates (ΣRONO_2) were
390 measured by the University of California-Berkeley thermal-dissociation laser-induced
391 fluorescence (TD-LIF) technique (Day et al., 2002; Wooldridge et al., 2010). Formaldehyde was
392 measured with the University of Colorado-Boulder difference frequency absorption spectrometer
393 (CAMS, or Compact Atmospheric Multi-species Spectrometer) (Weibring et al., 2010; Richter et
394 al., 2015). Finally, HCN, HNO_3 , and dihydroxy-toluene were measured by the California Institute
395 of Technology chemical ionization mass spectrometer (CIT-CIMS) (Crouse et al., 2006;
396 Schwantes et al., 2017).

397 **2.4.2 Supporting aerosol measurements**

398 Refractory Black carbon (BC) mass concentrations in the accumulation mode size range
399 measured by the NOAA Single Particle Soot Photometer (SP2) (Schwarz et al., 2013). SO_4^{2-} was
400 measured both by the University of New Hampshire mist-chamber ion-chromatograph (MC/IC,
401 fine mode only) (Talbot et al., 1997) and total particulate filters, analyzed off-line with ion
402 chromatography (fine and coarse mode with an estimated size cut of 4 μm) (Dibb et al., 2003;
403 McNaughton et al., 2007; Heim et al., 2018). Besides the CU-AMS, the Hankuk University of
404 Foreign Studies operated an AMS onboard as well (hereinafter referred to as K-AMS); however,
405 using a “capture vaporizer” (see Sect. 2.2 above). Briefly, the geometry and material of the
406 vaporizer has been modified to reduce the amount of particle bounce, and this leads to a CE of ~ 1
407 for all ambient species, albeit with more thermal decomposition (Jayne and Worsnop, 2015; Hu et
408 al., 2017a, 2017b, 2018a, 2018b; Xu et al., 2017).

409 Finally, the physical concentration and properties of the aerosol were measured by the
 410 NASA Langley Aerosol Research Group (LARGE). These included: (1) Size-resolved particle
 411 number concentrations (values used to estimate surface area and volume) were measured by a TSI
 412 Laser Aerosol Spectrometer (LAS, model 3340; TSI Inc., St. Paul, MN; calibrated with a range of
 413 NIST traceable polystyrene latex spheres (PSL), size range 100 – 5000 nm PSL mobility diameter),
 414 a scanning mobility particle sizer (SMPS, composed of a differential mobility analyzer, TSI model
 415 3081 long column with custom flow system and SMPS operated using TSI software) and a CPC
 416 (TSI model 3010, size range 10 – 200 nm PSL mobility diameter). (2) Scattering coefficients at
 417 450, 550 and 700 nm were measured with an integrating nephelometer (TSI, Inc. model 3563) and
 418 corrected for truncation errors per Anderson and Ogren (1998). (3) Absorption coefficients at 470,
 419 532 and 660 nm were measured with a Particle Soot Absorption Photometer (PSAP, Radiance
 420 Research) and corrected for filter scattering per Virkkula (2010). In order to calculate extinction,
 421 which is used in this study, the measured Angstrom exponent was used to adjust the scattering at
 422 550 nm to 532 nm (Ziemba et al., 2013).

423 3. PM₁ comparisons, composition, and transport during KORUS-AQ

424 3.1 Intercomparisons of airborne PM₁ during KORUS-AQ

425 The intercomparison of aerosol measurements less than 1 μm are summarized here and
 426 shown in Table 1, and the full detailed intercomparison is found in SI 8. The AMS and the other
 427 aerosol measurements agree within their combined uncertainties, similar to prior studies (DeCarlo
 428 et al., 2008; Dunlea et al., 2009; Hayes et al., 2013; Liu et al., 2017; Schroder et al., 2018).

429 **Table 1.** Overview of intercomparisons for KORUS-AQ CU-AMS versus other PM₁
 430 measurements. Uncertainties listed are 1σ .

<i>Instrument Comparison</i>	<i>What is being Compared</i>	<i>Slope</i>	<i>R²</i>	<i>Combined Uncertainty of Instruments</i>	<i>Uncertainty of Regression Slope</i>
MC/IC	SO ₄ Mass	0.95	0.76	±20%	±1%
Filters	SO ₄ Mass	0.80	0.86	±24%	±2%

AMS Scatter Plot (Total Campaign)	Total PM ₁ Mass/CE	0.95		±27%	±1%
AMS Scatter Plot (Lower PM ₁ Sizes) ^a	Mass/CE/ Transmission	1.02	0.91	±27%	±1%
AMS Scatter Plot (Higher PM ₁ Sizes) ^b	Mass/ Transmission	0.84	0.82	±27%	±1%
Extinction	Total PM ₁ Mass to 532 nm Extinction	6.00	0.87	±31%	±3%
LAS (all data)	PM ₁ Volume	1.56	0.86	±43%	±1%
LAS (Conc. Filter) ^c	PM ₁ Volume	1.19	0.91	±43%	±1%
LAS (Mass Filter) ^c	PM ₁ Volume	1.00	0.79	±43%	±1%

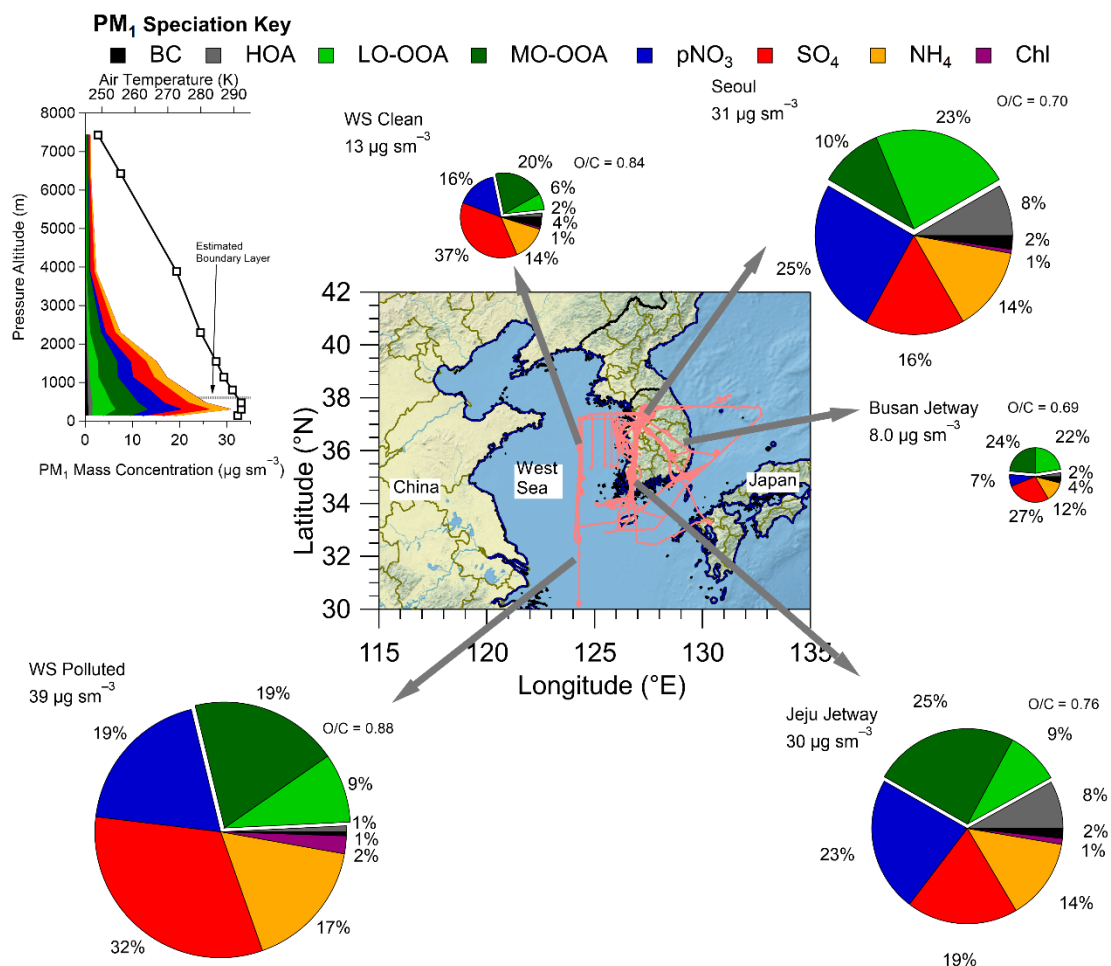
431 ^aComparison of K-AMS and CU-AMS for RFs 1 – 9, 11, 15, 19. ^bComparison of K-AMS and CU-
432 AMS for RFs 10, 12 – 14, 16 – 18, 20. ^cUsing the lower concentration and mass filter. See SI 8
433 and Fig. S27.

434
435 There are two comparisons that show lower agreement. The slope between AMS SO₄
436 versus filter SO₄ is 20% lower than unity. As previously mentioned, the filters collect aerosols
437 with diameters up to 4 μm, and Heim et al. (2018) concluded that the difference was due to
438 supermicron SO₄²⁻ throughout the campaign from the transport of dust from continental Asia to
439 South Korea. Thus, the differences in the diameter cut-off between the AMS and filters and
440 observations of supermicron SO₄²⁻ are the likely cause of the lower slope. The comparison of
441 calculated volume from AMS plus BC versus calculated volume from LAS indicate that the AMS
442 and BC calculated volume is higher. Part of the reason could be that LAS vaporizes BC (Kupc et
443 al., 2018); however, as shown in Figure 1, BC accounts for a small fraction of PM₁. As discussed
444 in SI 8, the LAS detector saturated at high particle number concentrations/high mass
445 concentrations. This has also been observed by Liu et al. (2017) in a prior airborne campaign with
446 the same instruments. Comparing the LAS and AMS plus BC volume at lower total mass
447 concentrations/particle number concentrations, the difference is reduced to ~10%, which is well
448 within the combined uncertainties.

449 3.2 PM₁ concentration and composition over South Korea during KORUS-AQ

450 We briefly describe the PM₁ composition observed over South Korea during the campaign
451 and compare it to prior observations in the same region and for other large urban areas around the
452 world. First, the comparison of PM₁ in the boundary layer (estimated to be ~600 m from
453 temperature profiles measured on the DC-8 during the entire campaign, as shown in Figure 1) in
454 the KORUS-AQ domain is discussed. As shown in Figure 1, the highest average PM₁ during
455 KORUS-AQ were observed over the West Sea during the “transport/polluted” research flight
456 (RF12, 24/May/2016), at 39 $\mu\text{g sm}^{-3}$, and over Seoul, at 31 $\mu\text{g sm}^{-3}$ (average of all flights over
457 Seoul). However, during the latter half of the mission, PM₁ was regularly greater than 60 $\mu\text{g sm}^{-3}$,
458 and as high as 100 $\mu\text{g sm}^{-3}$, over Seoul. During the rest of the flights, the average mass
459 concentration over the West Sea was a factor of 3 lower (13 $\mu\text{g sm}^{-3}$). Also, the Seoul and West
460 Sea PM₁ composition was different, where SO₄ and more-oxidized oxidized organic aerosol (MO-
461 OOA) dominated the West Sea PM₁ budget, indicative of transported, aged chemistry (Dunlea et
462 al., 2009; Lee et al., 2015). Also, the O/C ratio for the West Sea was 0.84 (WS Clean) to 0.88 (WS
463 polluted). Seoul showed higher fractions of less-oxidized OOA (LO-OOA) than MO-OOA, and
464 higher pNO₃ than SO₄, which is more typical of fresher, urban chemistry, with an average O/C
465 ratio of 0.70 (DeCarlo et al., 2008; Hennigan et al., 2008; Hayes et al., 2013; H. Kim et al., 2017;
466 Kim et al., 2018). The eastern side of South Korea had lower average PM₁ than observed over
467 Seoul. This region of South Korea is not as highly populated as around Seoul, reducing the sources
468 and production of PM₁ and is more representative of PM₁ background pollution/transport across
469 the country. The average PM₁ observed over the Jeju jetway was similar to what was observed
470 over Seoul. Also, this area had similar contributions from hydrocarbon-like organic aerosol (HOA)
471 and pNO₃ as Seoul, indicating local emissions, including industry, along with
472 transport/background, are impacting the PM₁ composition (e.g., Hayes et al., 2013). This part of

473 South Korea has some large population centers (e.g., Gwangju and Jeonju) and power plants (e.g.,
 474 Boryeong Power Station), which are consistent with the observed impact.



475
 476 **Figure 1.** Pie charts of the average boundary layer PM₁ composition by the different regions
 477 (defined in Table S2) sampled over South Korea during the campaign. The flight paths are shown
 478 in light red. The Busan jetway had no measurable Chl; therefore, Chl is not included in the pie
 479 chart. The pie charts area is proportional to PM₁ in each region. The average O/C for the OA is
 480 shown by each OA section in the pie charts. The map shows the DC-8 flight paths throughout
 481 KORUS-AQ. The average vertical profile of PM₁ species (along with temperature and continental
 482 PBL height) over all of South Korea is shown in the upper left.

483 The average PM₁ observed over Seoul during KORUS-AQ was similar to the mass
 484 concentration measured in Seoul in previous years (37, 38, 37, 27, and 22 μg m⁻³ for Choi et al.,
 485 2012, Kim et al., 2007, H. C. Kim et al., 2016, Park et al., 2012, and Kim and Zhang, 2017,

486 respectively). Also, the average PM₁ over the West Sea during clean conditions (13 μg sm⁻³) is in
487 line with what has been reported over Baengnyeong Island (Lee et al., 2015), located west of South
488 Korea in the West Sea (37°58'00" N, 124°37'04" S). Finally, the PM_{2.5} mass concentrations have
489 remained nearly constant for the last ~20 years (OECD, 2018).

490 The PM₁ composition over Seoul is dominated by pNO₃ and SOA, similar to what was
491 observed on the ground during the same time period (Kim et al., 2018). The composition over
492 Seoul is more similar to what has been observed over Mexico City during MILAGRO (DeCarlo
493 et al., 2008), and in Los Angeles during CalNex (Hayes et al., 2013) than observed over large
494 urban areas in Asia (Hu et al., 2016).

495 As the differences in PM₁ composition for the different regions mostly occurred in the
496 boundary layer, we show the average PM₁ profile observed during all of KORUS-AQ in the inset
497 of Figure 1, and the fractional contribution to the profile in Fig. S32. At low altitudes, the PM₁
498 mass is dominated by secondary PM₁ species that compose the largest fractions in the pie charts
499 in Figure 1 (LO-OOA, MO-OOA, pNO₃, and SO₄). The fractional contributions of SO₄ and MO-
500 OOA to PM₁ mass increase with altitude and become dominant above ~4 km, representative of
501 more aged aerosol, away from sources (e.g., Dunlea et al., 2009).

502 **3.3 Analysis of background and transport influence on PM₁**

503 Transport of aerosols and aerosol precursors from distant sources creates a larger-scale
504 background that needs to be quantified in order to understand the impact of local emissions on
505 aerosol production. Prior studies have shown the potential impact of long-distance transport in
506 creating a background aerosol mass over Seoul (H. S. Kim et al., 2007; Heo et al., 2009; Kim et
507 al., 2009, 2016, 2018; H. C. Kim et al., 2017; H. Kim et al., 2017; Jeong et al., 2017; Lee et al.,
508 2017; Seo et al., 2017). To investigate the influence of background and transported air to Seoul,

509 the FLEXPART Lagrangian model with WRF winds and meteorology is used. The application of
510 FLEXPART to this study is described in SI 7. Briefly, the model uses back trajectories from the
511 point where the DC-8 was sampling and calculates the amount of CO and NO₂ contributed by
512 different emission regions for each sampled air parcel.

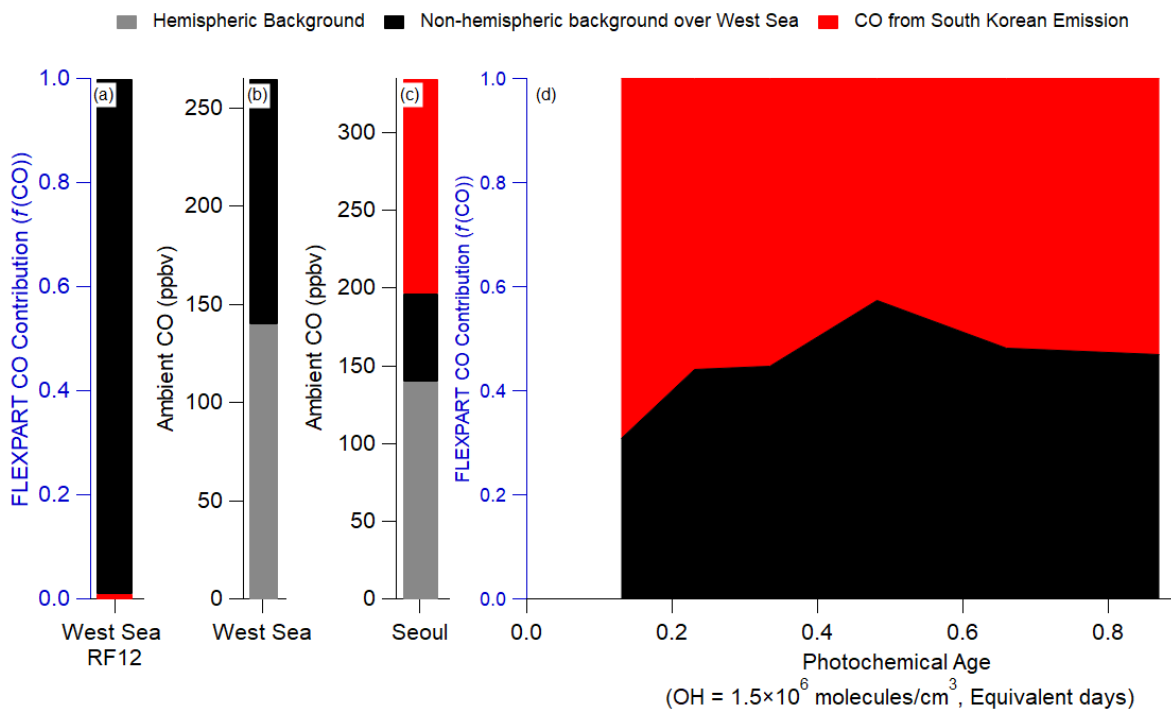
513 The CO concentration measured during KORUS-AQ can be described by Eq. (2). The
514 average CO mixing ratios observed during the campaign are used.

$$515 \quad \text{CO}_{\text{ambient}} = \text{CO}_{\text{hem. bckg.}} + \text{CO}_{\text{foreign}} + \text{CO}_{\text{South Korean}} \quad (2)$$

516 Here, CO_{hem. bckg.} is the hemispheric background of CO. In FLEXPART, the foreign emissions are
517 from China, Hong Kong, Japan, Laos, Macau, Myanmar, Mongolia, North Korea, Russia, Taiwan
518 and Vietnam. FLEXPART does not include the CO hemispheric background; therefore, that term
519 is estimated from upwind sites (Mt. Waliguan, China and Ulan Uul, Mongolia) (Novelli et al.,
520 2017) to be 140 ppbv CO. The West Sea is the simplest case, as FLEXPART predicted that all the
521 CO originated from the foreign sources listed above (Figure 2a). Thus, CO_{ambient} in the West Sea
522 can be attributed to 140 ppbv CO_{hem. bckg.} and 125 ppbv CO_{foreign} (Figure 2b). The advection of CO
523 from the West Sea to Seoul will lead to dilution and mixing of the CO_{foreign} with air containing
524 only the CO_{hem. bckg.}. With an average wind speed of 4 m/s over the West Sea, and a distance of
525 ~300 km, the air takes ~1 actual day to move from where the DC-8 sampled over the West Sea to
526 Seoul. The results from FLEXPART are used to estimate the dilution rate, ~0.7 day⁻¹, comparable
527 to the values determined in prior studies (McKeen et al., 1996; Price et al., 2004; Arnold et al.,
528 2007; Dzepina et al., 2011; Fried et al., 2011). CO_{foreign} over Seoul was determined by Eq. (3),
529 where $t = \sim 1$ day, $-k_{dil} = \sim 0.7 \text{ day}^{-1}$, and $C(0) = 125$ ppbv. Using the full equation from McKeen
530 et al. (1996), a similar value of 60 ppbv CO_{foreign} is derived.

$$531 \quad C(0) = C(t) \times \exp(-k_{dil} \times t) \quad (3)$$

532 With Eq. (2), the total CO background ($CO_{\text{foreign}} + CO_{\text{hem. bckg.}}$) is 200 ppbv, and the remainder of
 533 the observed ambient CO is attributed to local South Korean emissions (on average, 165 ppbv
 534 CO). Finally, results from FLEXPART show that the CO_{foreign} contribution (Figure 2d) remained
 535 nearly constant throughout the campaign at all observed photochemical ages. Therefore, 200 ppbv
 536 CO background for observations over Seoul will be used throughout this study.

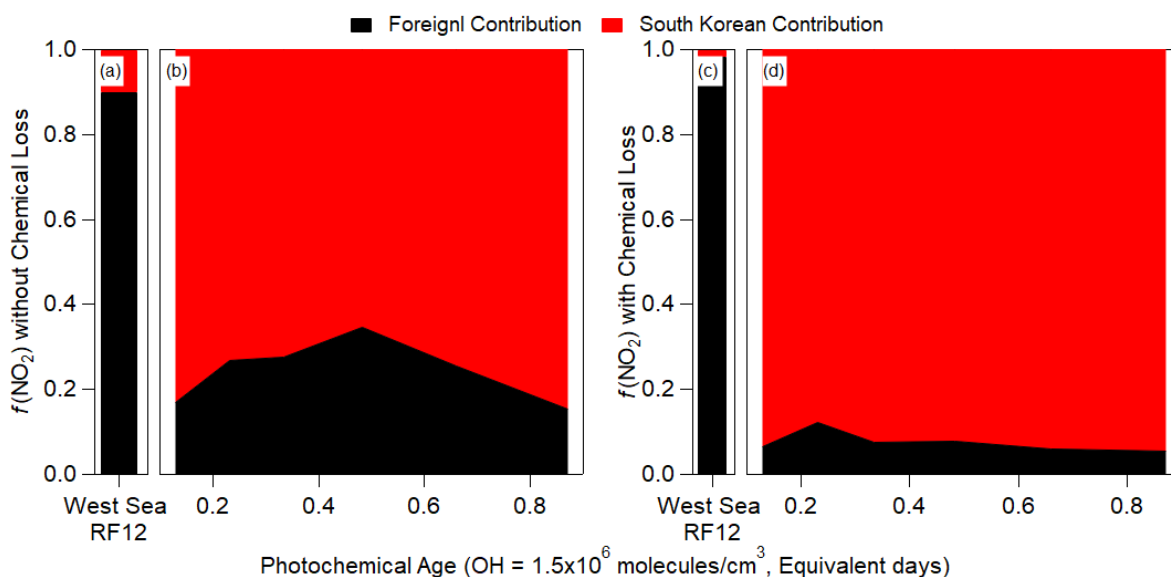


537
 538 **Figure 2.** Note differences in labels and values for each y-axis. Also, note that FLEXPART does
 539 not include hemispheric background; therefore, it is not included in (a) and (d); however, it is
 540 included for the actual observations in (b) and (c). (a) Fractional contribution of foreign versus
 541 South Korean CO emission over the West Sea from FLEXPART. (b) Estimated measured
 542 partitioning of the average CO observed over the West Sea. (c) Same as (b), but for over Seoul.
 543 (d) Same as (a), but for over Seoul. For all panels, CO does not include any chemical losses or
 544 production.

545 From the observed dilution-corrected OA concentrations (OA concentration divided by the
 546 hemispheric background subtracted CO mixing ratios) over the West Sea (13 and 40 $\mu\text{g sm}^{-3}$
 547 ppmv^{-1} for clean West Sea and RF12 West Sea, respectively), the CO_{foreign} over Seoul would
 548 correspond to 1 – 3 $\mu\text{g sm}^{-3}$ OA background (Eq. (4)).

549
$$OA_{\text{background}}(t) = CO_{\text{foreign}}(t) \times \left(\frac{OA}{CO} \right)_{\text{foreign}}(0) \quad (4)$$

550 The upper limit will be used for the remainder of the study. The corresponding observed
 551 background values for HOA, LO-OOA, and MO-OOA are 0, 1 ± 1 , and $2 \pm 2 \mu\text{g sm}^{-3}$, respectively.
 552 Finally, the background for key gas-phase and aerosol species (which are discussed below) are
 553 1.05 ± 0.28 (CH_2O), 69 ± 5 (O_x), 0.25 ± 0.06 (PAN), and 0.30 ± 0.10 (ΣROONO_2) ppbv, 0.44 ± 0.34
 554 (Dihydroxy toluene) pptv, and $2 \pm 2 \mu\text{g sm}^{-3}$ (pNO_3). Thus, the increase in OA mass concentration
 555 from the background values ($3 \mu\text{g sm}^{-3}$) to average Seoul values ($13 \mu\text{g sm}^{-3}$) must be due to South
 556 Korean emissions of POA and production of SOA.



557 **Figure 3.** Binned fractional contribution (South Korea/(South Korea + Foreign)) of the
 558 FLEXPART contributions to (a and b) NO_2 (without any chemical losses) and (c and d) NO_2 (with
 559 chemical losses ($\tau = 1$ day)) versus the observed (aircraft) photochemical age. For (a) and (c), the
 560 West Sea bars are the average fractional contributions for RF12.
 561

562 The contribution of foreign versus South Korean emissions of NO_2 from FLEXPART over
 563 Seoul and West Sea (Figure 3) is analyzed next. NO_2 is investigated since it has a photochemical
 564 lifetime of ~ 1 day (at $\text{OH} \approx 1.5 \times 10^6$ molecules/ cm^3). This lifetime is similar to short-lived
 565 hydrocarbons (e.g., xylene, S/IVOC, etc.) that are thought to dominate urban SOA production in
 566 this campaign and other megacities (de Gouw et al., 2005; Kleinman et al., 2007, 2008; DeCarlo

567 et al., 2010; Wood et al., 2010; Hayes et al., 2013, 2015, Hu et al., 2013, 2016; Ortega et al., 2016;
568 Ma et al., 2017; Schroder et al., 2018). In general, $f(\text{NO}_2)_{\text{foreign}}$ and $f(\text{NO}_2)_{\text{local}}$ (with and without
569 photochemical loss included in the FLEXPART model runs) is quite constant with photochemical
570 age (Figure 3), like CO. Unlike CO, the contribution of local NO_2 is ~70% (if photochemical
571 removal is not included) and ~90% (if photochemical removal is included). This strongly suggests
572 that most short-lived hydrocarbons over Seoul, which are believed to dominate urban SOA
573 production, are dominated by South Korean emissions and not transport from foreign sources.

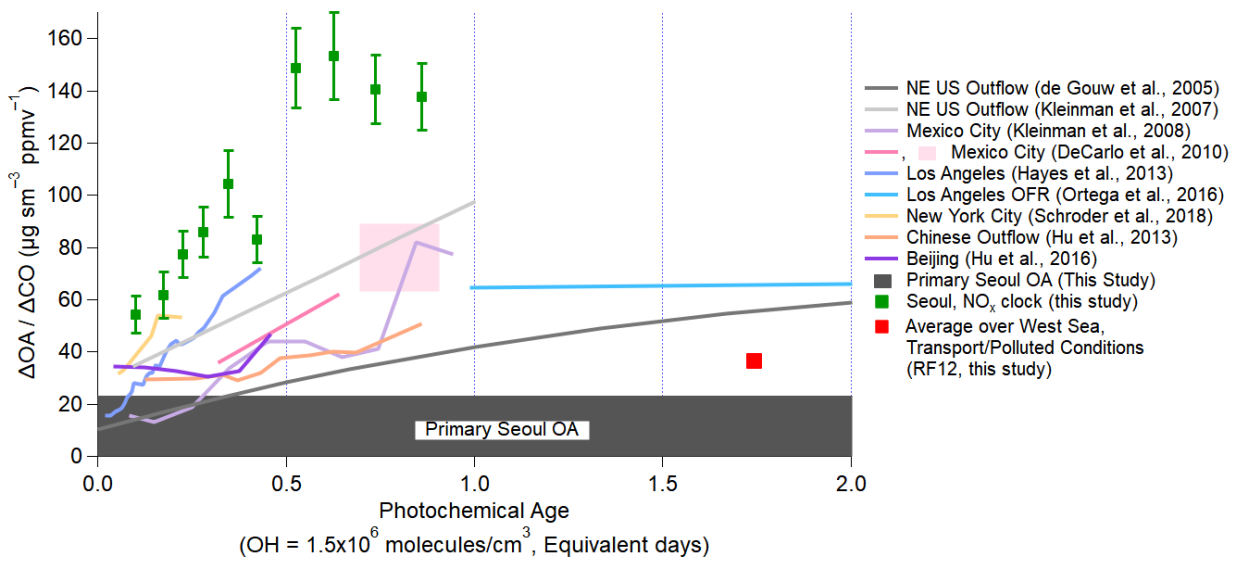
574 **4. SOA production over the Seoul Metropolitan Area**

575 **4.1 SOA production over Seoul during KORUS-AQ**

576 The conceptual model for analysis of photochemical SOA production over and downwind
577 of megacities has been discussed in detail in de Gouw (2005) and DeCarlo et al. (2010) and
578 subsequent studies (Hayes et al., 2013; Hu et al., 2013, 2016; Freney et al., 2014; Schroder et al.,
579 2018). An air mass with “background” values of OA and CO is advected over a megacity area,
580 where fresh emissions of POA, SOA precursors, and CO are emitted into the air mass. The SOA
581 precursors will oxidize to produce SOA and undergo dilution with the surrounding background air
582 masses. To correct for this dilution effect, the change of OA over background OA ($\Delta\text{OA} = \text{OA} -$
583 background OA) is divided by the change of CO over background CO ($\Delta\text{CO} = \text{CO} -$ background
584 CO), and this term is the dilution-corrected concentration. CO has been used in prior studies as a
585 surrogate for primary pollution emissions as this compound has high signal-to-noise between
586 urban plumes and background and a long photochemical lifetime (meaning minimal CO is lost due
587 to chemistry or produced from VOC oxidation over a ~1 day timescale (Griffin et al., 2007)) (de
588 Gouw et al., 2005; DeCarlo et al., 2010). Finally, $\Delta\text{OA}/\Delta\text{CO}$ is plotted versus estimated
589 photochemical age. The photochemical age approximately accounts for the chemical evolution of

590 precursors either into products which can be estimated from the time evolution of NO_x/NO_y , or the
 591 differences in removal rates of two hydrocarbons (o-xylene or m+p-xylene to ethylbenzene). See
 592 SI 5 for more information about the calculation of the photochemical age. The potential impact of
 593 SOA precursors being advected into Seoul is addressed in Sect. 4.4.

594 Throughout the paper, the estimated photochemical age from NO_x/NO_y will be used as this
 595 measurement has higher temporal coverage, and an emissions ratio is not needed to calculate the
 596 photochemical age (SI 5), but note that ages estimated from hydrocarbon-based clocks are
 597 consistent. For photochemical ages greater than 1 day (measurements over the West Sea), the
 598 aromatic photochemical clock is used (SI 5) as the NO_x/NO_y clock does not work well past 1
 599 equivalent day (SI 5). As discussed in Parrish et al. (2007), compounds used to calculate
 600 photochemical ages should have lifetimes on the order of the range in ages to be quantified. For
 601 example, photochemical age over Seoul is less than 1 equivalent day, which is equivalent to the
 602 NO_x lifetime; whereas, the photochemical age over the West Sea is expected to be a few equivalent
 603 days, which is bracketed by the lifetimes of benzene and toluene.



604
 605 **Figure 4.** Evolution of dilution-corrected OA versus equivalent photochemical age (days), where
 606 $\Delta\text{OA} = \text{OA} - \text{background OA}$ and $\Delta\text{CO} = \text{CO} - \text{background CO}$, during KORUS-AQ. Over Seoul

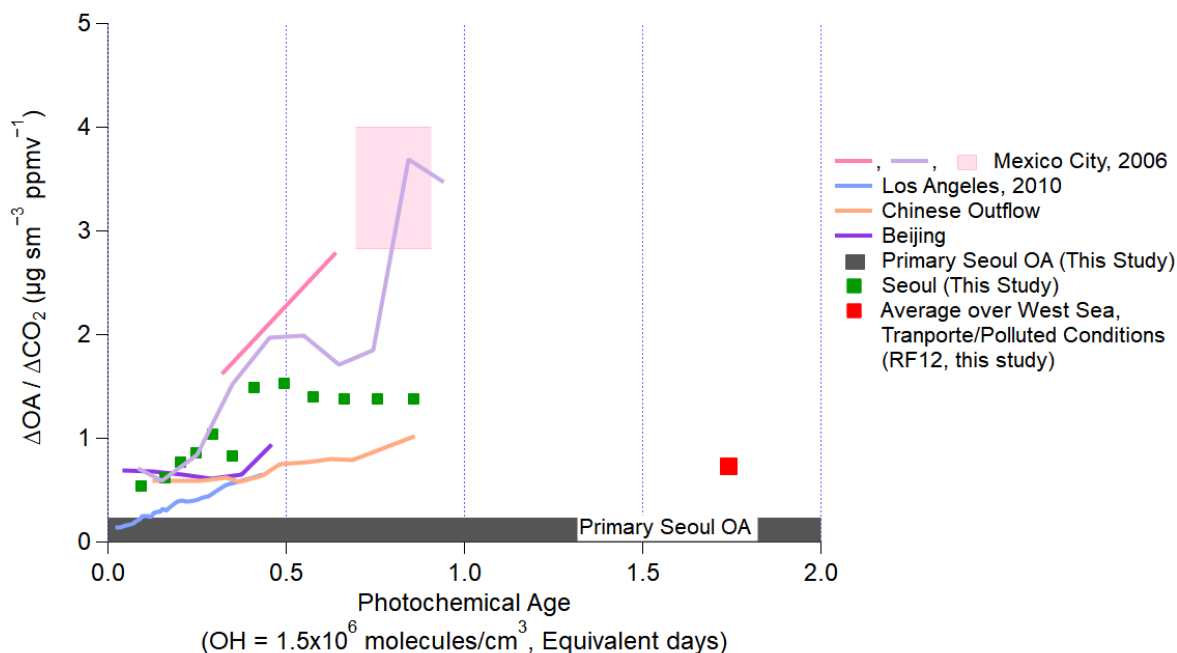
607 and the West Sea, the CO background is 200 (hemispheric plus foreign) and 140 ppbv (hemispheric
608 only), respectively. The vertical error bars for the observations during KORUS-AQ are the
609 standard error of $\Delta\text{OA}/\Delta\text{CO}$ for each bin. Photochemical age is determined by the NO_x/NO_y . The
610 dark grey bar at the bottom ($22 \mu\text{g sm}^{-3} \text{ppmv}^{-1}$) is the observed POA over Seoul during the
611 campaign. Observations from other megacities (de Gouw et al., 2005; Kleinman et al., 2007, 2008;
612 DeCarlo et al., 2010; Hayes et al., 2013; Hu et al., 2013, 2016; Ortega et al., 2016; Schroder et al.,
613 2018) are also shown, as lines, for comparison, and have been updated, as described in Schroder
614 et al. (2018).

615 Similar to prior studies, OA over Seoul increased rapidly within the first photochemical
616 equivalent day from the emission source (Figure 4). The dilution-corrected SOA production is very
617 rapid for photochemical ages less than 0.7 equivalent days (note that this would be only 4 actual
618 hours of exposure for average OH concentration of 6×10^6 molecules/cm³ observed during this
619 campaign). After that time, the dilution-corrected OA plateaus and remains nearly constant.
620 George et al. (2008) and Ortega et al. (2016) found that after $\sim 4 - 5$ equivalent days, OH
621 heterogeneous reactions start fragmenting the compounds in SOA, leading to a reduction in the
622 dilution-corrected OA mass with age. Compared to prior megacity studies, the dilution-corrected
623 OA produced over Seoul is between $40 - 80 \mu\text{g sm}^{-3} \text{ppmv}^{-1}$ higher at ~ 0.5 equivalent days of
624 photochemical aging and $\sim 70 \mu\text{g sm}^{-3} \text{ppmv}^{-1}$ higher than in Chinese megacities (Hu et al., 2013,
625 2016). Qualitatively, the time scale for the production and plateauing of dilution-corrected OA is
626 similar for Seoul, Los Angeles, and Mexico City; however, the amount of OA produced per CO is
627 larger for Seoul compared to Los Angeles and Seoul. It also appears not to be significantly
628 influenced by the outflow of upwind Chinese megacities, since Seoul SOA formation is very rapid
629 and occurs much faster than air mass transport from those megacities, and since the dilution-
630 corrected production is much larger in Seoul than in Chinese megacities.

631 Finally, though the absolute $\Delta\text{OA}/\Delta\text{CO}$ value changes depending on background CO used,
632 assuming a lower CO background does not change the general results that Seoul has higher and
633 more rapid SOA production than has been observed in prior megacities. As shown in Fig. S34, the

634 OA mass concentration increases versus CO mixing ratios as photochemical age increase, and in
635 Fig. S35, even assuming a lower CO background (140 ppbv), the dilution-corrected OA
636 concentration is still $\sim 100 \mu\text{g sm}^{-3} \text{ppmv}^{-1}$. This value is still higher than what has been observed
637 in prior cities (Figure 4). If the CO background is higher than assumed here (200 ppbv), the OA
638 production would be even higher.

639 To further investigate the potential influence from upwind megacities, we compare
640 $\Delta\text{OA}/\Delta\text{CO}$ over the West Sea versus that over Seoul (Figure 4). The average $\Delta\text{OA}/\Delta\text{CO}$ over the
641 West Sea during the “transport/polluted” conditions (RF12, 24/May/2016) is $\sim 40 \mu\text{g sm}^{-3} \text{ppmv}^{-1}$.
642 Since $40 \mu\text{g sm}^{-3} \text{ppmv}^{-1}$ has been observed in and downwind of China (Hu et al., 2013, 2016),
643 and observed over the West Sea during the “transport/polluted” event, this dilution-corrected OA
644 concentration is taken to be representative of transport events from China to South Korea. This
645 value has already been subtracted from the observations over Seoul. The fact that OA
646 concentrations are greater than POA concentrations at the youngest photochemical ages may be
647 due to (1) very rapid SOA production; (2) sunrise occurring 3 – 4 hours (sunrise between 5:10 –
648 5:30 LT) prior to sampling air over Seoul in the morning; and, (3) the imperfect characterization
649 provided by the average photochemical age when fresh emissions have been recently injected into
650 an air parcel.



651
 652 **Figure 5.** Same as Figure 4, but normalized by ΔCO_2 . The ratios to CO_2 are calculated using
 653 $\Delta\text{CO}/\Delta\text{CO}_2$ emissions ratios from prior studies in each megacity that occur during the same
 654 campaign or for the same time of year, since direct measurements of the CO_2 enhancements above
 655 background during the aircraft studies of each megacity are very challenging. (Table S4).

656 Here, we introduce another dilution-correction method to investigate SOA production over
 657 a megacity— $\Delta\text{OA}/\Delta\text{CO}_2$ (Figure 5). $\Delta\text{OA}/\Delta\text{CO}_2$ is a way to investigate the amount of OA
 658 produced per unit mass of fuel burned in each megacity. Note that although some SOA precursors
 659 are not emitted from combustion sources, such as volatile consumer products (McDonald et al.,
 660 2018), one can still define this ratio in an average sense for each megacity. It has been used
 661 previously for laboratory experiments (e.g., Gordon et al., 2013; Platt et al., 2013, 2017) and
 662 biomass burning (e.g., Akagi et al., 2012; Collier et al., 2016); however, to the best of the authors’
 663 knowledge, it has not been used for SOA production over a megacity. As noted above, CO has
 664 been typically used instead, given that it is always measured in pollution studies, and it typically
 665 has a higher signal-to-background ratio than CO_2 in urban areas. Also, during spring and summer,
 666 CO_2 is taken up by plants, which can reduce its signal-to-background ratio. However, the ratio of

667 other gases to CO can vary between urban areas depending on the average combustion efficiency
668 of the dominant sources (Silva et al., 2013). CO₂ better accounts for fuel consumption in an urban
669 area (Vay et al., 2009; Tang et al., 2018). Multiple recent studies have reported average emissions
670 ratios for different megacities based on high precision measurements of $\Delta\text{CO}/\Delta\text{CO}_2$ (Vay et al.,
671 2009; Wang et al., 2010; Peischl et al., 2013; Silva et al., 2013; Tohjima et al., 2014; Tang et al.,
672 2018). These results provide an ability to convert the $\Delta\text{OA}/\Delta\text{CO}$ determined in prior studies to
673 $\Delta\text{OA}/\Delta\text{CO}_2$ (Table S4). We find that for most of the megacities studied, $\Delta\text{OA}/\Delta\text{CO}_2$ is very
674 similar, though Mexico City and Seoul show higher values (approximately factor of 2). The range
675 of observed $\Delta\text{OA}/\Delta\text{CO}_2$ versus photochemical age is narrower, compared to the spread for all
676 megacities observed for $\Delta\text{OA}/\Delta\text{CO}$. Both analyses suggest that Seoul has larger relative emissions
677 of SOA precursors compared to other megacities, which could be targeted for air quality
678 improvement. However, more observations across other megacities and additional comparative
679 analyses would be beneficial.

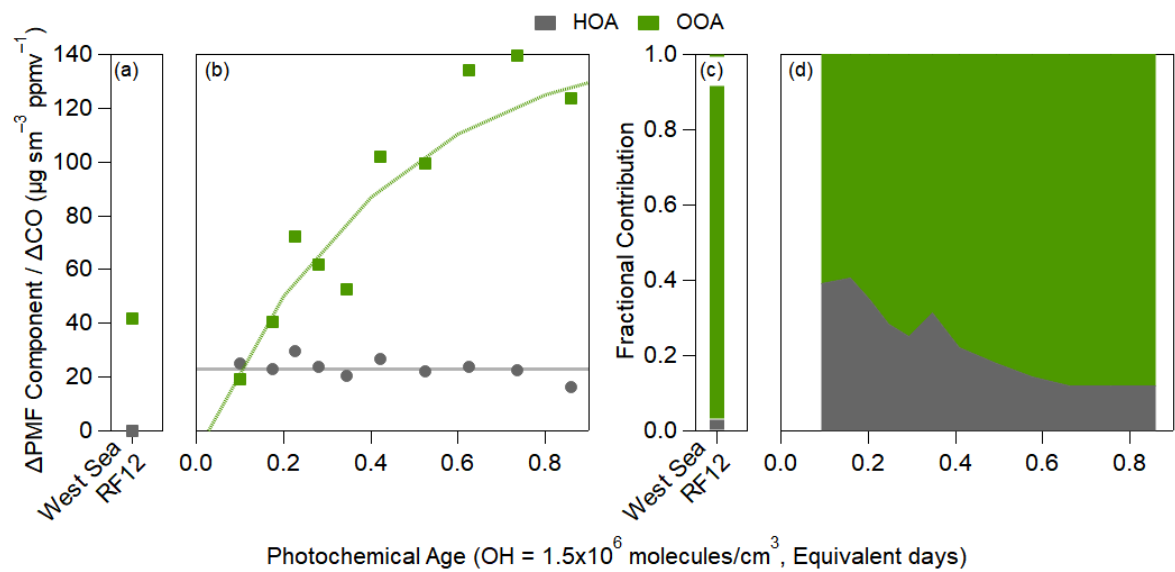
680 **4.2 Composition-based analysis of the foreign versus South Korean contribution to SOA** 681 **precursors and SOA over Seoul**

682 **4.2.1 Evolution of oxygenated organic aerosol over Seoul**

683 Here, we focus on the positive matrix factorization (PMF) (Ulbrich et al., 2009) factors for
684 OA resolved during KORUS-AQ, whose evolution over Seoul is shown in Figure 6. Total OOA
685 (LO-OOA plus MO-OOA) is used as a surrogate of total SOA. The fractional contribution of these
686 two factors can be found in Fig. S36. Rapid production of OOA is observed, accounting for all of
687 the observed growth in total OA over Seoul. LO-OOA, overall, is slightly more abundant than
688 MO-OOA (Fig. S36). LO-OOA has lower O/C compared to MO-OOA (Fig. S10); thus, the faster
689 production of LO-OOA likely represents the less oxidized OOA produced from the photooxidation

690 of SOA precursors (Hayes et al., 2013; Freney et al., 2014; Hu et al., 2016; Kim et al., 2018), while
 691 MO-OOA may represent the more oxidized species or those formed from later generations of
 692 oxidation (Robinson et al., 2007; Miracolo et al., 2010; Tritscher et al., 2011; Ortega et al., 2016;
 693 Sato et al., 2017; Schwantes et al., 2017).

694 The PMF factors have very different dilution-corrected concentrations over the West Sea
 695 during the “transport/polluted” event (Figure 6a). All Δ PMF factors/ Δ CO show much lower values
 696 than for aged air over Seoul. The discontinuity between the three factors between Seoul and West
 697 Sea indicate that transported OA, and transported SOA production, has limited impact on the OA
 698 over Seoul.



699
 700 **Figure 6.** Same as Figure 4, but for the PMF results of the OA evolution over (a) West Sea during
 701 the polluted event (West Sea RF12 at ~1.75 equivalent days) and (b) over Seoul. For (b), fit to
 702 HOA and OOA are $23 \mu\text{g sm}^{-3} \text{ppmv}^{-1}$ and $150 \times (1 - \exp(-2.3 \times \text{eq. day}))$, respectively. For the OOA
 703 equation, 150 equals the max SOA. Fractional contribution of the PMF factors over (c) West Sea
 704 (RF12) and (d) over Seoul.

705 The slope of Δ HOA/ Δ CO versus age was nearly zero $\mu\text{g sm}^{-3} \text{ppmv}^{-1}$ equivalent day⁻¹,
 706 indicating minimal evolution within these timescales. There are mixed results on whether HOA
 707 changes with photochemical age (DeCarlo et al., 2010; Hayes et al., 2013; Hu et al., 2013, 2016;

708 Freney et al., 2014; Schroder et al., 2018); however, due to the uncertainty that comes from the
709 CO background, it is difficult to determine whether these changes are real or not.

710 At the lowest photochemical ages, HOA is ~35% of the total $\Delta\text{OA}/\Delta\text{CO}$ (Figure 6d). Since
711 HOA remains approximately constant with age while OOA rapidly increases (Figure 6b), the HOA
712 contribution to total $\Delta\text{OA}/\Delta\text{CO}$ decreases to ~10% after ~1 equivalent day. It has been observed
713 in prior urban campaigns that HOA contributes 10 – 50% and total POA (HOA + other primary
714 OA factors in AMS) contributes 30 – 60% (Aiken et al., 2009; DeCarlo et al., 2010; Hayes et al.,
715 2013; Crippa et al., 2014; Hu et al., 2016; H. Kim et al., 2017; Kim et al., 2018). The fractional
716 contribution of HOA in Seoul is within this range.

717 A more detailed discussion of the behavior of AMS OA source tracers can be found in SI
718 11. In general, the AMS OA source tracers behave similarly to other urban campaigns (e.g., Hayes
719 et al., 2013; Freney et al., 2014). Some dilute biomass burning OA was evident, but this source
720 was not major most of the KORUS-AQ. Similarly, isoprene oxidation chemistry was not a major
721 contributor to SOA during this campaign.

722 **4.2.2 Correlation of SOA versus other fast photochemical products**

723 Results above support that a major fraction of the SOA observed over Seoul is rapidly
724 produced through photooxidation of South Korean SOA precursors. To further evaluate this result,
725 we analyze the correlation of OOA with other secondary species known to be rapidly produced
726 through photooxidation of organic precursors.

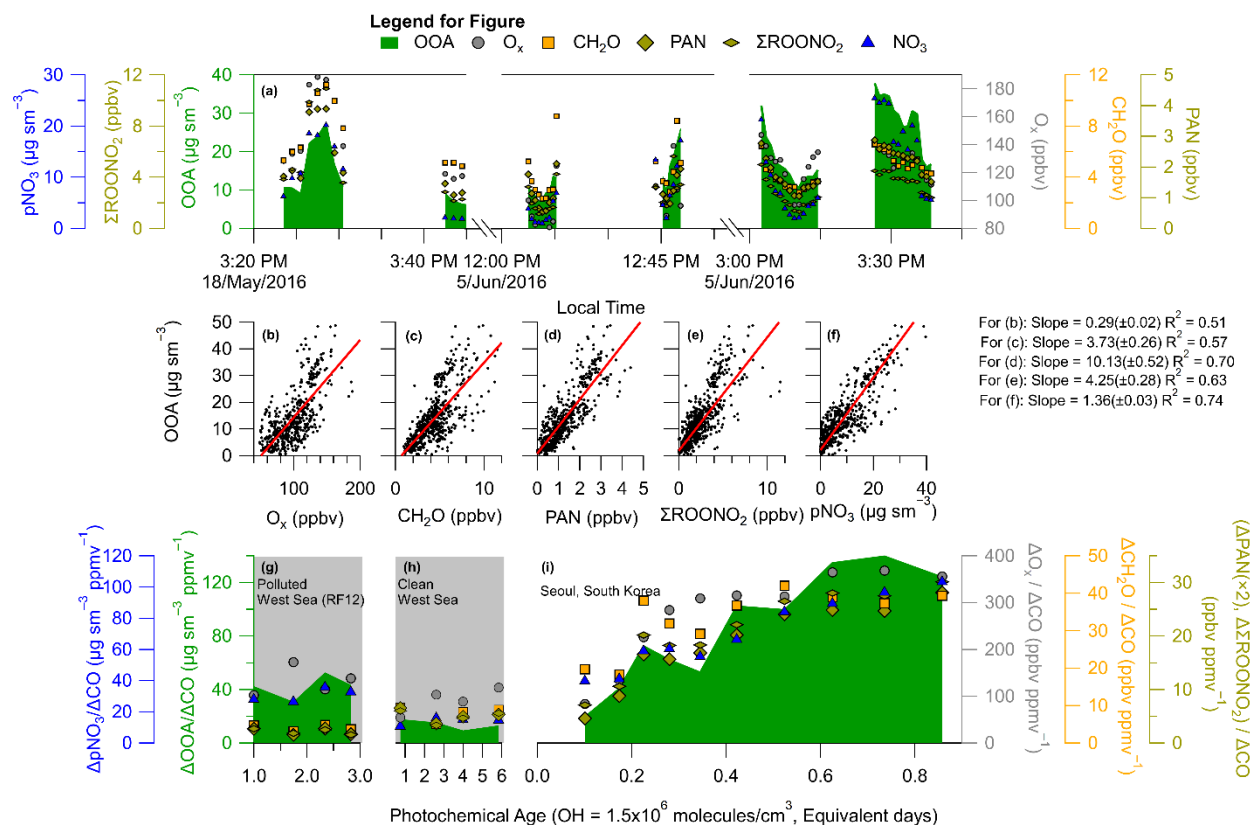
727 The other secondary species used in this study are odd oxygen (O_x), formaldehyde (CH_2O),
728 peroxy acetyl nitrate (PAN), the sum of all acyl peroxy nitrates (ΣROONO_2), and pNO_3 . O_x
729 (approximated as $\text{NO}_2 + \text{O}_3$) is used instead of O_3 to account for titration of O_3 in the presence of
730 fresh NO emissions. Prior studies have used O_x to provide insights into SOA production (Herndon

731 et al., 2008; Wood et al., 2010; Hayes et al., 2013; Morino et al., 2014; Zhang et al., 2015; Hu et
732 al., 2016) since O_x has a similar lifetime to SOA (~1 week) (Jacob, 2000; Goldberg et al., 2015;
733 Hodzic et al., 2015; Ortega et al., 2016), and O_x is also produced through the photooxidation of
734 organic compounds. However, since both O_x and SOA have longer lifetimes, the correlation
735 observed between these two species may have a contribution from transport of polluted air masses.
736 To reduce the influence of transport on this analysis, the correlation of OOA with CH_2O , PAN,
737 and $\Sigma ROONO_2$ is also investigated. The benefit of these species is that they have estimated
738 lifetimes of less than 3 hours during daytime in KORUS-AQ (typical temperature for transported
739 air 17°C). Also, it has been shown that dilution-corrected pNO_3 decreases rapidly from urban
740 centers, possibly due to dilution with surrounding air low in HNO_3 and NH_3 and irreversible uptake
741 of HNO_3 onto coarser particles (e.g., DeCarlo et al., 2008).

742 Example time series of OOA with O_x , CH_2O , PAN, $\Sigma ROONO_2$, and pNO_3 during three
743 different afternoon Seoul overpasses are shown in Figure 7a. All gas and aerosol species exhibit
744 similar behavior, indicating that these species are undergoing photochemical production during
745 these afternoon passes, similar to what has been observed in other urban environments during the
746 afternoon (Perring et al., 2010; Fried et al., 2011; Parrish et al., 2012; Hayes et al., 2013; Zhang et
747 al., 2015). OOA also tracks the evolution of these species, consistent with OOA also being a
748 secondary product from hydrocarbon photooxidation.

749 Analyzing the entire KORUS-AQ campaign, correlations with $R^2 > 0.50$ are observed
750 between OOA and O_x , CH_2O , PAN, $\Sigma ROONO_2$, and pNO_3 for the overpass observations after
751 12:00 LT (Figure 7b-f). These correlations for these secondary species produced through the
752 oxidation of hydrocarbons, in the afternoon, when photochemical production dominates over

753 mixing and losses, further supports that the OOA production observed in Figure 4 and 6 is
 754 dominated by the photochemistry of locally emitted hydrocarbons.



755
 756 **Figure 7.** (a) Time series of OOA (OOA = LO-OOA + MO-OOA), O_x, CH₂O, PAN, ΣROONO₂,
 757 and pNO₃ during RF09 (18/May/2016), and RF18 (05/June/2016) noon and afternoon overpasses.
 758 Gaps in time series correspond to climbing out of the boundary layer. OOA versus (b) O_x (O_x =
 759 O₃ + NO₂), (c) CH₂O, (d) PAN, (e) ΣROONO₂, and (f) pNO₃ over Seoul, South Korea, during
 760 KORUS-AQ. For panels (b) – (f), the observations are after 12:00 local time (03:00 UTC), the
 761 black dots are all data, and the slopes (red line) is an ODR fit to the data. (g – i) Same as Figure 6
 762 for ΔOOA/ΔCO versus photochemical age, and including the dilution-corrected production of O_x,
 763 CH₂O, PAN, ΣROONO₂, and pNO₃. (g) is over the West Sea (RF12), (h) is over the West Sea
 764 (normal conditions) and (i) is over Seoul. Similar to Figure 4, the Δ corresponds to subtracting the
 765 background values for the respective species.

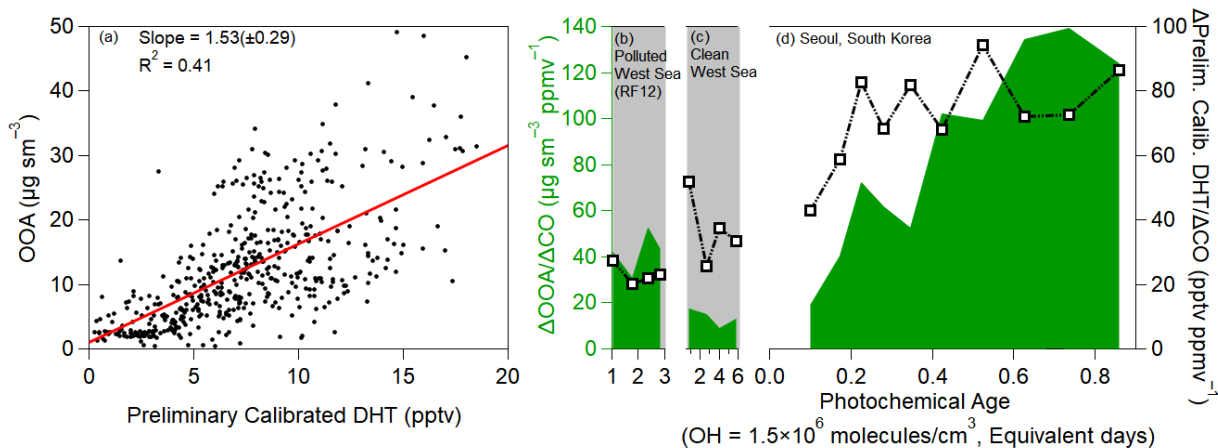
766 O_x, CH₂O, PAN, ΣROONO₂, and pNO₃, when dilution-corrected with ΔCO, show a similar
 767 trend as OOA (Figure 7i). From the lowest observed photochemical age (~0.1 equivalent day) to
 768 the highest (~0.85 equivalent day), O_x, CH₂O, PAN, ΣROONO₂, and pNO₃ increase by factors of
 769 4, 2, 7, 4, and 2, respectively. Over Mexico City, increases of factors of ~2 (CH₂O) (Fried et al.,

2011) and ~ 3 (ΣROONO_2) (Perring et al., 2010) were observed, which are comparable to the Seoul observations. These rapid increases can only be explained by photooxidation of South Korean primary emissions (hydrocarbons and NO_x).

The influence of the upwind, background air masses over the West Sea are investigated and shown in Figure 7g and h. Over the West Sea, the dilution-corrected concentration of SOA, O_x , CH_2O , PAN, ΣROONO_2 , and pNO_3 were all nearly constant. This indicates that the secondary short-lived gas-phase species have reached steady state. Also, since dilution-corrected SOA concentration is flat, this suggests that the SOA precursors have been depleted, and the SOA production has ended, with SOA concentration reaching the plateau that is typically observed after ~ 1 equivalent day (Ortega et al., 2016). The low PAN concentration and influence from transport over the West Sea was also observed by Lee et al. (2012) over Baengyeoung Island, a regional background monitoring location for Seoul and South Korea, during August 2010 and March – April 2011. This further indicates low amounts of PAN are transported due to its thermal decomposition and very short lifetime, and any production, and correlation, of PAN with OOA would suggest local, photochemical production.

Besides the ubiquitous (but less specific) secondary species from organic compound oxidation, OOA shows a robust correlation with dihydroxy toluene (DHT) (Figure 8), a known SOA precursor from toluene photooxidation (Schwantes et al., 2017). DHT is very short lived, with a photochemical lifetime of less than 1 hour, and it is formed under both low and high NO conditions (Schwantes et al., 2017). The lower correlation, compared to the ubiquitous secondary species, is possibly due to DHT forming from one precursor (toluene) instead of the broad range of precursors that form OOA and O_x , PAN, and CH_2O . The correlation of OOA with a known SOA precursor, that is very short-lived, again supports that OOA production is dominated by

793 photooxidation of locally emitted hydrocarbons, including toluene. The increasing ratio of OOA
 794 to DHT also suggests that SOA production is fastest at low equivalent ages and is starting to
 795 plateau at higher ages.

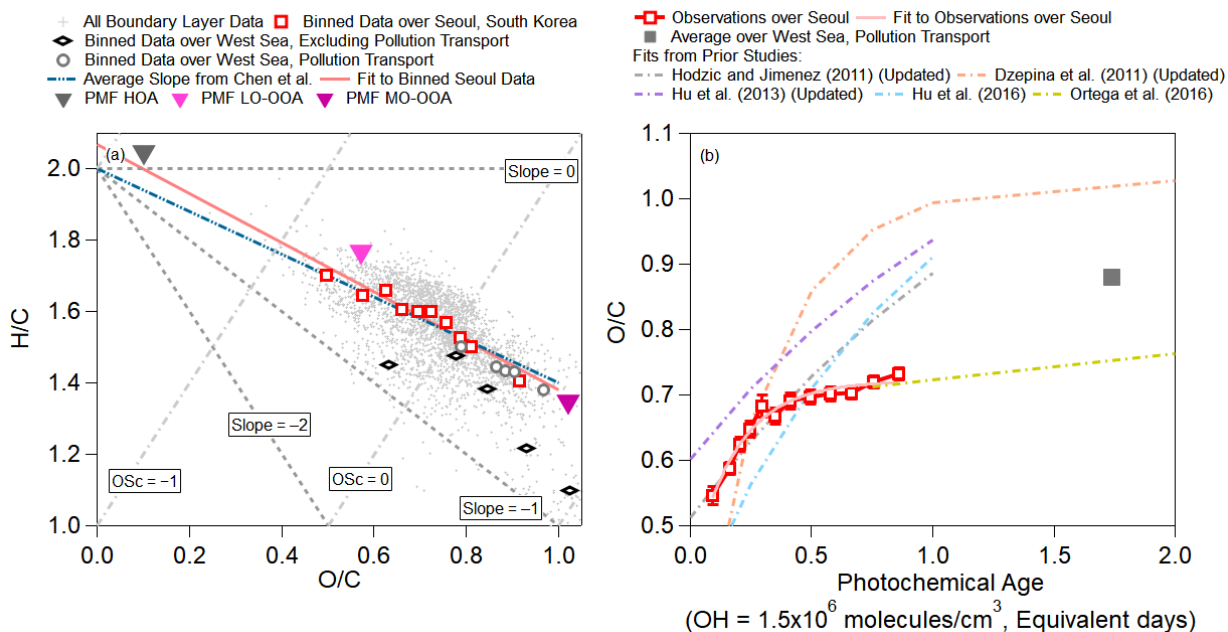


796
 797 **Figure 8.** (a) Scatter plot of OOA versus DHT over Seoul, South Korea, during KORUS-AQ, after
 798 12:00 local time (03:00 UTC). (b) Same as Figure 7f, but for DHT over the West Sea (RF12). (c)
 799 Same as Figure 7g, but for DHT over the West Sea. (d) Same as Figure 7i, but for DHT over Seoul.
 800 As an important note, concentrations of DHT are based on a preliminary calibration; however, any
 801 further calibrations are not expected to impact the relative trend and general correlation.

802 The correlation between OOA and secondary species that have very short lifetimes further
 803 suggest that the observed OOA is dominantly due to photooxidation of local emissions to produce
 804 SOA and the other secondary species and not transport. This is due to the fact that the short
 805 photochemical lifetimes of PAN, CH_2O , DHT, and ΣROONO_2 would cause the secondary species
 806 to be in steady state. The observations over the West Sea, which is mainly upwind of Seoul and
 807 thus background air, show much lower ratios. These two observations further suggest that local
 808 SMA emissions are the precursors that undergo the rapid photooxidation to produce SOA, pNO_3 ,
 809 and the other secondary species.

810 4.2.3 Oxidation state of SOA

811 We investigate the oxidation state of the observed OA with the van Krevelen diagram
 812 (Heald et al., 2010) in Figure 9a. The slope over Seoul (-0.69) is close to the average slope for
 813 numerous studies summarized by Chen et al. (2015) (-0.60) and similar to the range of slopes
 814 (-0.7 to -1.0) for studies impacted by urban pollution (Aiken et al., 2009; Docherty et al., 2011;
 815 Ge et al., 2012), including Los Angeles during CalNex (ranges from -0.64 to -0.68 from Hayes
 816 et al. (2013) and Ortega et al. (2016)) or chamber studies investigating the photooxidation of
 817 combustion exhausts (Heald et al., 2010; Lambe et al., 2012; Jathar et al., 2013; Presto et al., 2014;
 818 Tkacik et al., 2014; Liu et al., 2015). This generally indicates that the photochemistry controlling
 819 the production of SOA is similar in urban areas, including photooxidation of diesel and gasoline
 820 emissions, evaporative diesel and gasoline, and cooking emissions (Hayes et al., 2015; Woody et
 821 al., 2016; Janssen et al., 2017; Ma et al., 2017; Kim et al., 2018).



822
 823 **Figure 9.** (a) Van Krevelen diagram for all of KORUS-AQ. $OSc = (O/C - 2 \times H/C)$ (Kroll et al.,
 824 2011). The observations are binned, into deciles, for observations over Seoul, South Korea, and
 825 binned, into 5 bins, for clean West Sea, and polluted West Sea. The teal line represents the average
 826 slope reported in Chen et al. (2015) of -0.60 , and the light red line represents the slope (slope =

827 $-0.69(\pm 0.15)$, y-intercept= $2.07(\pm 0.11)$) observed over Seoul, South Korea, during the campaign.
828 (b) Binned O/C from observations versus photochemical age, over Seoul, South Korea, and
829 averaged O/C versus photochemical clock over polluted West Sea. The light red line is the fit to
830 the observations over Seoul during KORUS-AQ. The values of O/C versus photochemical age
831 from Hodzic and Jimenez (2011), Dzepina et al. (2011), Hu et al. (2013), are updated with
832 calibrations of Canagaratna et al. (2015); whereas, Hu et al. (2016), and Ortega et al. (2016) did
833 not need updates.

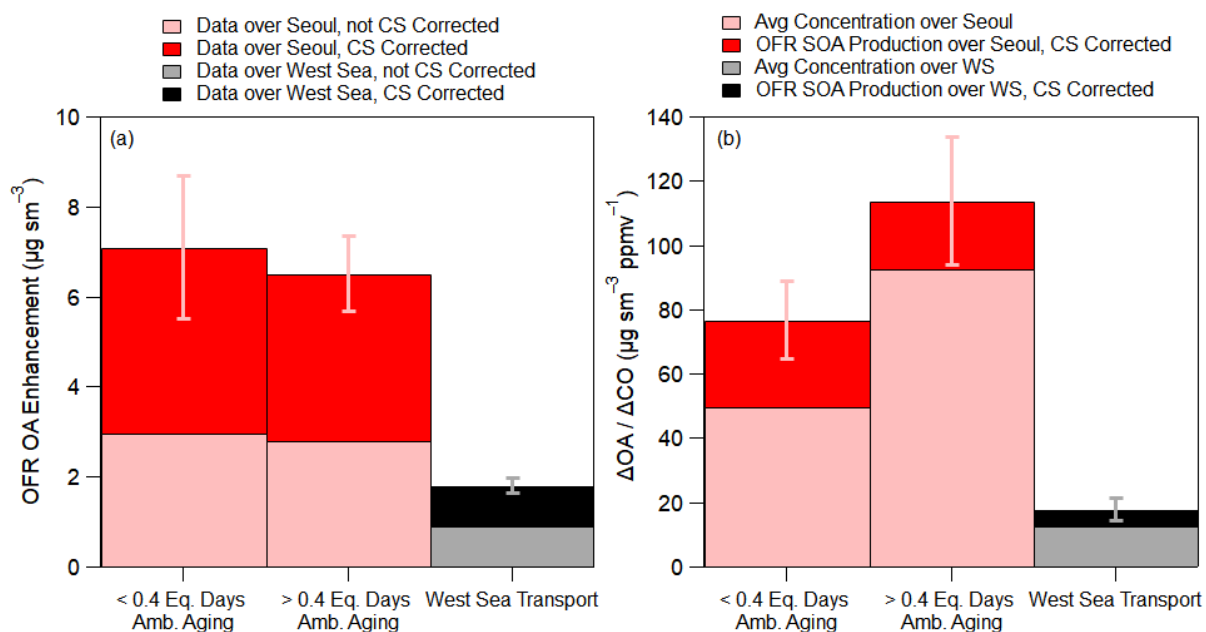
834 The “transport/polluted” evolution of H/C versus O/C falls on the same slope as the
835 observations over Seoul; however, the values lie at higher O/C ratios, indicative of more aged
836 OOA. O/C versus H/C during the “transported/polluted” event over the West Sea is also
837 comparable to the H/C versus O/C slope (-0.63) observed in Chinese outflow at Changdao (Hu et
838 al., 2013). On the other hand, O/C versus H/C over the West Sea during “clean” events show
839 distinctly lower values and a steeper evolution (slope = -1.1).

840 The evolution of O/C with photochemical age over Seoul and over the West Sea is shown
841 in Figure 9b, along with results from prior studies (Dzepina et al., 2011; Hodzic and Jimenez,
842 2011; Hu et al., 2013, 2016; Ortega et al., 2016). Note that older studies have been updated with
843 the calibration of Canagaratna et al. (2015). For the first 0.5 equivalent days, O/C is nearly identical
844 to the Mexico City observations (Hodzic and Jimenez, 2011); however, after 0.5 equivalent days,
845 the O/C ratio growth slows down. The O/C evolution then becomes more similar to that observed
846 when processing Los Angeles air in an OFR (Ortega et al., 2016). The evolution of O/C over Seoul
847 is at the low end of the range of values observed from prior megacities. The average O/C value
848 observed over the West Sea during RF12 is more similar to the values observed after 1 equivalent
849 day in two sites in China (Hu et al., 2013, 2016).

850 **4.4 Influence of local versus transported SOA precursors to SOA production over Seoul**

851 OFR results can be used to investigate the role of SOA production from South Korean and
852 Seoul emissions versus long-distance transported SOA precursors. As shown in prior studies
853 (Ortega et al., 2016; Palm et al., 2016, 2017, 2018), the SOA potential decreases drastically in the

854 daytime, as the most reactive compounds to OH have already oxidized and formed SOA. Thus,
 855 these results will not directly capture the full emitted SOA potential for Seoul, South Korea. Also,
 856 recent studies indicate that lower volatility species (e.g., S/IVOCs) can be lost to tubing walls, or
 857 their transfer can be greatly delayed (Pagonis et al., 2017; Deming et al., 2018). Thus, it is likely
 858 that the OFR inlet line on the DC-8 acted at least as a partial sink of S/IVOCs and thus reduced
 859 the measured potential SOA. As a reminder, a correction is included for the condensational sink
 860 (CS) of LVOC in the OFR based on Eq. (1).



861
 862 **Figure 10.** (a) Comparison of OFR OA enhancement (OFR OA enhancement = OA exiting OFR
 863 – ambient OA) over Seoul, South Korea, and the West Sea, corrected for evaporation losses. The
 864 difference between the two stacked shaded bars is that the lighter (bottom) shade has no CS
 865 correction whereas the darker shade does. (b) The lighter color represents the average dilution-
 866 corrected observed ambient OA preexisting concentration corresponding to the OFR observations
 867 of the same air mass. The darker color represents the dilution-corrected SOA production in the
 868 OFR. The average additional photochemical age added in the OFR is ~ 4 days ($\text{OH}_{\text{exp}} \sim 5.4 \times 10^{11}$
 869 molecules/ $\text{cm}^3 \times \text{s}$) for both over Seoul and West Sea. Also, the observations for the West Sea are
 870 for all flights, not including RF12, where the average $\Delta\text{OA}/\Delta\text{CO}$ was $13 \mu\text{g sm}^{-3} \text{ppmv}^{-1}$. For both
 871 (a) and (b), the OFR observations over Seoul are split between lower and higher equivalent ages
 872 (see x-axis). The average ambient ages for the two bars are 0.17 and 0.63 equivalent days. Error
 873 bars are the standard errors of the observations.

874 The average OA enhancement in the OFR (OA Enhancement = OA in OFR – Ambient
875 OA) in Seoul is slightly greater for the less aged ambient air (7.1 ± 1.6 versus $6.5 \pm 0.8 \mu\text{g sm}^{-3}$) but
876 both values lie within the range of the measurements (Figure 10a). The less aged ambient air show
877 slightly higher OA enhancement suggests that more SOA precursors might have been present and
878 available to form SOA mass (Ortega et al., 2016; Palm et al., 2016, 2017, 2018). The OA
879 enhancement observed over Seoul was a factor of 3.5 greater than observed over the West Sea (~ 7
880 $\mu\text{g sm}^{-3}$ over Seoul versus $\sim 2 \mu\text{g sm}^{-3}$ over the West Sea). The much higher SOA formation
881 potential observed over Seoul versus the West Sea indicates that the majority of the precursors that
882 led to the observed SOA and SOA production over Seoul originated from local emissions,
883 consistent with results above.

884 Plotting the OA enhancements as $\Delta\text{OA}/\Delta\text{CO}$, similar to Figure 4, the amount of ambient
885 SOA production, not including pre-existing OA, for ambient air that has aged less than 0.4
886 equivalent days is $27(\pm 12) \mu\text{g sm}^{-3} \text{ppmv}^{-1}$, a 50% increase compared to the average $\Delta\text{OA}/\Delta\text{CO}$
887 observed over Seoul at the same ambient photochemical age (Figure 10b). For air older than 0.4
888 equivalent days, the increase is slightly smaller ($21(\pm 20) \mu\text{g sm}^{-3} \text{ppmv}^{-1}$ above ambient pre-
889 existing OA) since a large fraction of the most reactive, high aerosol producing compounds have
890 already been depleted and produced ambient SOA (Ortega et al., 2016; Palm et al., 2016, 2017,
891 2018).

892 Finally, there is still a small amount of SOA production potential in the air transported over
893 the West Sea to Seoul. The average potential, not including pre-existing OA, is $5(\pm 4) \mu\text{g sm}^{-3}$
894 ppmv^{-1} . This is a factor of 4 – 5 less than the potential SOA production observed in the OFR for
895 Seoul. Including the pre-existing dilution-corrected OA for the West Sea observation ($18 \mu\text{g sm}^{-3}$
896 ppmv^{-1}), the concentration is approximately a factor of 8.5 less than the maximum ambient

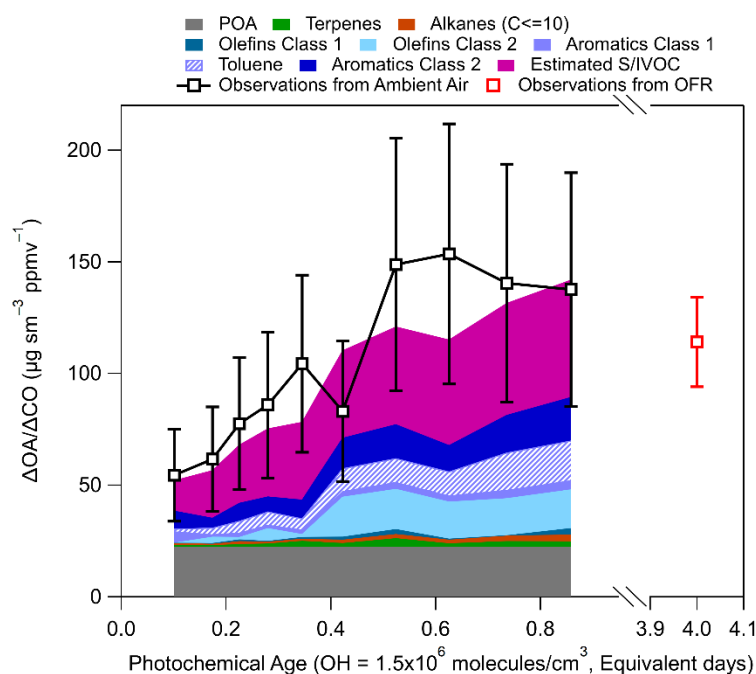
897 dilution-corrected OA concentration and a factor of 6 – 8 less than the total dilution corrected OA
898 concentration exiting the OFR. Some of this remaining production would have been further
899 consumed during transport between the West Sea and Seoul (typically 1 day); therefore, it is not
900 expected to significantly impact the SOA production over Seoul. This further indicates that, during
901 this campaign, the transported SOA precursors to Seoul from foreign sources did not contribute
902 significantly to the overall observed SOA production.

903 **4.5 Calculated precursor contributions to the SOA production over Seoul**

904 We use a simple SOA model (Dzepina et al., 2009; Zhao et al., 2014) to calculate the
905 contribution of various precursors to SOA over Seoul (Figure 11, details in Sect. SI 6). Observed
906 hydrocarbons (Table 2), from WAS, along with estimated S/IVOC (Robinson et al., 2007; Dzepina
907 et al., 2009; Hayes et al., 2015) and SOA yields updated to account for vapor wall losses (Ma et
908 al., 2017) were used to estimate (SI Eq. (S3) and (S4)) the contribution of various precursors to
909 SOA production observed over Seoul. Dzepina et al. (2009) and Hayes et al. (2015) both found
910 that the “Robinson” parameterization of SOA from S/IVOC was consistent with SOA production
911 in Mexico City and Los Angeles for observations at 1 equivalent day or less; thus, the same
912 parameterizations are used here.

913 The percent difference between the modeled and measured total OA ranged between –24
914 to 34% with an average value of the observations being 11% higher. This provides confidence that
915 the calculation described in SI 6 captures the chemical production of SOA over Seoul. Also, the
916 difference between the estimated and measured OA is comparable to, or better than, found in other
917 studies that utilized a similar modeling approaches (Dzepina et al., 2009; Zhao et al., 2014, 2016;
918 Hayes et al., 2015; Huang et al., 2015; Ma et al., 2017), and within the uncertainty of the measured
919 OA (38%, 2σ).

920 This box model does not explicitly consider volatile consumer products (VCPs) (Khare
 921 and Gentner, 2018; McDonald et al., 2018), S/IVOC from cooking emissions (e.g., Hayes et al.,
 922 2013; Ots et al., 2016), or glyoxal (Volkamer et al., 2006; Knote et al., 2014), although
 923 contributions from these components may be partially included in the empirical estimation of
 924 S/IVOC. Modeled SOA in Los Angeles, using estimates of S/IVOC from $\Delta\text{HOA}/\Delta\text{CO}$, including
 925 $\sim 2/3$ of VCPs and not including glyoxal, were able to capture the observed SOA in the first 0.5
 926 equivalent days (Hayes et al., 2015; McDonald et al., 2018), similar to the results here.



927
 928 **Figure 11.** Calculated SOA production for KORUS-AQ. POA is from observations shown in
 929 Figure 6, and the observations of $\Delta\text{OA}/\Delta\text{CO}$ are from Figure 4. The SOA precursor classes are
 930 defined in Table 2. Note, Toluene is part of Aromatics Class 1 (light purple), but it is shown
 931 separately for discussion. The error bars represent the uncertainty in OA ($\pm 38\%$). The OFR
 932 observations, and error bars, are from Figure 10.

933 **Table 2.** Definition of classes used in Figure 11. The VOCs listed in the table were all measured
 934 by WAS.

<i>Class</i>	<i>Included Compounds or Parameterization</i>
Terpenes	alpha-pinene, beta-pinene
Alkanes (C \leq 10)	methyl-cyclopentane, cyclohexane, methyl-cyclohexane, n-hetpane, n-octane, n-nonane, n-decane,
Olefins Class 1	1-butene, i-butene, cis-butene, trans-butene
Olefins Class 2	Styrene, 1,3-butadiene
Aromatics Class 1	benzene, toluene, isopropylbenzene, n-propylbenzene, ethylbenzene,
Aromatics Class 2	m+p-xylene, o-xylene, 3-ethyltoluene, 4-ethyltoluene, 1,2,3-trimethylbenzene, 1,2,4-trimethylbenzene, 1,3,5-trimethylbenzene
Estimated S/IVOC	$6.7^a \times \Delta\text{HOA}/\Delta\text{CO}$ ($\Delta\text{HOA}/\Delta\text{CO} = 22 \mu\text{g sm}^{-3} \text{ppmv}^{-1}$ from Figure 6)

935 ^aThis value is taken from Dzepina et al. (2009), which is based on partitioning calculations.

936 The most important calculated SOA precursors are S/IVOC and the most reactive
 937 aromatics (Table 2). These two classes of compounds comprise ~70% of the total modeled SOA
 938 over Seoul. The calculation further supports the conclusions from multiple previous studies
 939 (Dzepina et al., 2009, 2011; Hodzic et al., 2010; Chen et al., 2015; Hayes et al., 2015; Ma et al.,
 940 2017) that aromatics and primary S/IVOC dominate SOA formation over different urban
 941 environments. A consistent feature across most species in both classes of compounds is that they
 942 all have photochemical lifetimes of less than 1 equivalent day and less than 4 actual hours for the
 943 average observed daytime OH (6×10^6 molecules/cm³) over Seoul. With the typical wind speeds
 944 during KORUS-AQ (~4 m/s), the lifetime of these species would limit their transport
 945 approximately 60 km during daytime. Since these compounds have short photochemical lifetimes,
 946 and they compose the majority of the calculated SOA budget, our conclusion that the SOA
 947 production over Seoul originates from local emissions is further supported.

948 Numerous prior studies have shown the importance of S/IVOC in order to explain the
 949 observed SOA production (Robinson et al., 2007; Dzepina et al., 2009, 2011; Grieshop et al., 2009;
 950 Pye and Seinfeld, 2010; Hodzic et al., 2010; Zhao et al., 2014; Jathar et al., 2014; Chen et al.,
 951 2015; Hayes et al., 2015; Palm et al., 2016, 2017, 2018; Ortega et al., 2016; Janssen et al., 2017;

952 Ma et al., 2017). Until recently, it has been analytically challenging to measure these compounds
953 (Ait-Helal et al., 2014; Zhao et al., 2014; Hunter et al., 2017), and they can make up a small fraction
954 of the total measured, and speciated, hydrocarbons in an urban location (Ait-Helal et al., 2014;
955 Zhao et al., 2014). However, due to the higher initial molecular weight, S/IVOC already have a
956 low saturation concentration ($C^* \sim 1 - 1000 \mu\text{g m}^{-3}$ for SVOC and $\sim 1 \times 10^4 - 1 \times 10^6 \mu\text{g m}^{-3}$ for
957 IVOC), especially compared to aromatic compounds ($C^* \sim 10^7 \mu\text{g m}^{-3}$); thus, any addition of
958 functional groups will more easily lead to the partitioning of oxidized S/IVOC to the particle phase
959 (Robinson et al., 2007; Hayes et al., 2015; Ma et al., 2017). In urban environments, S/IVOC
960 emissions come from numerous sources, including transportation, cooking, and VCPs (Robinson
961 et al., 2007; Hayes et al., 2015; Woody et al., 2016; Janssen et al., 2017; Ma et al., 2017; McDonald
962 et al., 2018).

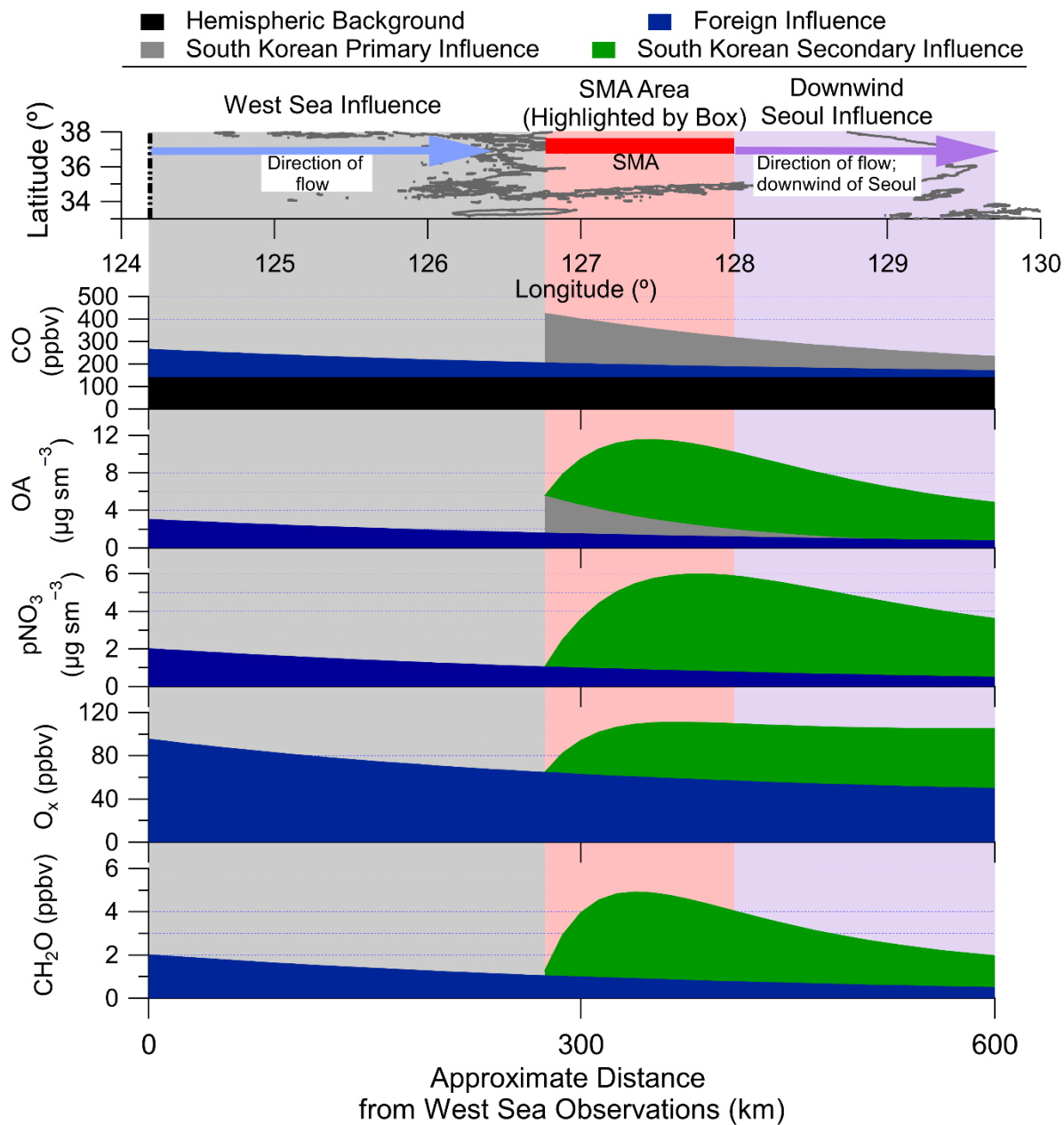
963 The next most important compound is toluene, composing $9(\pm 3)\%$ of the estimated SOA
964 production. Though this single compound is as important as the rest of Aromatics Class 1, Olefins
965 Class 1 and 2, alkanes, and terpenes (Table 2) combined, it does not contribute the majority of the
966 calculated SOA budget, as was recently suggested in another study (Wu et al., 2016). The average
967 aerosol yield for toluene used in this study ($Y \approx 0.30$) is similar to the value used in Wu et al.
968 (2016) and recommended by Hildebrandt et al. (2015). The aerosol yield is similar for all
969 aromatics; however, the more reactive aromatics will contribute more SOA per unit precursor at
970 shorter photochemical ages. The longer photochemical lifetime (factor of 2) for toluene decreases
971 the overall amount of SOA produced compared to the very reactive aromatics.

972 **4.6 Conceptual model representing rapid photochemical production**

973 A conceptual model representing rapid photochemical production of SOA, pNO_3 , O_x , and
974 CH_2O is presented here. For the model, the flow is simplified to be from the west to the east. The

975 lateral and vertical dilution have been represented as the equivalent first order rate, constrained by
976 observations ($\sim 0.7 \text{ day}^{-1}$). Also, the hemispheric and foreign transport is accurate on average based
977 on observations, and is discussed in Sect. 3.3. For the production over Seoul, it is represented by
978 photochemical aging, constrained by observations (Figure 7i), as a first order rate. Thus, the
979 important processes are represented with realistic quantitative constraints, but in a simple enough
980 system to demonstrate the impact of the secondary chemistry from Seoul.

981 The results are shown in Figure 12. The figure summarizes and demonstrates the results
982 discussed throughout the paper. First, as discussed in Sect. 3.2 and 4.2, there is no clear net
983 production of the pollutants over the West Sea. Instead, they undergo dilution as the air travels
984 across the West Sea. Then, as the air enters SMA area, there are fresh injections of primary
985 emissions (CO, HOA, hydrocarbons, and NO_x). These primary emissions undergo rapid
986 photooxidation to produce SOA, pNO_3 , O_x , and CH_2O , as detailed in Sect. 4.2. As demonstrated
987 in Figure 12, most of the production occurs with SMA prior to dilution taking over. This
988 demonstrates that the emissions and subsequent chemistry from SMA are directly impacting the
989 residents of SMA. Thus, control of the primary pollutants, including the SOA precursors discussed
990 in Sect. 4.5 (aromatics and S/IVOC), and NO_x , would substantially reduce concentration of the
991 secondary photochemical products impacting SMA, even during period of higher foreign transport
992 than observed during KORUS-AQ.



993

994 **Figure 12.** Conceptual model representing the transport of background into Seoul, and the
 995 emissions of primary species (CO and HOA) and photochemical production of secondary species
 996 (SOA, pNO₃, O_x, and CH₂O) impacting Seoul.

997 **5. Summary**

998 A suite of aerosol- and gas-phase measurements were made over Seoul and the West Sea
999 during May and June, 2016, as part of the KORUS-AQ campaign. The results from this study are
1000 summarized below.

1001 (1) Using a combination of a Lagrangian backtrajectory model (FLEXPART) and
1002 observations, the hemispheric CO background was estimated to be 140 ppbv, the CO foreign
1003 background over Seoul was estimated to be 60 ppbv, and the remainder of the CO over Seoul was
1004 due to South Korean emissions. The CO background analysis allows estimating background values
1005 for other species used throughout this study. In particular, the OA background was estimated to be
1006 between 1 – 3 $\mu\text{g sm}^{-3}$.

1007 (2) FLEXPART was also used for source analysis of NO_2 , as a surrogate for SOA
1008 precursors. NO_2 has a photochemical lifetime of less than 1 day (similar to the dominant urban
1009 SOA precursors). Results from FLEXPART indicate that greater than 90% of NO_2 originates from
1010 South Korea, consistent with most of the important SOA and pNO_3 precursors also originating
1011 there.

1012 (3) Factor analysis of OA showed that the OA growth over Seoul was dominated by OOA
1013 (surrogate for SOA). This OOA (background subtracted) was low at low photochemical ages and
1014 rapidly increased throughout the day as photochemistry occurred. This points to local emissions
1015 controlling SOA production over Seoul.

1016 (4) OOA was correlated with secondary gas-phase species, including O_x ($\text{O}_3 + \text{NO}_2$),
1017 formaldehyde, peroxy acetyl nitrates, sum of acyl peroxy nitrates, dihydroxy toluene, and pNO_3 .
1018 Correlation with these species indicates that the SOA was produced from local emissions and

1019 photochemistry since some of these compounds (CH_2O and PAN) had photochemical lifetimes of
1020 less than three daytime hours during KORUS-AQ.

1021 (5) Using an airborne OFR for the first time, the amount of potential SOA produced from
1022 air sampled over Seoul was a factor of three higher than for air sampled over the West Sea (a
1023 background inflow location). This points to local SOA precursor emissions from Seoul, and
1024 subsequent rapid photochemistry, causing the increase in SOA observed over Seoul. The air
1025 sampled over West Sea did not have enough SOA precursors to cause the SOA production
1026 observed over Seoul.

1027 (6) A simple box model showed good agreement with the measured SOA growth. This
1028 allows an estimation of the contribution of various precursors to SOA over Seoul. Hydrocarbons
1029 with a photochemical lifetime of less than one day dominate the production of SOA. Specifically,
1030 short lived aromatic compounds (i.e., ethyltoluenes, xylenes, trimethylbenzenes) and S/IVOC are
1031 the main precursors to SOA, accounting for 70% of the calculated SOA. Toluene was found to
1032 contribute 9% of the calculated SOA.

1033 (7) Over Seoul, a large megacity with numerous sources of emissions, local emissions and
1034 their photochemical products overwhelm the foreign influence during KORUS-AQ. However, for
1035 smaller cities or more rural areas in South Korea that are not downwind of Seoul or other large
1036 sources, the foreign influence can more easily overwhelm the smaller local emissions. Thus,
1037 outside of the Seoul Metropolitan Area, the foreign influence has a greater impact on the air
1038 quality. During periods in which the foreign influence is larger than during KORUS-AQ (due to
1039 more favorable transport conditions), it will be more comparable to the importance of the Seoul
1040 emissions. However, given the apparently stronger emissions of SOA precursors than in other
1041 megacities, reducing South Korean emissions should improve air quality under all conditions.

1042 **Author Contribution**

1043 BAN, PCJ, DAD, JCS, and JLJ collected the AMS data; BA, AJB, CAC, and KLT collected the
1044 data from LARGE; DRB collected the WAS data; WHB collected the OH, HO₂, and OHR
1045 data; YC and JPD collected the CO measurements from Picarro; JD and ES collected
1046 MC/IC and filter measurements; GD and SEP collected H₂O and ambient CO
1047 measurements; AF collected CH₂O measurements; LGH collected PAN, PPN, and SO₂
1048 measurements; MJK collected HNO₃, DHT, and HCN measurements; CK ran the
1049 FLEXPART analysis; KDL collected the BC measurements; TL and TP collected the
1050 KAMS data; and, JHW provided the emissions for the FLEXPART analysis. JAdG assisted
1051 in the analysis of the photochemical clocks and SOA production. BAN and JLJ prepared
1052 the original manuscript, and all authors contributed to the review and editing of the
1053 manuscript.

1054
1055 **Acknowledgements**

1056 This study was supported by NASA grants NNX15AT96G & 80NSSC18K0630, and EPA STAR
1057 83587701-0. It has not been formally reviewed by EPA. The views expressed in this
1058 document are solely those of the authors and do not necessarily reflect those of EPA. EPA
1059 does not endorse any products or commercial services mentioned in this publication. MJK
1060 was funded by NSF award number 1524860. Joost de Gouw worked as a part-time
1061 consultant for Aerodyne Research Inc during the preparation phase of this manuscript. The
1062 authors acknowledge Joshua Schwarz and Anne Perring for the use of their black carbon
1063 data, Ronald Cohen, Paul Wooldridge, and Paul Romer for use of their ΣRONO₂ and
1064 ΣROONO₂ data, Paul Wennberg and John Crouse for the use of their HCN, DHT, and
1065 HNO₃ data, Armin Wisthaler for the use of their PTR-MS data, and Andrew Weinheimer
1066 and Denise Montzka for the use of their O₃, NO_x, and NO_y data. Finally, the authors
1067 acknowledge the NOAA ESRL GMD CCGG for the use of the CO measurements in
1068 Mongolia and China for the background measurements.

1069
1070 **Data Availability**

1071 Measurements and FLEXPART results from the KORUS-AQ campaign are available at
1072 <https://www-air.larc.nasa.gov/cgi-bin/ArcView/korusaq>. Measurements for the CO
1073 background are available at ftp://aftp.cmdl.noaa.gov/data/trace_gases/co/flask/surface/.

1074
1075 **Competing Interests**

1076 The authors declare that they have no conflict of interest.

1 **References**

- 2 Aiken, A. C., Salcedo, D., Cubison, M. J., Huffman, J. A., DeCarlo, P. F., Ulbrich, I. M., Docherty,
3 K. S., Sueper, D., Kimmel, J. R., Worsnop, D. R., Trimborn, A., Northway, M., Stone, E. A.,
4 Schauer, J. J., Volkamer, R. M., Fortner, E., de Foy, B., Wang, J., Laskin, A., Shutthanandan, V.,
5 Zheng, J., Zhang, R., Gaffney, J., Marley, N. A., Paredes-Miranda, G., Arnott, W. P., Molina, L.
6 T., Sosa, G. and Jimenez, J. L.: Mexico City aerosol analysis during MILAGRO using high
7 resolution aerosol mass spectrometry at the urban supersite (T0) – Part 1: Fine particle composition
8 and organic source apportionment, *Atmos. Chem. Phys.*, 9(9), 6633–6653, doi:10.5194/acpd-9-
9 8377-2009, 2009.
- 10 Ait-Helal, W., Borbon, A., Sauvage, S., De Gouw, J. A., Colomb, A., Gros, V., Freutel, F., Crippa,
11 M., Afif, C., Baltensperger, U., Beekmann, M., Doussin, J.-F. F., Durand-Jolibois, R., Fronval, I.,
12 Grand, N., Leonardis, T., Lopez, M., Michoud, V., Miet, K., Perrier, S., Prévôt, A. S. H.,
13 Schneider, J., Siour, G., Zapf, P. and Locoge, N.: Volatile and intermediate volatility organic
14 compounds in suburban Paris: Variability, origin and importance for SOA formation, *Atmos.*
15 *Chem. Phys.*, 14(19), 10439–10464, doi:10.5194/acp-14-10439-2014, 2014.
- 16 Akagi, S. K., Craven, J. S., Taylor, J. W., Mcmeeking, G. R., Yokelson, R. J., Burling, I. R.,
17 Urbanski, S. P., Wold, C. E., Seinfeld, J. H., Coe, H., Alvarado, M. J. and Weise, D. R.: Evolution
18 of trace gases and particles emitted by a chaparral fire in California, *Atmos. Chem. Phys.*, 12,
19 1397–1421, doi:10.5194/acp-12-1397-2012, 2012.
- 20 Aknan, A. and Chen, G.: KORUS-AQ DC-8 Aircraft Dataset, [online] Available from:
21 <https://www-air.larc.nasa.gov/cgi-bin/ArcView/korusaq> (Accessed 6 December 2018), 2018.
- 22 Al-Saadi, J., Carmichael, G., Crawford, J., Emmons, L., Korean, S. K., Group, S., Song, C.-K.,
23 Chang, L.-S., Lee, G., Kim, J. and Park, R.: NASA Contributions to KORUS-AQ: An International
24 Cooperative Air Quality Field Study in Korea, 2015.
- 25 Anderson, T. L. and Ogren, J. A.: Determining Aerosol Radiative Properties Using the TSI 3563
26 Integrating Nephelometer, *Aerosol Sci. Technol.*, 29(1), 57–69,
27 doi:10.1080/02786829808965551, 1998.
- 28 Arnold, S. R., Methven, J., Evans, M. J., Chipperfield, M. P., Lewis, A. C., Hopkins, J. R.,
29 Mcquaid, J. B., Watson, N., Purvis, R. M., Lee, J. D., Atlas, E. L., Blake, D. R. and Rappenglück,
30 B.: Statistical inference of OH concentrations and air mass dilution rates from successive
31 observations of nonmethane hydrocarbons in single air masses, *J. Geophys. Res. Atmos.*, 112,
32 D10S40, doi:10.1029/2006JD007594, 2007.
- 33 Bahreini, R., Dunlea, E. J., Matthew, B. M., Simons, C., Docherty, K. S., DeCarlo, P. F., Jimenez,
34 J. L., Brock, C. A. and Middlebrook, A. M.: Design and Operation of a Pressure-Controlled Inlet
35 for Airborne Sampling with an Aerodynamic Aerosol Lens, *Aerosol Sci. Technol.*, 42(6), 465–
36 471, doi:10.1080/02786820802178514, 2008.
- 37 Bahreini, R., Ervens, B., Middlebrook, A. M., Warneke, C., de Gouw, J. A., DeCarlo, P. F.,
38 Jimenez, J. L., Brock, C. A., Neuman, J. A., Ryerson, T. B., Stark, H., Atlas, E., Brioude, J., Fried,
39 A., Holloway, J. S., Peischl, J., Richter, D., Walega, J., Weibring, P., Wollny, A. G. and
40 Fehsenfeld, F. C.: Organic aerosol formation in urban and industrial plumes near Houston and
41 Dallas, Texas, *J. Geophys. Res.*, 114(16), D00F16, doi:10.1029/2008JD011493, 2009.
- 42 Baklanov, A., Molina, L. T. and Gauss, M.: Megacities, Air Quality and Climate, *Atmos. Environ.*,
43 126, 235–249, doi:10.1016/j.atmosenv.2015.11.059, 2016.

- 1 Blake, N. J., Blake, D. R., Sive, B. C., Katzenstein, A. S., Meinardi, S., Wingenter, O. W., Atlas,
2 E. L., Flocke, F., Ridley, B. A. and Rowland, F. S.: The seasonal evolution of NMHC's and light
3 alkyl nitrates at middle to northern latitudes during TOPSE, *J. Geophys. Res.*, 108(D4), 8359,
4 2003.
- 5 Campuzano-Jost, P., Day, D. A., Nault, B. A., Schroder, J. C. and Jimenez, J. L.: Temporal
6 Variability of the Pieber Effect and Some Notes on AMS Detection Limits, in 17th AMS Users'
7 Meeting, Portland. [online] Available from: [http://cires1.colorado.edu/jimenez-](http://cires1.colorado.edu/jimenez-group/UsrMtg/UsersMtg17/10-14-2016_PCJ_AMSUsersMtg_Prez.pdf)
8 [group/UsrMtg/UsersMtg17/10-14-2016_PCJ_AMSUsersMtg_Prez.pdf](http://cires1.colorado.edu/jimenez-group/UsrMtg/UsersMtg17/10-14-2016_PCJ_AMSUsersMtg_Prez.pdf) (Accessed 5 April 2018),
9 2016.
- 10 Canagaratna, M. R., Jayne, J. T., Jimenez, J. L., Allan, J. D., Alfarra, M. R., Zhang, Q., Onasch,
11 T. B., Drewnick, F., Coe, H., Middlebrook, A. M., Delia, A., Williams, L. R., Trimborn, A. M.,
12 Northway, M. J., DeCarlo, P. F., Kolb, C. E., Davidovits, P. and Worsnop, D. R.: Chemical and
13 microphysical characterization of ambient aerosols with the Aerodyne Aerosol Mass
14 Spectrometer, *Mass Spectrom. Rev.*, 26(2), 185–222, doi:10.1002/mas, 2007.
- 15 Canagaratna, M. R., Jimenez, J. L., Kroll, J. H., Chen, Q., Kessler, S. H., Massoli, P., Hildebrandt
16 Ruiz, L., Fortner, E., Williams, L. R., Wilson, K. R., Surratt, J. D., Donahue, N. M., Jayne, J. T.
17 and Worsnop, D. R.: Elemental ratio measurements of organic compounds using aerosol mass
18 spectrometry: characterization, improved calibration, and implications, *Atmos. Chem. Phys.*,
19 15(1), 253–272, doi:10.5194/acp-15-253-2015, 2015.
- 20 Cappa, C. D. and Jimenez, J. L.: Quantitative estimates of the volatility of ambient organic aerosol,
21 *Atmos. Chem. Phys.*, 10(12), 5409–5424, doi:10.5194/acp-10-5409-2010, 2010.
- 22 Cappa, C. D., Jathar, S. H., Kleeman, M. J., Docherty, K. S., Jimenez, J. L., Seinfeld, J. H. and
23 Wexler, A. S.: Simulating secondary organic aerosol in a regional air quality model using the
24 statistical oxidation model – Part 2: Assessing the influence of vapor wall losses, *Atmos. Chem.*
25 *Phys.*, 16(5), 3041–3059, doi:10.5194/acp-16-3041-2016, 2016.
- 26 Chen, Q., Heald, C. L., Jimenez, J. L., Canagaratna, M. R., He, L., Huang, X.-F., Campuzano-Jost,
27 P., Palm, B. B., Poulain, L., Kuwata, M., Martin, S. T., Abbatt, J. P. D., Lee, A. K. Y., Liggio, J.,
28 Zhang, Q., He, L. and Huang, X.-F.: Elemental composition of organic aerosol: The gap between
29 ambient and laboratory measurements, *Geophys. Res. Lett.*, 42(10), 4182–4189,
30 doi:10.1002/2015GL063693, 2015.
- 31 Choi, J. K., Heo, J. B., Ban, S. J., Yi, S. M. and Zoh, K. D.: Chemical characteristics of PM_{2.5}
32 aerosol in Incheon, Korea, *Atmos. Environ.*, 60, 583–592, doi:10.1016/j.atmosenv.2012.06.078,
33 2012.
- 34 Cohen, A. J., Brauer, M., Burnett, R., Anderson, H. R., Frostad, J., Estep, K., Balakrishnan, K.,
35 Brunekreef, B., Dandona, L., Dandona, R., Feigin, V., Freedman, G., Hubbell, B., Jobling, A.,
36 Kan, H., Knibbs, L., Liu, Y., Martin, R., Morawska, L., Pope, C. A., Shin, H., Straif, K., Shaddick,
37 G., Thomas, M., van Dingenen, R., van Donkelaar, A., Vos, T., Murray, C. J. L. and Forouzanfar,
38 M. H.: Estimates and 25-year trends of the global burden of disease attributable to ambient air
39 pollution: an analysis of data from the Global Burden of Diseases Study 2015., *Lancet* (London,
40 England), 389(10082), 1907–1918, doi:10.1016/S0140-6736(17)30505-6, 2017.
- 41 Collier, S., Zhou, S., Onasch, T. B., Jaffe, D. A., Kleinman, L., Sedlacek, A. J., Briggs, N. L., Hee,
42 J., Fortner, E., Shilling, J. E., Worsnop, D., Yokelson, R. J., Parworth, C., Ge, X., Xu, J.,
43 Butterfield, Z., Chand, D., Dubey, M. K., Pekour, M. S., Springston, S. and Zhang, Q.: Regional

1 Influence of Aerosol Emissions from Wildfires Driven by Combustion Efficiency: Insights from
2 the BBOP Campaign, *Environ. Sci. Technol.*, 50(16), 8613–8622, doi:10.1021/acs.est.6b01617,
3 2016.

4 Craven, J. S., Metcalf, A. R., Bahreini, R., Middlebrook, A., Hayes, P. L., Duong, H. T.,
5 Sorooshian, A., Jimenez, J. L., Flagan, R. C. and Seinfeld, J. H.: Los Angeles Basin airborne
6 organic aerosol characterization during CalNex, *J. Geophys. Res. Atmos.*, 118(19), 11,453–11,467,
7 doi:10.1002/jgrd.50853, 2013.

8 Crippa, M., Canonaco, F., Lanz, V. A., Äijälä, M., Allan, J. D., Carbone, S., Capes, G., Ceburnis,
9 D., Dall’Osto, M., Day, D. A., DeCarlo, P. F., Ehn, M., Eriksson, A., Freney, E., Hildebrandt Ruiz,
10 L. H., Hillamo, R., Jimenez, J. L., Junninen, H., Kiendler-Scharr, A., Kortelainen, A.-M., Kulmala,
11 M., Laaksonen, A., Mensah, A. A., Mohr, C., Nemitz, E., O’Dowd, C., Ovadnevaite, J., Pandis, S.
12 N., Petäjä, T., Poulain, L., Saarikoski, S., Sellegri, K., Swietlicki, E., Tiitta, P., Worsnop, D. R.,
13 Baltensperger, U. and Prévôt, A. S. H.: Organic aerosol components derived from 25 AMS data
14 sets across Europe using a consistent ME-2 based source apportionment approach, *Atmos. Chem.*
15 *Phys.*, 14(12), 6159–6176, doi:10.5194/acp-14-6159-2014, 2014.

16 Crounse, J., McKinney, K. A., Kwan, A. J. and Wennberg, P. O.: Measurement of gas-phase
17 hydroperoxides by chemical ionization mass spectrometry, *Anal. Chem.*, 78(19), 6726–6732,
18 doi:doi:10.1021/ac0604235, 2006.

19 Cubison, M. J., Ortega, A. M., Hayes, P. L., Farmer, D. K., Day, D. A., Lechner, M. J., Brune, W.
20 H., Apel, E., Diskin, G. S., Fisher, J. A., Fuelberg, H. E., Hecobian, A., Knapp, D. J., Mikoviny,
21 T., Riemer, D., Sachse, G. W., Sessions, W., Weber, R. J., Weinheimer, A. J., Wisthaler, A. and
22 Jimenez, J. L.: Effects of aging on organic aerosol from open biomass burning smoke in aircraft
23 and laboratory studies, *Atmos. Chem. Phys.*, 11(23), 12049–12064, doi:10.5194/acp-11-12049-
24 2011, 2011.

25 Day, D. A., Wooldridge, P. J., Dillon, M. B., Thornton, J. A. and Cohen, R. C.: A thermal
26 dissociation laser-induced fluorescence instrument for in situ detection of NO₂, peroxy nitrates,
27 alkyl nitrates, and HNO₃, *J. Geophys. Res.*, 107(D5-6), 4046, doi:10.1029/2001JD000779, 2002.

28 DeCarlo, P. F., Kimmel, J. R., Trimborn, A., Northway, M. J., Jayne, J. T., Aiken, A. C., Gonin,
29 M., Fuhrer, K., Horvath, T., Docherty, K. S., Worsnop, D. R. and Jimenez, J. L.: Field-Deployable,
30 High-Resolution, Time-of-Flight Aerosol Mass Spectrometer, *Anal. Chem.*, 78(24), 8281–8289,
31 doi:10.1021/ac061249n, 2006.

32 DeCarlo, P. F., Dunlea, E. J., Kimmel, J. R., Aiken, A. C., Sueper, D., Crounse, J., Wennberg, P.
33 O., Emmons, L., Shinozuka, Y., Clarke, A., Zhou, J., Tomlinson, J., Collins, D. R., Knapp, D.,
34 Weinheimer, A. J., Montzka, D. D., Campos, T. and Jimenez, J. L.: Fast airborne aerosol size and
35 chemistry measurements above Mexico City and Central Mexico during the MILAGRO campaign,
36 *Atmos. Chem. Phys.*, 8(14), 4027–4048, doi:10.5194/acp-8-4027-2008, 2008.

37 DeCarlo, P. F., Ulbrich, I. M., Crounse, J., de Foy, B., Dunlea, E. J., Aiken, A. C., Knapp, D.,
38 Weinheimer, A. J., Campos, T., Wennberg, P. O. and Jimenez, J. L.: Investigation of the sources
39 and processing of organic aerosol over the Central Mexican Plateau from aircraft measurements
40 during MILAGRO, *Atmos. Chem. Phys.*, 10(12), 5257–5280, doi:10.5194/acp-10-5257-2010,
41 2010.

42 Deming, B., Pagonis, D., Liu, X., Talukdar, R. K., Roberts, J. M., Veres, P. R., Krechmer, J. E.,
43 de Gouw, J. A., Jimenez, J. L. and Ziemann, P. J.: Measurements of Delays of Gas-Phase

- 1 Compounds in a Wide Variety of Tubing Materials due to Gas-Wall Partitioning, *Atmos. Meas.*
2 *Tech.*, In Prep., 2018.
- 3 Dibb, J. E., Talbot, R. W., Scheuer, E. M., Seid, G., Avery, M. A. and Singh, H. B.: Aerosol
4 chemical composition in Asian continental outflow during the TRACE-P campaign: Comparison
5 with PEM-West B, *J. Geophys. Res.*, 108(D21), 8815, doi:10.1029/2002JD003111, 2003.
- 6 Diskin, G. S., Podolske, J. R., Sachse, G. W. and Slate, T. A.: Open-path airborne tunable diode
7 laser hygrometer, vol. 4817, edited by A. Fried, p. 196, International Society for Optics and
8 Photonics., 2002.
- 9 Docherty, K. S., Aiken, A. C., Huffman, J. A., Ulbrich, I. M., DeCarlo, P. F., Sueper, D., Worsnop,
10 D. R., Snyder, D. C., Peltier, R. E., Weber, R. J., Grover, B. D., Eatough, D. J., Williams, B. J.,
11 Goldstein, A. H., Ziemann, P. J. and Jimenez, J. L.: The 2005 Study of Organic Aerosols at
12 Riverside (SOAR-1): instrumental intercomparisons and fine particle composition, *Atmos. Chem.*
13 *Phys.*, 11(23), 12387–12420, doi:DOI 10.5194/acp-11-12387-2011, 2011.
- 14 Drewnick, F., Hings, S. S., Alfarra, M. R., Prevot, A. S. H. and Borrmann, S.: Aerosol
15 quantification with the Aerodyne Aerosol Mass Spectrometer: detection limits and ionizer
16 background effects, *Atmos. Meas. Tech.*, 2(1), 33–46, doi:10.5194/amt-2-33-2009, 2009.
- 17 Dunlea, E. J., DeCarlo, P. F., Aiken, A. C., Kimmel, J. R., Peltier, R. E., Weber, R. J., Tomlison,
18 J., Collins, D. R., Shinzuka, Y., McNaughton, C. S., Howell, S. G., Clarke, A. D., Emmons, L.
19 K., Apel, E. C., Pfister, G. G., van Donkelaar, A., Martin, R. V., Millett, D. B., Heald, C. L. and
20 Jimenez, J. L.: Evolution of Asian aerosols during transpacific transport in INTEX-B, *Atmos.*
21 *Chem. Phys.*, 9(19), 7257–7287, doi:10.5194/acp-9-7257-2009, 2009.
- 22 Dzepina, K., Volkamer, R. M. R., Madronich, S., Tulet, P., Ulbrich, I. M., Zhang, Q., Cappa, C.
23 D., Ziemann, P. J. and Jimenez, J. L.: Evaluation of recently-proposed secondary organic aerosol
24 models for a case study in Mexico City, *Atmos. Chem. Phys.*, 9(15), 5681–5709, doi:10.5194/acp-
25 9-5681-2009, 2009.
- 26 Dzepina, K., Cappa, C. D., Volkamer, R. M., Madronich, S., DeCarlo, P. F., Zaveri, R. A. and
27 Jimenez, J. L.: Modeling the Multiday Evolution and Aging of Secondary Organic Aerosol During
28 MILAGRO 2006, *Environ. Sci. Technol.*, 45(8), 3496–3503, doi:10.1021/es103186, 2011.
- 29 Faloona, I. C., Tan, D., Leshner, R. L., Hazen, N. L., Frame, C. L., Simpas, J. B., Harder, H.,
30 Martinez, M., Di Carlo, P., Ren, X. and Brune, W. H.: A Laser-induced Fluorescence Instrument
31 for Detecting Tropospheric OH and HO₂: Characteristics and Calibration, *J. Atmos. Chem.*, 47(2),
32 139–167, doi:10.1023/B:JOCH.0000021036.53185.0e, 2004.
- 33 Farmer, D. K., Matsunaga, A., Docherty, K. S., Surratt, J. D., Seinfeld, J. H., Ziemann, P. J. and
34 Jimenez, J. L.: Response of an aerosol mass spectrometer to organonitrates and organosulfates and
35 implications for atmospheric chemistry, *Proc. Natl. Acad. Sci. U. S. A.*, 107(15), 6670–6675,
36 doi:10.1073/pnas.0912340107, 2010.
- 37 Freney, E. J., Sellegri, K., Canonaco, F., Colomb, A., Borbon, A., Michoud, V., Doussin, J.-F.,
38 Crumeyrolle, S., Amarouche, N., Pichon, J.-M., Bourianne, T., Gomes, L., Prevot, A. S. H.,
39 Beekmann, M. and Schwarzenböeck, A.: Characterizing the impact of urban emissions on regional
40 aerosol particles: airborne measurements during the MEGAPOLI experiment, *Atmos. Chem.*
41 *Phys.*, 14(3), 1397–1412, doi:10.5194/acp-14-1397-2014, 2014.
- 42 Fried, A., Cantrell, C., Olson, J., Crawford, J. H., Weibring, P., Walega, J., Richter, D.,

1 Junkermann, W., Volkamer, R., Sinreich, R., Heikes, B. G., O'Sullivan, D., Blake, D. R., Blake,
2 N., Meinardi, S., Apel, E., Weinheimer, A., Knapp, D., Perring, A., Cohen, R. C., Fuelberg, H.,
3 Shetter, R. E., Hall, S. R., Ullmann, K., Brune, W. H., Mao, J., Ren, X., Huey, L. G., Singh, H. B.,
4 Hair, J. W., Riemer, D., Diskin, G. and Sachse, G.: Detailed comparisons of airborne formaldehyde
5 measurements with box models during the 2006 INTEX-B and MILAGRO campaigns: Potential
6 evidence for significant impacts of unmeasured and multi-generation volatile organic carbon
7 compounds, *Atmos. Chem. Phys.*, 11(22), 11867–11894, doi:10.5194/acp-11-11867-2011, 2011.

8 Ge, X., Setyan, A., Sun, Y. and Zhang, Q.: Primary and secondary organic aerosols in Fresno,
9 California during wintertime: Results from high resolution aerosol mass spectrometry, *J. Geophys.*
10 *Res. Atmos.*, 117(D19), n/a-n/a, doi:10.1029/2012JD018026, 2012.

11 George, I. J., Slowik, J. and Abbatt, J. P. D.: Chemical aging of ambient organic aerosol from
12 heterogeneous reaction with hydroxyl radicals, *Geophys. Res. Lett.*, 35(13), L13811,
13 doi:10.1029/2008GL033884, 2008.

14 Goldberg, D. L., Vinciguerra, T. P., Hosley, K. M., Loughner, C. P., Canty, T. C., Salawitch, R. .
15 and Dickerson, R. R.: Evidence for an increase in the ozone photochemical lifetime in the eastern
16 United States using a regional air quality model, *J. Geophys. Res. Atmos.*, 120, 12,778-12,793,
17 doi:10.1002/2015JD02390, 2015.

18 Gordon, T. D., Tkacik, D. S., Presto, A. A., Zhang, M., Jathar, S. H., Nguyen, N. T., Massetti, J.,
19 Truong, T., Cicero-Fernandez, P., Maddox, C., Rieger, P., Chattopadhyay, S., Maldonado, H.,
20 Maricq, M. M. and Robinson, A. L.: Primary Gas- and Particle-Phase Emissions and Secondary
21 Organic Aerosol Production from Gasoline and Diesel Off-Road Engines, *Environ. Sci. Technol.*,
22 47(24), 14137–14146, doi:10.1021/es403556e, 2013.

23 de Gouw, J. A., Middlebrook, A. M., Warneke, C., Goldan, P. D., Kuster, W. C., Roberts, J. M.,
24 Fehsenfeld, F. C., Worsnop, D. R., Canagaratna, M. R., Pszenny, A. A. P., Keene, W. C.,
25 Marchewka, M. L., Bertman, S. B. and Bates, T. S.: Budget of organic carbon in a polluted
26 atmosphere: Results from the New England Air Quality Study in 2002, *J. Geophys. Res.*, 110(16),
27 D16305, doi:10.1029/2004JD005623, 2005.

28 de Gouw, J. A., Brock, C. A., Atlas, E. L., Bates, T. S., Fehsenfeld, F. C., Goldan, P. D., Holloway,
29 J. S., Kuster, W. C., Lerner, B. M., Matthew, B. M., Middlebrook, A. M., Onasch, T. B., Peltier,
30 R. E., Quinn, P. K., Senff, C. J., Stohl, A., Sullivan, A. P., Trainer, M., Warneke, C., Weber, R. J.
31 and Williams, E. J.: Sources of particulate matter in the northeastern United States in summer: 1.
32 Direct emissions and secondary formation of organic matter in urban plumes, *J. Geophys. Res.*,
33 113(8), D08301, doi:10.1029/2007JD009243, 2008.

34 de Gouw, J. A., Welsh-Bon, D., Warneke, C., Kuster, W. C., Alexander, L., Baker, A. K.,
35 Beyersdorf, A. J., Blake, D. R., Canagaratna, M., Celada, a. T., Huey, L. G., Junkermann, W.,
36 Onasch, T. B., Salcido, A., Sjostedt, S. J., Sullivan, A. P., Tanner, D. J., Vargas, O., Weber, R. J.,
37 Worsnop, D. R., Yu, X. Y. and Zaveri, R.: Emission and chemistry of organic carbon in the gas
38 and aerosol phase at a sub-urban site near Mexico City in March 2006 during the MILAGRO
39 study, *Atmos. Chem. Phys.*, 9(10), 3425–3442, doi:10.5194/acp-9-3425-2009, 2009.

40 Grieshop, A. P., Miracolo, M. A., Donahue, N. M. and Robinson, A. L.: Constraining the Volatility
41 Distribution and Gas-Particle Partitioning of Combustion Aerosols Using Isothermal Dilution and
42 Thermodenuder Measurements, *Environ. Sci. Technol.*, 43(13), 4750–4756,
43 doi:10.1021/Es8032378, 2009.

1 Griffin, R. J., Chen, J., Carmody, K., Vutukuru, S. and Dabdub, D.: Contribution of gas phase
2 oxidation of volatile organic compounds to atmospheric carbon monoxide levels in two areas of
3 the United States, *J. Geophys. Res. Atmos.*, 112(D10), doi:10.1029/2006JD007602, 2007.

4 Guo, H., Sullivan, A. P., Campuzano-Jost, P., Schroder, J. C., Lopez-Hilfiker, F. D., Dibb, J. E.,
5 Jimenez, J. L., Thornton, J. A., Brown, S. S., Nenes, A. and Weber, R. J.: Fine particle pH and the
6 partitioning of nitric acid during winter in the northeastern United States, *J. Geophys. Res. Atmos.*,
7 121(17), 10,355–10,376, doi:10.1002/2016JD025311, 2016.

8 Guo, H., Liu, J., Froyd, K. D., Roberts, J. M., Veres, P. R., Hayes, P. L., Jimenez, J. L., Nenes, A.
9 and Weber, R. J.: Fine particle pH and gas–particle phase partitioning of inorganic species in
10 Pasadena, California, during the 2010 CalNex campaign, *Atmos. Chem. Phys.*, 17(9), 5703–5719,
11 doi:10.5194/acp-17-5703-2017, 2017.

12 Hallquist, M., Wenger, J. C., Baltensperger, U., Rudich, Y., Simpson, D., Claeys, M., Dommen,
13 J., Donahue, N. M., George, C., Goldstein, A. H., Hamilton, J. F., Herrmann, H., Hoffmann, T.,
14 Iinuma, Y., Jang, M., Jenkin, M. E., Jimenez, J. L., Kiendler-Scharr, A., Maenhaut, W.,
15 McFiggans, G., Mentel, T. F., Monod, A., Prévôt, A. S. H., Seinfeld, J. H., Surratt, J. D.,
16 Szmigielski, R. and Wildt, J.: The formation, properties and impact of secondary organic aerosol:
17 current and emerging issues, *Atmos. Chem. Phys.*, 9(14), 5155–5236, doi:10.5194/acp-9-5155-
18 2009, 2009.

19 Hayes, P. L., Ortega, A. M., Cubison, M. J., Froyd, K. D., Zhao, Y., Cliff, S. S., Hu, W. W.,
20 Toohey, D. W., Flynn, J. H., Lefer, B. L., Grossberg, N., Alvarez, S., Rappenglück, B., Taylor, J.
21 W., Allan, J. D., Holloway, J. S., Gilman, J. B., Kuster, W. C., de Gouw, J. A., Massoli, P., Zhang,
22 X., Liu, J., Weber, R. J., Corrigan, A. L., Russell, L. M., Isaacman, G., Worton, D. R., Kreisberg,
23 N. M., Goldstein, A. H., Thalman, R., Waxman, E. M., Volkamer, R., Lin, Y. H., Surratt, J. D.,
24 Kleindienst, T. E., Offenberg, J. H., Dusanter, S., Griffith, S., Stevens, P. S., Brioude, J., Angevine,
25 W. M. and Jimenez, J. L.: Organic aerosol composition and sources in Pasadena, California, during
26 the 2010 CalNex campaign, *J. Geophys. Res.*, 118(16), 9233–9257, doi:10.1002/jgrd.50530, 2013.

27 Hayes, P. L., Carlton, A. G., Baker, K. R., Ahmadov, R., Washenfelder, R. A., Alvarez, S.,
28 Rappenglück, B., Gilman, J. B., Kuster, W. C., de Gouw, J. A., Zotter, P., Prévôt, A. S. H., Szidat,
29 S., Kleindienst, T. E., Ma, P. K. and Jimenez, J. L.: Modeling the formation and aging of secondary
30 organic aerosols in Los Angeles during CalNex 2010, *Atmos. Chem. Phys.*, 15(10), 5773–5801,
31 doi:10.5194/acp-15-5773-2015, 2015.

32 Heald, C. L., Kroll, J. H., Jimenez, J. L., Docherty, K. S., Decarlo, P. F., Aiken, A. C., Chen, Q.,
33 Martin, S. T., Farmer, D. K. and Artaxo, P.: A simplified description of the evolution of organic
34 aerosol composition in the atmosphere, *Geophys. Res. Lett.*, 37(8), L08803,
35 doi:10.1029/2010GL042737, 2010.

36 Heim, E., Dibb, J., Scheuer, E., Campuzano-Jost, P., Nault, B. A., Jimenez, J. L., Peterson, D.,
37 Knote, C., Fenn, M., Hair, J., Beyersdorf, A. J. and Anderson, B. E.: Asian Dust Observed during
38 KORUS-AQ Facilitates the Uptake and Incorporation of Soluble Pollutants during Transport to
39 South Korea: The Hwangsa Anthropogenic Model, *J. Geophys. Res. Atmos.*, submitted, 2018.

40 Hennigan, C. J., Sullivan, A. P., Fountoukis, C. I., Nenes, A., Hecobian, A., Vargas, O., Peltier,
41 R. E., Hanks, A. T. C., Huey, L. G., Lefer, B. L., Russell, A. G. and Weber, R. J.: On the volatility
42 and production mechanisms of newly formed nitrate and water soluble organic aerosol in Mexico
43 City, *Atmos. Chem. Phys.*, 8(14), 3761–3768, doi:10.5194/acp-8-3761-2008, 2008.

- 1 Heo, J.-B., Hopke, P. K. and Yi, S.-M.: Source apportionment of PM_{2.5} in Seoul, Korea, *Atmos.*
2 *Chem. Phys.*, 9(14), 4957–4971, doi:10.5194/acp-9-4957-2009, 2009.
- 3 Herndon, S. C., Onasch, T. B., Wood, E. C., Kroll, J. H., Canagaratna, M. R., Jayne, J. T., Zavala,
4 M. A., Knighton, W. B., Mazzoleni, C., Dubey, M. K., Ulbrich, I. M., Jimenez, J. L., Seila, R., de
5 Gouw, J. A., de Foy, B., Fast, J., Molina, L. T., Kolb, C. E. and Worsnop, D. R.: Correlation of
6 secondary organic aerosol with odd oxygen in Mexico City, *Geophys. Res. Lett.*, 35(15),
7 doi:10.1029/2008GL034058, 2008.
- 8 Hersey, S. P., Craven, J. S., Metcalf, A. R., Lin, J., Lathem, T., Suski, K. J., Cahill, J. F., Duong,
9 H. T., Sorooshian, A., Jonsson, H. H., Shiraiwa, M., Zuend, A., Nenes, A., Prather, K. A., Flagan,
10 R. C. and Seinfeld, J. H.: Composition and hygroscopicity of the Los Angeles Aerosol: CalNex, *J.*
11 *Geophys. Res. Atmos.*, 118(7), 3016–3036, doi:10.1002/jgrd.50307, 2013.
- 12 Hildebrandt Ruiz, L., Paciga, A. L., Cerully, K. M., Nenes, A., Donahue, N. M. and Pandis, S. N.:
13 Formation and aging of secondary organic aerosol from toluene: changes in chemical composition,
14 volatility, and hygroscopicity, *Atmos. Chem. Phys.*, 15(14), 8301–8313, doi:10.5194/acp-15-
15 8301-2015, 2015.
- 16 Hodzic, A. and Jimenez, J. L.: Modeling anthropogenically controlled secondary organic aerosols
17 in a megacity: A simplified framework for global and climate models, *Geosci. Model Dev.*, 4(4),
18 901–917, doi:10.5194/gmd-4-901-2011, 2011.
- 19 Hodzic, A., Jimenez, J. L., Madronich, S., Canagaratna, M. R., DeCarlo, P. F., Kleinman, L. and
20 Fast, J.: Modeling organic aerosols in a megacity: Potential contribution of semi-volatile and
21 intermediate volatility primary organic compounds to secondary organic aerosol formation,
22 *Atmos. Chem. Phys.*, 10(12), 5491–5514, doi:10.5194/acp-10-5491-2010, 2010.
- 23 Hodzic, A., Madronich, S., Kasibhatla, P. S., Tyndall, G., Aumont, B., Jimenez, J. L., Lee-Taylor,
24 J. and Orlando, J.: Organic photolysis reactions in tropospheric aerosols: effect on secondary
25 organic aerosol formation and lifetime, *Atmos. Chem. Phys.*, 15(16), 9253–9269, doi:10.5194/acp-
26 15-9253-2015, 2015.
- 27 Hong, J.-W. and Hong, J.: Changes in the Seoul Metropolitan Area Urban Heat Environment with
28 Residential Redevelopment, *J. Appl. Meteorol. Climatol.*, 55, 1091–1106, doi:10.1175/JAMC-D-
29 15-0321.1, 2016.
- 30 Hu, W., Hu, M., Hu, W., Jimenez, J. L., Yuan, B., Chen, W., Wang, M., Wu, Y., Chen, C., Wang,
31 Z., Peng, J., Zeng, L. and Shao, M.: Chemical composition, sources and aging process of sub-
32 micron aerosols in Beijing: contrast between summer and winter, *J. Geophys. Res. Atmos.*,
33 doi:10.1002/2015JD024020, 2016.
- 34 Hu, W., Campuzano-Jost, P., Day, D. A., Croteau, P., Canagaratna, M. R., Jayne, J. T., Worsnop,
35 D. R. and Jimenez, J. L.: Evaluation of the new capture vaporizer for aerosol mass spectrometers
36 (AMS) through field studies of inorganic species, *Aerosol Sci. Technol.*, 51(6), 735–754,
37 doi:10.1080/02786826.2017.1296104, 2017a.
- 38 Hu, W., Campuzano-Jost, P., Day, D. A., Croteau, P., Canagaratna, M. R., Jayne, J. T., Worsnop,
39 D. R. and Jimenez, J. L.: Evaluation of the new capture vapourizer for aerosol mass spectrometers
40 (AMS) through laboratory studies of inorganic species, *Atmos. Meas. Tech.*, 10(6), 2897–2921,
41 doi:10.5194/amt-10-2897-2017, 2017b.
- 42 Hu, W., Day, D. A., Campuzano-Jost, P., Nault, B. A., Park, T., Lee, T., Croteau, P., Canagaratna,

1 M. R., Jayne, J. T., Worsnop, D. R. and Jimenez, J. L.: Evaluation of the new capture vaporizer
2 for Aerosol Mass Spectrometers: Characterization of organic aerosol mass spectra, *Aerosol Sci.*
3 *Technol.*, 52(7), 752–739, doi:10.1080/02786826.2018.1454584, 2018a.

4 Hu, W., Day, D. A., Campuzano-Jost, P., Nault, B. A., Park, T., Lee, T., Croteau, P., Canagaratna,
5 M. R., Jayne, J. T., Worsnop, D. R. and Jimenez, J. L.: Evaluation of the New Capture Vaporizer
6 for Aerosol Mass Spectrometers (AMS): Elemental Composition and Source Apportionment of
7 Organic Aerosols (OA), *ACS Earth Sp. Chem.*, 2(4), 410–421,
8 doi:10.1021/acsearthspacechem.8b00002, 2018b.

9 Hu, W. W., Hu, M., Yuan, B., Jimenez, J. L., Tang, Q., Peng, J. F., Hu, W., Shao, M., Wang, M.,
10 Zeng, L. M., Wu, Y. S., Gong, Z. H., Huang, X. F. and He, L. Y.: Insights on organic aerosol aging
11 and the influence of coal combustion at a regional receptor site of central eastern China, *Atmos.*
12 *Chem. Phys.*, 13(19), 10095–10112, doi:10.5194/acp-13-10095-2013, 2013.

13 Huang, C., Wang, H. L., Li, L., Wang, Q., Lu, Q., de Gouw, J. A., Zhou, M., Jing, S. A., Lu, J.
14 and Chen, C. H.: VOC species and emission inventory from vehicles and their SOA formation
15 potentials estimation in Shanghai, China, *Atmos. Chem. Phys.*, 15(19), 11081–11096,
16 doi:10.5194/acp-15-11081-2015, 2015.

17 Huey, L. G., Tanner, D. J., Slusher, D. L., Dibb, J. E., Arimoto, R., Chen, G., Davis, D., Buhr, M.
18 P., Nowak, J. B., Mauldin III, R. L., Eisele, F. L. and Kosciuch, E.: CIMS measurements of HNO₃
19 and SO₂ at the South Pole during ISCAT 2000, *Atmos. Environ.*, 38(32), 5411–5421,
20 doi:10.1016/J.ATMOENV.2004.04.037, 2004.

21 Huffman, J. A., Docherty, K. S., Aiken, A. C., Cubison, M. J., Ulbrich, I. M., DeCarlo, P. F.,
22 Sueper, D., Jayne, J. T., Worsnop, D. R., Ziemann, P. J. and Jimenez, J. L.: Chemically-resolved
23 aerosol volatility measurements from two megacity field studies, *Atmos. Chem. Phys.*, 9(1), 7161–
24 7182, doi:doi:10.5194/acp-9-7161-2009, 2009.

25 Hunter, J. F., Day, D. A., Palm, B. B., Yatavelli, R. L. N., Chan, A. W. H., Kaser, L., Cappellin,
26 L., Hayes, P. L., Cross, E. S., Carrasquillo, A. J., Campuzano-Jost, P., Stark, H., Zhao, Y., Hohaus,
27 T., Smith, J. N., Hansel, A., Karl, T., Goldstein, A. H., Guenther, A., Worsnop, D. R., Thornton,
28 J. A., Heald, C. L., Jimenez, J. L. and Kroll, J. H.: Comprehensive characterization of atmospheric
29 organic carbon at a forested site, *Nat. Geosci.*, 10(10), 748–753, doi:10.1038/ngeo3018, 2017.

30 Jacob, D. J.: Heterogeneous chemistry and tropospheric ozone, *Atmos. Environ.*, 34, 2131–2159,
31 doi:10.1016/S1352-2310(99)00462-8, 2000.

32 Janssen, R. H. H., Tsimpidi, A. P., Karydis, V. A., Pozzer, A., Lelieveld, J., Crippa, M., Prévôt,
33 A. S. H., Ait-Helal, W., Borbon, A., Sauvage, S. and Locoge, N.: Influence of local production
34 and vertical transport on the organic aerosol budget over Paris, *J. Geophys. Res. Atmos.*, 1–21,
35 doi:10.1002/2016JD026402, 2017.

36 Jathar, S. H., Miracolo, M. A., Tkacik, D. S., Donahue, N. M., Adams, P. J. and Robinson, A. L.:
37 Secondary Organic Aerosol Formation from Photo-Oxidation of Unburned Fuel: Experimental
38 Results and Implications for Aerosol Formation from Combustion Emissions, *Environ. Sci.*
39 *Technol.*, 47(22), 12886–12893, doi:10.1021/es403445q, 2013.

40 Jathar, S. H., Gordon, T. D., Hennigan, C. J., Pye, H. O. T., Pouliot, G., Adams, P. J., Donahue,
41 N. M. and Robinson, A. L.: Unspeciated organic emissions from combustion sources and their
42 influence on the secondary organic aerosol budget in the United States., *Proc. Natl. Acad. Sci. U.*

- 1 S. A., 111(29), 10473–10478, doi:10.1073/pnas.1323740111, 2014.
- 2 Jayne, J. T. and Worsnop, D. R.: Particle Capture Device Aerodyne Research, 2015.
- 3 Jeong, U., Kim, J., Lee, H. and Lee, Y. G.: Assessing the effect of long-range pollutant
4 transportation on air quality in Seoul using the conditional potential source contribution function
5 method, *Atmos. Environ.*, 150, 33–44, doi:10.1016/j.atmosenv.2016.11.017, 2017.
- 6 Jimenez, J. L., Canagaratna, M. R., Donahue, N. M., Prévôt, A. S. H., Zhang, Q., Kroll, J. H.,
7 DeCarlo, P. F., Allan, J. D., Coe, H., Ng, N. L., Aiken, A. C., Docherty, K. S., Ulbrich, I. M.,
8 Grieshop, A. P., Robinson, A. L., Duplissy, J., Smith, J. D., Wilson, K. R., Lanz, V. A., Hueglin,
9 C., Sun, Y. L., Tian, J., Laaksonen, A., Raatikainen, T., Rautiainen, J., Vaattovaara, P., Ehn, M.,
10 Kulmala, M., Tomlinson, J. M., Collins, D. R., Cubison, M. J., Dunlea, E. J., Huffman, J. A.,
11 Onasch, T. B., Alfarra, M. R., Williams, P. I., Bower, K., Kondo, Y., Schneider, J., Drewnick, F.,
12 Borrmann, S., Weimer, S., Demerjian, K., Salcedo, D., Cottrell, L., Griffin, R., Takami, A.,
13 Miyoshi, T., Hatakeyama, S., Shimono, A., Sun, J. Y., Zhang, Y. M., Dzepina, K., Kimmel, J. R.,
14 Sueper, D., Jayne, J. T., Herndon, S. C., Trimborn, A. M., Williams, L. R., Wood, E. C.,
15 Middlebrook, A. M., Kolb, C. E., Baltensperger, U. and Worsnop, D. R.: Evolution of Organic
16 Aerosols in the Atmosphere, *Science* (80-.), 326(5959), 1525–1529,
17 doi:10.1126/science.1180353, 2009.
- 18 Jimenez, J. L., Campuzano-Jost, P., Day, D. A., Nault, B. A., Schroder, J. C. and Cubison, M. J.:
19 Frequently AMS Questions for AMS Data Users, [online] Available from:
20 http://cires.colorado.edu/jimenez-group/wiki/index.php?title=FAQ_for_AMS_Data_Users,
21 accessed month-year (Accessed 6 December 2018), 2018.
- 22 Kang, E., Root, M. J., Toohey, D. W. and Brune, W. H.: Introducing the concept of Potential
23 Aerosol Mass (PAM), *Atmos. Chem. Phys.*, 7(22), 5727–5744, doi:10.5194/acp-7-5727-2007,
24 2007.
- 25 Kang, E., Lee, M., Brune, W. H., Lee, T., Park, T., Ahn, J. and Shang, X.: Photochemical aging
26 of aerosol particles in different air masses arriving at Baengnyeong Island, Korea, *Atmos. Chem.*
27 *Phys.*, 18(9), 6661–6677, doi:10.5194/acp-18-6661-2018, 2018.
- 28 Khare, P. and Gentner, D. R.: Considering the future of anthropogenic gas-phase organic
29 compound emissions and the increasing influence of non-combustion sources on urban air quality,
30 *Atmos. Chem. Phys.*, 18(8), 5391–5413, doi:10.5194/acp-18-5391-2018, 2018.
- 31 Kim, B. M., Seo, J., Kim, J. Y., Lee, J. Y. and Kim, Y.: Transported vs. local contributions from
32 secondary and biomass burning sources to PM_{2.5}, *Atmos. Environ.*, 144, 24–36,
33 doi:10.1016/j.atmosenv.2016.08.072, 2016.
- 34 Kim, H., Zhang, Q., Bae, G.-N., Kim, J. Y. and Lee, S. B.: Sources and atmospheric processing of
35 wintertime aerosols in Seoul, Korea: Insights from real-time measurements using a high-resolution
36 aerosol mass spectrometer, *Atmos. Chem. Phys. Discuss.*, 17(3), 2009–2003, doi:10.5194/acp-17-
37 2009-2017, 2017.
- 38 Kim, H., Zhang, Q. and Heo, J.: Influence of Intense secondary aerosol formation and long-range
39 transport on aerosol chemistry and properties in the Seoul Metropolitan Area during spring time :
40 Results from KORUS-AQ, *Atmos. Chem. Phys.*, 18, 7149–7168, doi:10.5194/acp-2017-947,
41 2018.
- 42 Kim, H. C., Kim, E. H., Kim, B. U. and Kim, S.: Regional Contributions to the Particulate Matter

1 Concentration in the Seoul Metropolitan Area, Korea: Seasonal Variation and Sensitivity to
2 Meteorology, *Atmos. Chem. Phys.*, 17(17), 10315–10332, doi:10.5194/acp-17-10315-2017, 2017.

3 Kim, H. S., Huh, J. B., Hopke, P. K., Holsen, T. M. and Yi, S. M.: Characteristics of the major
4 chemical constituents of PM_{2.5} and smog events in Seoul, Korea in 2003 and 2004, *Atmos.*
5 *Environ.*, 41(32), 6762–6770, doi:10.1016/j.atmosenv.2007.04.060, 2007.

6 Kim, S., Huey, L. G., Stickel, R. E., Tanner, D. J., Crawford, J. H., Olson, J. R., Chen, G., Brune,
7 W. H., Ren, X., Leshner, R., Wooldridge, P. J., Bertram, T. H., Perring, A., Cohen, R. C., Lefer, B.
8 L., Shetter, R. E., Avery, M., Diskin, G. and Sokolik, I.: Measurement of HO₂ NO₂ in the free
9 troposphere during the Intercontinental Chemical Transport Experiment–North America 2004, *J.*
10 *Geophys. Res.*, 112, D12S01, doi:10.1029/2006JD007676, 2007.

11 Kim, Y. J., Woo, J. H., Ma, Y. Il, Kim, S., Nam, J. S., Sung, H., Choi, K. C., Seo, J., Kim, J. S.,
12 Kang, C. H., Lee, G., Ro, C. U., Chang, D. and Sunwoo, Y.: Chemical characteristics of long-
13 range transport aerosol at background sites in Korea, *Atmos. Environ.*, 43(34), 5556–5566,
14 doi:10.1016/j.atmosenv.2009.03.062, 2009.

15 Kimmel, J. R., Farmer, D. K., Cubison, M. J., Sueper, D., Tanner, C., Nemitz, E., Worsnop, D. R.,
16 Gonin, M. and Jimenez, J. L.: Real-time aerosol mass spectrometry with millisecond resolution,
17 *Int. J. Mass Spectrom.*, 303(1), 15–26, doi:10.1016/j.ijms.2010.12.004, 2011.

18 Kleinman, L., Kuang, C., Sedlacek, A., Senum, G., Springston, S., Wang, J., Zhang, Q., Jayne, J.,
19 Fast, J., Hubbe, J., Shilling, J. and Zaveri, R.: What do correlations tell us about anthropogenic-
20 biogenic interactions and SOA formation in the Sacramento plume during CARES?, *Atmos.*
21 *Chem. Phys.*, 16(3), 1729–1746, doi:10.5194/acp-16-1729-2016, 2016.

22 Kleinman, L. I., Daum, P. H., Lee, Y.-N., Senum, G. I., Springston, S. R., Wang, J., Berkowitz,
23 C., Hubbe, J., Zaveri, R. A., Brechtel, F. J., Jayne, J., Onasch, T. B. and Worsnop, D.: Aircraft
24 observations of aerosol composition and ageing in New England and Mid-Atlantic States during
25 the summer 2002 New England Air Quality Study field campaign, *J. Geophys. Res.*, 112(D9),
26 D09310, doi:10.1029/2006JD007786, 2007.

27 Kleinman, L. I., Springston, S. R., Daum, P. H., Lee, Y.-N., Nunnermacker, L. J., Senum, G. I.,
28 Wang, J., Weinstein-Lloyd, J., Alexander, M. L., Hubbe, J., Ortega, J., Canagaratna, M. R. and
29 Jayne, J.: The time evolution of aerosol composition over the Mexico City plateau, *Atmos. Chem.*
30 *Phys.*, 8(6), 1559–1575, doi:10.5194/acp-8-1559-2008, 2008.

31 Kleinman, L. I., Springston, S. R., Wang, J., Daum, P. H., Lee, Y.-N. N., Nunnermacker, L. J.,
32 Senum, G. I., Weinstein-Lloyd, J., Alexander, M. L., Hubbe, J., Ortega, J., Zaveri, R. A.,
33 Canagaratna, M. R. and Jayne, J.: The time evolution of aerosol size distribution over the Mexico
34 City plateau, *Atmos. Chem. Phys.*, 9(13), 4261–4278, doi:10.5194/acpd-9-1621-2009, 2009.

35 Knote, C., Hodzic, A., Jimenez, J. L., Volkamer, R., Orlando, J. J., Baidar, S., Brioude, J., Fast, J.,
36 Gentner, D. R., Goldstein, A. H., Hayes, P. L., Knighton, W. B., Oetjen, H., Setyan, A., Stark, H.,
37 Thalman, R., Tyndall, G., Washenfelder, R., Waxman, E. and Zhang, Q.: Simulation of semi-
38 explicit mechanisms of SOA formation from glyoxal in aerosol in a 3-D model, *Atmos. Chem.*
39 *Phys.*, 14(12), 6213–6239, doi:10.5194/acp-14-6213-2014, 2014.

40 Krechmer, J. E., Pagonis, D., Ziemann, P. J. and Jimenez, J. L.: Quantification of Gas-Wall
41 Partitioning in Teflon Environmental Chambers Using Rapid Bursts of Low-Volatility Oxidized
42 Species Generated in Situ, *Environ. Sci. Technol.*, 50(11), 5757–5765,

1 doi:10.1021/acs.est.6b00606, 2016.

2 Krechmer, J. E., Day, D. A., Ziemann, P. J. and Jimenez, J. L.: Direct Measurements of
3 Gas/Particle Partitioning and Mass Accommodation Coefficients in Environmental Chambers,
4 *Environ. Sci. Technol.*, 51(20), 11867–11875, doi:10.1021/acs.est.7b02144, 2017.

5 Kroll, J. H. and Seinfeld, J. H.: Chemistry of secondary organic aerosol: Formation and evolution
6 of low-volatility organics in the atmosphere, *Atmos. Environ.*, 42(16), 3593–3624,
7 doi:10.1016/J.ATMOSENV.2008.01.003, 2008.

8 Kroll, J. H., Donahue, N. M., Jimenez, J. L., Kessler, S. H., Canagaratna, M. R., Wilson, K. R.,
9 Altieri, K. E., Mazzoleni, L. R., Wozniak, A. S., Bluhm, H., Mysak, E. R., Smith, J. D., Kolb, C.
10 E. and Worsnop, D. R.: Carbon oxidation state as a metric for describing the chemistry of
11 atmospheric organic aerosol., *Nat. Chem.*, 3(2), 133–139, doi:10.1038/nchem.948, 2011.

12 Kupc, A., Williamson, C., Wagner, N. L., Richardson, M. and Brock, C. A.: Modification,
13 calibration, and performance of the Ultra-High Sensitivity Aerosol Spectrometer for particle size
14 distribution and volatility measurements during the Atmospheric Tomography Mission (ATom)
15 airborne campaign, *Atmos. Meas. Tech.*, 11(1), 369–383, doi:10.5194/amt-11-369-2018, 2018.

16 Lambe, A. T., Ahern, A. T., Williams, L. R., Slowik, J. G., Wong, J. P. S., Abbatt, J. P. D., Brune,
17 W. H., Ng, N. L., Wright, J. P., Croasdale, D. R., Worsnop, D. R., Davidovits, P. and Onasch, T.
18 B.: Characterization of aerosol photooxidation flow reactors: heterogeneous oxidation, secondary
19 organic aerosol formation and cloud condensation nuclei activity measurements, *Atmos. Meas.*
20 *Tech.*, 4(3), 445–461, doi:10.5194/amt-4-445-2011, 2011.

21 Lambe, A. T., Onasch, T. B., Croasdale, D. R., Wright, J. P., Martin, A. T., Franklin, J. P., Massoli,
22 P., Kroll, J. H., Canagaratna, M. R., Brune, W. H., Worsnop, D. R. and Davidovits, P.: Transitions
23 from Functionalization to Fragmentation Reactions of Laboratory Secondary Organic Aerosol
24 (SOA) Generated from the OH Oxidation of Alkane Precursors, *Environ. Sci. Technol.*, 46(10),
25 5430–5437, doi:10.1021/Es300274t, 2012.

26 Landrigan, P. J., Fuller, R., Acosta, N. J. R., Adeyi, O., Arnold, R., Basu, N., Baldé, A. B.,
27 Bertollini, R., Bose-O'Reilly, S., Boufford, J. I., Breyse, P. N., Chiles, T., Mahidol, C., Coll-Seck,
28 A. M., Cropper, M. L., Fobil, J., Fuster, V., Greenstone, M., Haines, A., Hanrahan, D., Hunter, D.,
29 Khare, M., Krupnick, A., Lanphear, B., Lohani, B., Martin, K., Mathiasen, K. V, McTeer, M. A.,
30 Murray, C. J. L., Ndahimananjara, J. D., Perera, F., Potočnik, J., Preker, A. S., Ramesh, J.,
31 Rockström, J., Salinas, C., Samson, L. D., Sandilya, K., Sly, P. D., Smith, K. R., Steiner, A.,
32 Stewart, R. B., Suk, W. A., van Schayck, O. C. P., Yadama, G. N., Yumkella, K. and Zhong, M.:
33 The Lancet Commission on pollution and health, *Lancet*, 391(10119), 462–512,
34 doi:10.1016/S0140-6736(17)32345-0, 2018.

35 Lee, G., Choi, H. S., Lee, T., Choi, J., Park, J. S. and Ahn, J. Y.: Variations of regional background
36 peroxyacetyl nitrate in marine boundary layer over Baengyeong Island, South Korea, *Atmos.*
37 *Environ.*, 61, 533–541, doi:10.1016/j.atmosenv.2012.07.075, 2012.

38 Lee, H. M., Park, R. J., Henze, D. K., Lee, S., Shim, C., Shin, H. J., Moon, K. J. and Woo, J. H.:
39 PM_{2.5} source attribution for Seoul in May from 2009 to 2013 using GEOS-Chem and its adjoint
40 model, *Environ. Pollut.*, 221, 377–384, doi:10.1016/j.envpol.2016.11.088, 2017.

41 Lee, S., Ho, C.-H., Lee, Y. G., Choi, H.-J. and Song, C.-K.: Influence of transboundary air
42 pollutants from China on the high-PM₁₀ episode in Seoul, Korea for the period October 16–20,

- 1 2008, *Atmos. Environ.*, 77, 430–439, doi:10.1016/J.ATMOSENV.2013.05.006, 2013.
- 2 Lee, T., Choi, J., Lee, G., Ahn, J., Park, J. S., Atwood, S. A., Schurman, M., Choi, Y., Chung, Y.
3 and Collett, J. L.: Characterization of aerosol composition, concentrations, and sources at
4 Baengnyeong Island, Korea using an aerosol mass spectrometer, *Atmos. Environ.*, 120, 297–306,
5 doi:10.1016/j.atmosenv.2015.08.038, 2015.
- 6 Lelieveld, J., Evans, J. S., Fnais, M., Giannadaki, D. and Pozzer, A.: The contribution of outdoor
7 air pollution sources to premature mortality on a global scale, *Nature*, 525(7569), 367–371,
8 doi:10.1038/nature15371, 2015.
- 9 Li, R., Palm, B. B., Ortega, A. M., Hlywiak, J., Hu, W., Peng, Z., Day, D. A., Knote, C., Brune,
10 W. H., de Gouw, J. A. and Jimenez, J. L.: Modeling the radical chemistry in an oxidation flow
11 reactor: radical formation and recycling, sensitivities, and the OH exposure estimation equation.,
12 *J. Phys. Chem. A*, 119(19), 4418–4432, doi:10.1021/jp509534k, 2015.
- 13 Liu, T., Wang, X., Deng, W., Hu, Q., Ding, X., Zhang, Y., He, Q., Zhang, Z., Lü, S., Bi, X., Chen,
14 J. and Yu, J.: Secondary organic aerosol formation from photochemical aging of light-duty
15 gasoline vehicle exhausts in a smog chamber, *Atmos. Chem. Phys.*, 15(15), 9049–9062,
16 doi:10.5194/acp-15-9049-2015, 2015.
- 17 Liu, X., Huey, L. G., Yokelson, R. J., Selimovic, V., Simpson, I. J., Müller, M., Jimenez, J. L.,
18 Campuzano-Jost, P., Beyersdorf, A. J., Blake, D. R., Butterfield, Z., Choi, Y., Crouse, J. D., Day,
19 D. A., Diskin, G. S., Dubey, M. K., Fortner, E., Hanisco, T. F., Hu, W., King, L. E., Kleinman, L.,
20 Meinardi, S., Mikoviny, T., Onasch, T. B., Palm, B. B., Peischl, J., Pollack, I. B., Ryerson, T. B.,
21 Sachse, G. W., Sedlacek, A. J., Shilling, J. E., Springston, S., St. Clair, J. M., Tanner, D. J., Teng,
22 A. P., Wennberg, P. O., Wisthaler, A. and Wolfe, G. M.: Airborne measurements of western U.S.
23 wildfire emissions: Comparison with prescribed burning and air quality implications, *J. Geophys.*
24 *Res.*, 122(11), 6108–6129, doi:10.1002/2016JD026315, 2017.
- 25 Ma, P. K., Zhao, Y., Robinson, A. L., Worton, D. R., Goldstein, A. H., Ortega, A. M., Jimenez, J.-
26 L., Zotter, P., Prévôt, A. S. H., Szidat, S. and Hayes, P. L.: Evaluating the impact of new
27 observational constraints on P-S/IVOC emissions, multi-generation oxidation, and chamber wall
28 losses on SOA modeling for Los Angeles, CA, *Atmos. Chem. Phys.*, 17(15), 9237–9259,
29 doi:10.5194/acp-17-9237-2017, 2017.
- 30 Mao, J., Ren, X., Brune, W. H., Olson, J. R., Crawford, J. H., Fried, a., Huey, L. G., Cohen, R.
31 C., Heikes, B., Singh, H. B., Blake, D. R., Sachse, G. W., Diskin, G. S., Hall, S. R. and Shetter, R.
32 E.: Airborne measurement of OH reactivity during INTEX-B, *Atmos. Chem. Phys.*, 9(1), 163–
33 173, doi:10.5194/acp-9-163-2009, 2009.
- 34 Matsunaga, A. and Ziemann, P. J.: Gas-Wall Partitioning of Organic Compounds in a Teflon Film
35 Chamber and Potential Effects on Reaction Product and Aerosol Yield Measurements, *Aerosol*
36 *Sci. Technol.*, 44(10), 881–892, doi:10.1080/02786826.2010.501044, 2010.
- 37 McDonald, B. C., de Gouw, J. A., Gilman, J. B., Jathar, S. H., Akherati, A., Cappa, C. D., Jimenez,
38 J. L., Lee-Taylor, J., Hayes, P. L., McKeen, S. A., Cui, Y. Y., Kim, S.-W., Gentner, D. R.,
39 Isaacman-VanWertz, G., Goldstein, A. H., Harley, R. A., Frost, G. J., Roberts, J. M., Ryerson, T.
40 B. and Trainer, M.: Volatile chemical products emerging as largest petrochemical source of urban
41 organic emissions., *Science*, 359(6377), 760–764, doi:10.1126/science.aaq0524, 2018.
- 42 McKeen, S. A., Liu, S. C., Hsie, E.-Y., Lin, X., Bradshaw, J. D., Smyth, S., Gregory, G. L. and

1 Blake, D. R.: Hydrocarbon ratios during PEM-WEST A: A model perspective, *J. Geophys. Res.*
2 *Atmos.*, 101(D1), 2087–2109, doi:10.1029/95JD02733, 1996.

3 McMeeking, G. R., Bart, M., Chazette, P., Haywood, J. M., Hopkins, J. R., McQuaid, J. B.,
4 Morgan, W. T., Raut, J.-C., Ryder, C. L., Savage, N., Turnbull, K. and Coe, H.: Airborne
5 measurements of trace gases and aerosols over the London metropolitan region, *Atmos. Chem.*
6 *Phys.*, 12(11), 5163–5187, doi:10.5194/acp-12-5163-2012, 2012.

7 McNaughton, C. S., Clarke, A. D., Howell, S. G., Pinkerton, M., Anderson, B., Thornhill, L.,
8 Hudgins, C., Winstead, E., Dibb, J. E., Scheuer, E. and Maring, H.: Results from the DC-8 Inlet
9 Characterization Experiment (DICE): Airborne versus surface sampling of mineral dust and sea
10 salt aerosols, *Aerosol Sci. Technol.*, 41(2), 136–159, doi:10.1080/02786820601118406, 2007.

11 Middlebrook, A. M., Bahreini, R., Jimenez, J. L. and Canagaratna, M. R.: Evaluation of
12 Composition-Dependent Collection Efficiencies for the Aerodyne Aerosol Mass Spectrometer
13 using Field Data, *Aerosol Sci. Technol.*, 46(3), 258–271, doi:10.1080/02786826.2011.620041,
14 2012.

15 Miracolo, M. A., Presto, A. A., Lambe, A. T., Hennigan, C. J., Donahue, N. M., Kroll, J. H.,
16 Worsnop, D. R. and Robinson, A. L.: Photo-Oxidation of Low-Volatility Organics Found in Motor
17 Vehicle Emissions: Production and Chemical Evolution of Organic Aerosol Mass, *Environ. Sci.*
18 *Technol.*, 44(5), 1638–1643, doi:10.1021/es902635c, 2010.

19 Mitroo, D., Sun, Y., Combet, D. P., Kumar, P. and Williams, B. J.: Assessing the degree of plug
20 flow in oxidation flow reactors (OFRs): a study on a potential aerosol mass (PAM) reactor, *Atmos.*
21 *Meas. Tech.*, 11, 1741–1756, doi:10.5194/amt-11-1741-2018, 2018.

22 Monks, P. S., Granier, C., Fuzzi, S., Stohl, A., Williams, M. L., Akimoto, H., Amann, M.,
23 Baklanov, A., Baltensperger, U., Bey, I., Blake, N., Blake, R. S., Carslaw, K., Cooper, O. R.,
24 Dentener, F., Fowler, D., Fragkou, E., Frost, G. J., Generoso, S., Ginoux, P., Grewe, V., Guenther,
25 A., Hansson, H. C., Henne, S., Hjorth, J., Hofzumahaus, A., Huntrieser, H., Isaksen, I. S. A.,
26 Jenkin, M. E., Kaiser, J., Kanakidou, M., Klimont, Z., Kulmala, M., Laj, P., Lawrence, M. G., Lee,
27 J. D., Lioussé, C., Maione, M., McFiggans, G., Metzger, A., Mieville, A., Moussiopoulos, N.,
28 Orlando, J. J., O’Dowd, C. D., Palmer, P. I. I., Parrish, D. D., Petzold, A., Platt, U., Pöschl, U.,
29 Prévôt, A. S. H., Reeves, C. E., Reimann, S., Rudich, Y., Sellegri, K., Steinbrecher, R., Simpson,
30 D., ten Brink, H., Theloke, J., van der Werf, G. R., Vautard, R., Vestreng, V., Vlachokostas, C.
31 and von Glasow, R.: Atmospheric composition change - global and regional air quality, *Atmos.*
32 *Environ.*, 43(33), 5268–5350, doi:10.1016/j.atmosenv.2009.08.021, 2009.

33 Morino, Y., Tanabe, K., Sato, K. and Ohara, T.: Secondary organic aerosol model intercomparison
34 based on secondary organic aerosol to odd oxygen ratio in Tokyo, *J. Geophys. Res. Atmos.*,
35 119(23), 13,489–13,505, doi:10.1002/2014JD021937, 2014.

36 Müller, M., Mikoviny, T., Feil, S., Haidacher, S., Hanel, G., Hartungen, E., Jordan, A., Märk, L.,
37 Mutschlechner, P., Schottkowsky, R., Sulzer, P., Crawford, J. H. and Wisthaler, A.: A compact
38 PTR-ToF-MS instrument for airborne measurements of volatile organic compounds at high
39 spatiotemporal resolution, *Atmos. Meas. Tech.*, 7(11), 3763–3772, doi:10.5194/amt-7-3763-2014,
40 2014.

41 Murphy, B. N., Donahue, N. M., Fountoukis, C. and Pandis, S. N.: Simulating the oxygen content
42 of ambient organic aerosol with the 2D volatility basis set, *Atmos. Chem. Phys.*, 11(15), 7859–
43 7873, doi:10.5194/acp-11-7859-2011, 2011.

1 Murphy, B. N., Woody, M. C., Jimenez, J. L., Carlton, A. M. G., Hayes, P. L., Liu, S., Ng, N. L.,
2 Russell, L. M., Setyan, A., Xu, L., Young, J., Zaveri, R. A., Zhang, Q. and Pye, H. O. T.:
3 Semivolatile POA and parameterized total combustion SOA in CMAQv5.2: impacts on source
4 strength and partitioning, *Atmos. Chem. Phys.*, 17(18), 11107–11133, doi:10.5194/acp-17-11107-
5 2017, 2017.

6 Myhre, G., Shindell, D., Bréon, F.-M., Collins, W., Fuglestedt, J., Huang, J., Koch, D., Lamarque,
7 J.-F., Lee, D., Mendoza, B., Nakajima, T., Robock, A., Stephens, G., Takemura, T. and Zhang, H.:
8 Anthropogenic and Natural Radiative Forcing, in *Climate Change 2013: The Physical Science*
9 *Basis. Contribution of Working Group I to the Fifth Assessment Report of the Intergovernmental*
10 *Panel on Climate Change*, edited by T. F. Stocker, D. Qin, G.-K. Plattner, M. Tignor, S. K. Allen,
11 J. Boschung, A. Nauels, Y. Xia, V. Bex, and P. M. Midgley, p. 659, Cambridge University Press,
12 Cambridge, United Kingdom and New York, NY, USA, United Kingdom and New York, NY,
13 USA. [online] Available from: <https://www.ipcc.ch/report/ar5/wg1/>, 2013.

14 Novelli, P. C., Crotwell, A., Lang, P. M. and Mund, J.: Atmospheric Carbon Monoxide Dry Air
15 Mole Fractions from the NOAA ESRL Carbon Cycle Cooperative Global Air Sampling Network,
16 1988-2016, Version: 2017-07-28, [online] Available from:
17 ftp://aftp.cmdl.noaa.gov/data/trace_gases/co/flask/surface/, 2017.

18 OECD: Exposure to PM2.5 in countries and regions : Exposure to PM2.5 in macroregions, [online]
19 Available from: <https://stats.oecd.org/index.aspx?queryid=72722> (Accessed 1 August 2018),
20 2018.

21 Ortega, A. M., Hayes, P. L., Peng, Z., Palm, B. B., Hu, W., Day, D. A., Li, R., Cubison, M. J.,
22 Brune, W. H., Graus, M., Warneke, C., Gilman, J. B., Kuster, W. C., de Gouw, J. A., Gutiérrez-
23 Montes, C. and Jimenez, J. L.: Real-time measurements of secondary organic aerosol formation
24 and aging from ambient air in an oxidation flow reactor in the Los Angeles area, *Atmos. Chem.*
25 *Phys.*, 16(11), 7411–7433, doi:10.5194/acp-16-7411-2016, 2016.

26 Ots, R., Vieno, M., Allan, J. D., Reis, S., Nemitz, E., Young, D. E., Coe, H., Di Marco, C.,
27 Detournay, A., Mackenzie, I. A., Green, D. C. and Heal, M. R.: Model simulations of cooking
28 organic aerosol (COA) over the UK using estimates of emissions based on measurements at two
29 sites in London, *Atmos. Chem. Phys.*, 16(21), 13773–13789, doi:10.5194/acp-16-13773-2016,
30 2016.

31 Pagonis, D., Krechmer, J. E., de Gouw, J., Jimenez, J. L. and Ziemann, P. J.: Effects of gas–wall
32 partitioning in Teflon tubing and instrumentation on time-resolved measurements of gas-phase
33 organic compounds, *Atmos. Meas. Tech.*, 10(12), 4687–4696, doi:10.5194/amt-10-4687-2017,
34 2017.

35 Palm, B. B., Campuzano-Jost, P., Ortega, A. M., Day, D. A., Kaser, L., Jud, W., Karl, T., Hansel,
36 A., Hunter, J. F., Cross, E. S., Kroll, J. H., Peng, Z., Brune, W. H. and Jimenez, J. L.: In situ
37 secondary organic aerosol formation from ambient pine forest air using an oxidation flow reactor,
38 *Atmos. Chem. Phys.*, 16(5), 2943–2970, doi:10.5194/acp-16-2943-2016, 2016.

39 Palm, B. B., Campuzano-Jost, P., Day, D. A., Ortega, A. M., Fry, J. L., Brown, S. S., Zarzana, K.
40 J., Dube, W., Wagner, N. L., Draper, D. C., Kaser, L., Jud, W., Karl, T., Hansel, A., Gutiérrez-
41 Montes, C. and Jimenez, J. L.: Secondary organic aerosol formation from in situ OH, O₃, and NO₃
42 oxidation of ambient forest air in an oxidation flow reactor, *Atmos. Chem. Phys.*, 17(8), 5331–
43 5354, doi:10.5194/acp-17-5331-2017, 2017.

1 Palm, B. B., de Sá, S. S., Day, D. A., Campuzano-Jost, P., Hu, W., Seco, R., Sjostedt, S. J., Park,
2 J.-H., Guenther, A. B., Kim, S., Brito, J., Wurm, F., Artaxo, P., Thalman, R., Wang, J., Yee, L. D.,
3 Wernis, R., Isaacman-VanWertz, G., Goldstein, A. H., Liu, Y., Springston, S. R., Souza, R.,
4 Newburn, M. K., Alexander, M. L., Martin, S. T. and Jimenez, J. L.: Secondary organic aerosol
5 formation from ambient air in an oxidation flow reactor in central Amazonia, *Atmos. Chem. Phys.*,
6 18(1), 467–493, doi:10.5194/acp-18-467-2018, 2018.

7 Park, M.-S., Park, S.-H., Chae, J.-H., Choi, M.-H., Song, Y., Kang, M. and Roh, J.-W.: High-
8 resolution urban observation network for user-specific meteorological information service in the
9 Seoul Metropolitan Area, South Korea, *Atmos. Meas. Tech*, 10, 1575–1594, doi:10.5194/amt-10-
10 1575-2017, 2017.

11 Park, M. E., Song, C. H., Park, R. S., Lee, J., Kim, J., Lee, S., Woo, J.-H., Carmichael, G. R., Eck,
12 T. F., Holben, B. N., Lee, S.-S., Song, C. K. and Hong, Y. D.: New approach to monitor
13 transboundary particulate pollution over Northeast Asia, *Atmos. Chem. Phys*, 14, 659–674,
14 doi:10.5194/acp-14-659-2014, 2014.

15 Park, S. S., Kim, J.-H. and Jeong, J.-U.: Abundance and sources of hydrophilic and hydrophobic
16 water-soluble organic carbon at an urban site in Korea in summer., *J. Environ. Monit.*, 14(1), 224–
17 32, doi:10.1039/c1em10617a, 2012.

18 Parrish, D. D., Stohl, A., Forster, C., Atlas, E. L., Blake, D. R., Goldan, P. D., Kuster, W. C. and
19 de Gouw, J. A.: Effects of mixing on evolution of hydrocarbon ratios in the troposphere, *J.*
20 *Geophys. Res.*, 112(D10), D10S34, doi:10.1029/2006JD007583, 2007.

21 Parrish, D. D., Ryerson, T. B., Mellqvist, J., Johansson, J., Fried, A., Richter, D., Walega, J. G.,
22 Washenfelder, R. A., de Gouw, J. A., Peischl, J., Aikin, K. C., McKeen, S. A., Frost, G. J.,
23 Fehsenfeld, F. C. and Herndon, S. C.: Primary and secondary sources of formaldehyde in urban
24 atmospheres: Houston Texas region, *Atmos. Chem. Phys.*, 12(7), 3273–3288, doi:10.5194/acp-12-
25 3273-2012, 2012.

26 Peischl, J., Ryerson, T. B., Brioude, J., Aikin, K. C., Andrews, A. E., Atlas, E., Blake, D., Daube,
27 B. C., de Gouw, J. A., Dlugokencky, E., Frost, G. J., Gentner, D. R., Gilman, J. B., Goldstein, A.
28 H., Harley, R. A., Holloway, J. S., Kofler, J., Kuster, W. C., Lang, P. M., Novelli, P. C., Santoni,
29 G. W., Trainer, M., Wofsy, S. C. and Parrish, D. D.: Quantifying sources of methane using light
30 alkanes in the Los Angeles basin, California, *J. Geophys. Res. Atmos.*, 118(10), 4974–4990,
31 doi:10.1002/jgrd.50413, 2013.

32 Peng, J. F., Hu, M., Wang, Z. B., Huang, X. F., Kumar, P., Wu, Z. J., Guo, S., Yue, D. L., Shang,
33 D. J., Zheng, Z. and He, L. Y.: Submicron aerosols at thirteen diversified sites in China: size
34 distribution, new particle formation and corresponding contribution to cloud condensation nuclei
35 production, *Atmos. Chem. Phys.*, 14(18), 10249–10265, doi:10.5194/acp-14-10249-2014, 2014.

36 Peng, Z., Day, D. A., Stark, H., Li, R., Lee-Taylor, J., Palm, B. B., Brune, W. H. and Jimenez, J.
37 L.: HO_x radical chemistry in oxidation flow reactors with low-pressure mercury lamps
38 systematically examined by modeling, *Atmos. Meas. Tech.*, 8(11), 4863–4890, doi:10.5194/amt-
39 8-4863-2015, 2015.

40 Peng, Z., Day, D. A., Ortega, A. M., Palm, B. B., Hu, W., Stark, H., Li, R., Tsigaridis, K., Brune,
41 W. H. and Jimenez, J. L.: Non-OH chemistry in oxidation flow reactors for the study of
42 atmospheric chemistry systematically examined by modeling, *Atmos. Chem. Phys.*, 16(7), 4283–
43 4305, doi:10.5194/acp-16-4283-2016, 2016.

1 Perring, A. E., Bertram, T. H., Farmer, D. K., Wooldridge, P. J., Dibb, J., Blake, N. J., Blake, D.
2 R., Singh, H. B., Fuelberg, H., Diskin, G., Sachse, G. and Cohen, R. C.: The production and
3 persistence of ΣRONO_2 in the Mexico City plume, *Atmos. Chem. Phys.*, 10(15), 7215–7229,
4 doi:10.5194/acp-10-7215-2010, 2010.

5 Platt, S. M., El Haddad, I., Zardini, A. A., Clairotte, M., Astorga, C., Wolf, R., Slowik, J. G.,
6 Temime-Roussel, B., Marchand, N., Ježek, I., Drinovec, L., Močnik, G., Möhler, O., Richter, R.,
7 Barmet, P., Bianchi, F., Baltensperger, U. and Prévôt, A. S. H.: Secondary organic aerosol
8 formation from gasoline vehicle emissions in a new mobile environmental reaction chamber,
9 *Atmos. Chem. Phys.*, 13(18), 9141–9158, doi:10.5194/acp-13-9141-2013, 2013.

10 Platt, S. M., El Haddad, I., Pieber, S. M., Zardini, A. A., Suarez-Bertoa, R., Clairotte, M.,
11 Daellenbach, K. R., Huang, R.-J., Slowik, J. G., Hellebust, S., Temime-Roussel, B., Marchand,
12 N., de Gouw, J., Jimenez, J. L., Hayes, P. L., Robinson, A. L., Baltensperger, U., Astorga, C. and
13 Prévôt, A. S. H.: Gasoline cars produce more carbonaceous particulate matter than modern filter-
14 equipped diesel cars, *Sci. Rep.*, 7(1), 4926, doi:10.1038/s41598-017-03714-9, 2017.

15 Presto, A. A., Gordon, T. D. and Robinson, A. L.: Primary to secondary organic aerosol: Evolution
16 of organic emissions from mobile combustion sources, *Atmos. Chem. Phys.*, 14(10), 5015–5036,
17 doi:10.5194/acp-14-5015-2014, 2014.

18 Price, H. U., Jaffe, D. A., Cooper, O. R. and Doskey, P. V: Photochemistry, ozone production, and
19 dilution during long-range transport episodes from Eurasia to the northwest United States, *J.*
20 *Geophys. Res. Atmos.*, 109, D23S13, doi:10.1029/2003JD004400, 2004.

21 Pye, H. O. T. and Seinfeld, J. H.: A global perspective on aerosol from low-volatility organic
22 compounds, *Atmos. Chem. Phys. Atmos. Chem. Phys.*, 10(9), 4377–4401, doi:10.5194/acp-10-
23 4377-2010, 2010.

24 Richter, D., Weibring, P., Walega, J. G., Fried, A., Spuler, S. M. and Taubman, M. S.: Compact
25 highly sensitive multi-species airborne mid-IR spectrometer, *Appl. Phys. B*, 119(1), 119–131,
26 doi:10.1007/s00340-015-6038-8, 2015.

27 Robinson, A. L., Donahue, N. M., Shrivastava, M. K., Weitkamp, E. A., Sage, A. M., Grieshop,
28 A. P., Lane, T. E., Pierce, J. R. and Pandis, S. N.: Rethinking Organic Aerosols: Semivolatile
29 Emissions and Photochemical Aging, *Science* (80-.), 315(5816), 1259–1262,
30 doi:10.1126/science.1133061, 2007.

31 Sachse, G. W., Hill, G. F., Wade, L. O. and Perry, M. G.: Fast-Response, High-Precision Carbon
32 Monoxide Sensor using a Tunable Diode Laser Absorption Technique, *J. Geophys. Res.*, 92(D2),
33 2071–2081, doi:doi:10.1029/JD092iD02p02071, 1987.

34 Sato, K., Nakashima, Y., Morino, Y., Imamura, T., Kurokawa, J. and Kajii, Y.: Total OH reactivity
35 measurements for the OH-initiated oxidation of aromatic hydrocarbons in the presence of NO_x ,
36 *Atmos. Environ.*, 171, 272–278, doi:10.1016/j.atmosenv.2017.10.036, 2017.

37 Schroder, J. C., Campuzano-Jost, P., Day, D. A., Shah, V., Larson, K., Sommers, J. M., Sullivan,
38 A. P., Campos, T., Reeves, J. M., Hills, A., Hornbrook, R. S., Blake, N. J., Scheuer, E., Guo, H.,
39 Fibiger, D. L., McDuffie, E. E., Hayes, P. L., Weber, R. J., Dibb, J. E., Apel, E. C., Jaeglé, L.,
40 Brown, S. S., Thornton, J. A. and Jimenez, J. L.: Sources and Secondary Production of Organic
41 Aerosols in the Northeastern US during WINTER, *J. Geophys. Res. Atmos.*,
42 doi:10.1029/2018JD028475, 2018.

1 Schwantes, R. H., Schilling, K. A., McVay, R. C., Lignell, H., Coggon, M. M., Zhang, X.,
2 Wennberg, P. O. and Seinfeld, J. H.: Formation of Highly Oxygenated Low-Volatility Products
3 from Cresol Oxidation, *Atmos. Chem. Phys.*, 7(5), 3453–3474, doi:10.5194/acp-17-3453-2017,
4 2017.

5 Schwarz, J. P., Samset, B. H., Perring, A. E., Spackman, J. R., Gao, R. S., Stier, P., Schulz, M.,
6 Moore, F. L., Ray, E. A. and Fahey, D. W.: Global-scale seasonally resolved black carbon vertical
7 profiles over the Pacific, *Geophys. Res. Lett.*, 40(20), 5542–5547, doi:10.1002/2013GL057775,
8 2013.

9 Seo, J., Kim, J. Y., Youn, D., Lee, J. Y., Kim, H., Lim, Y. Bin, Kim, Y. and Jin, H. C.: On the
10 multi-day haze in the Asian continental outflow: An important role of synoptic condition combined
11 with regional and local sources, *Atmos. Chem. Phys.*, 17(15), 9311–9332, doi:10.5194/acp-17-
12 9311-2017, 2017.

13 Shingler, T., Crosbie, E., Ortega, A., Shiraiwa, M., Zuend, A., Beyersdorf, A., Ziemba, L.,
14 Anderson, B., Thornhill, L., Perring, A. E., Schwarz, J. P., Campazano-Jost, P., Day, D. A.,
15 Jimenez, J. L., Hair, J. W., Mikoviny, T., Wisthaler, A. and Sorooshian, A.: Airborne
16 characterization of subsaturated aerosol hygroscopicity and dry refractive index from the surface
17 to 6.5km during the SEAC4RS campaign, *J. Geophys. Res.*, 121(8), 4188–4210,
18 doi:10.1002/2015JD024498, 2016.

19 Shrivastava, M., Cappa, C. D., Fan, J., Goldstein, A. H., Guenther, A. B., Jimenez, J. L., Kuang,
20 C., Laskin, A., Martin, S. T., Ng, N. L., Petaja, T., Pierce, J. R., Rasch, P. J., Roldin, P., Seinfeld,
21 J. H., Shilling, J., Smith, J. N., Thornton, J. A., Volkamer, R., Wang, J., Worsnop, D. R., Zaveri,
22 R. A., Zelenyuk, A. and Zhang, Q.: Recent advances in understanding secondary organic aerosol:
23 Implications for global climate forcing, *Rev. Geophys.*, 55(2), 509–559,
24 doi:10.1002/2016RG000540, 2017.

25 Shrivastava, M. K., Lane, T. E., Donahue, N. M., Pandis, S. N. and Robinson, A. L.: Effects of
26 gas particle partitioning and aging of primary emissions on urban and regional organic aerosol
27 concentrations, *J. Geophys. Res.*, 113(D18), D18301, doi:10.1029/2007JD009735, 2008.

28 Silva, S. J., Arellano, A. F. and Worden, H. M.: Toward anthropogenic combustion emission
29 constraints from space-based analysis of urban CO₂/CO sensitivity, *Geophys. Res. Lett.*, 40(18),
30 4971–4976, doi:10.1002/grl.50954, 2013.

31 Slusher, D. L., Huey, L. G., Tanner, D. J., Flocke, F. M. and Roberts, J. M.: A thermal dissociation–
32 chemical ionization mass spectrometry (TD-CIMS) technique for the simultaneous measurement
33 of peroxyacyl nitrates and dinitrogen pentoxide, *J. Geophys. Res.*, 109(D19), D19315,
34 doi:10.1029/2004JD004670, 2004.

35 Stith, J. L., Ramanathan, V., Cooper, W. A., Roberts, G. C., DeMott, P. J., Carmichael, G., Hatch,
36 C. D., Adhikary, B., Twohy, C. H., Rogers, D. C., Baumgardner, D., Prenni, A. J., Campos, T.,
37 Gao, R., Anderson, J. and Feng, Y.: An overview of aircraft observations from the Pacific Dust
38 Experiment campaign, *J. Geophys. Res.*, 114(D5), D05207, doi:10.1029/2008JD010924, 2009.

39 Sueper, D.: ToF-AMS Data Analysis Software Webpage, [online] Available from:
40 http://cires1.colorado.edu/jimenez-group/wiki/index.php/ToF-AMS_Analysis_Software
41 (Accessed 4 January 2017), 2018.

42 Talbot, R. W., Dibb, J. E., Lefer, B. L., Scheuer, E. M., Bradshaw, J. D., Sandholm, S. T., Smyth,

1 S., Blake, D. R., Blake, N. J., Sachse, G. W., Collins, J. E. and Gregory, G. L.: Large-scale
2 distributions of tropospheric nitric, formic, and acetic acids over the western Pacific basin during
3 wintertime, *J. Geophys. Res.*, 102(D23), 28303–28313, 1997.

4 Tang, W., Arellano, A. F., DiGangi, J. P., Choi, Y., Diskin, G. S., Agustí-Panareda, A., Parrington,
5 M., Massart, S., Gaubert, B., Lee, Y., Kim, D., Jung, J., Hong, J., Hong, J.-W., Kanaya, Y., Lee,
6 M., Stauffer, R. M., Thompson, A. M., Flynn, J. H. and Woo, J.-H.: Evaluating High-Resolution
7 Forecasts of Atmospheric CO and CO₂ from a Global Prediction System during KORUS-AQ Field
8 Campaign, *Atmos. Chem. Phys. Discuss.*, 1–41, doi:10.5194/acp-2018-71, 2018.

9 Tkacik, D. S., Lambe, A. T., Jathar, S., Li, X., Presto, A. A., Zhao, Y., Blake, D., Meinardi, S.,
10 Jayne, J. T., Croteau, P. L. and Robinson, A. L.: Secondary Organic Aerosol Formation from in-
11 Use Motor Vehicle Emissions Using a Potential Aerosol Mass Reactor., *Environ. Sci. Technol.*,
12 48(19), 11235–42, doi:10.1021/es502239v, 2014.

13 Tohjima, Y., Kubo, M., Minejima, C., Mukai, H., Tanimoto, H., Ganshin, A., Maksyutov, S.,
14 Katsumata, K., Machida, T. and Kita, K.: Temporal changes in the emissions of CH₄ and CO from
15 China estimated from CH₄ / CO₂ and CO / CO₂ correlations observed at Hateruma Island, *Atmos.*
16 *Chem. Phys.*, 14(3), 1663–1677, doi:10.5194/acp-14-1663-2014, 2014.

17 Tritscher, T., Dommen, J., DeCarlo, P. F., Gysel, M., Barmet, P. B., Praplan, A. P., Weingartner,
18 E., Prévôt, A. S. H., Riipinen, I., Donahue, N. M. and Baltensperger, U.: Volatility and
19 hygroscopicity of aging secondary organic aerosol in a smog chamber, *Atmos. Chem. Phys.*,
20 11(22), 11477–11496, doi:10.5194/acp-11-11477-2011, 2011.

21 Tsimpidi, A. P., Karydis, V. A., Zavala, M., Lei, W., Molina, L., Ulbrich, I. M., Jimenez, J. L. and
22 Pandis, S. N.: Evaluation of the volatility basis-set approach for the simulation of organic aerosol
23 formation in the Mexico City metropolitan area, *Atmos. Chem. Phys.*, 10(2), 525–546,
24 doi:10.5194/acp-10-525-2010, 2010.

25 Tsimpidi, A. P., Karydis, V. A., Pandis, S. N. and Lelieveld, J.: Global-scale combustion sources
26 of organic aerosols: sensitivity to formation and removal mechanisms, *Atmos. Chem. Phys.*,
27 17(12), 7345–7364, doi:10.5194/acp-17-7345-2017, 2017.

28 Ulbrich, I. M., Canagaratna, M. R., Zhang, Q., Worsnop, D. R. and Jimenez, J. L.: Interpretation
29 of organic components from Positive Matrix Factorization of aerosol mass spectrometric data,
30 *Atmos. Chem. Phys.*, 9(9), 2891–2918, doi:10.5194/acp-9-2891-2009, 2009.

31 UNDESA, P. D.: World Urbanization Prospects: The 2014 Revision., 2015.

32 Vay, S. A., Tyler, S. C., Choi, Y., Blake, D. R., Blake, N. J., Sachse, G. W., Diskin, G. S. and
33 Singh, H. B.: Sources and transport of $\Delta^{14}\text{C}$ in CO₂ within the Mexico City Basin and vicinity,
34 *Atmos. Chem. Phys.*, 9, 4973–4985, doi:10.159/acp-9-4973-2009, 2009.

35 Virkkula, A.: Correction of the Calibration of the 3-wavelength Particle Soot Absorption
36 Photometer (3λ PSAP), *Aerosol Sci. Technol.*, 44, 706–712, doi:10.1080/02786826.2010.482110,
37 2010.

38 Volkamer, R., Jimenez, J. L., San Martini, F., Dzepina, K., Zhang, Q., Salcedo, D., Molina, L. T.,
39 Worsnop, D. R. and Molina, M. J.: Secondary organic aerosol formation from anthropogenic air
40 pollution: Rapid and higher than expected, *Geophys. Res. Lett.*, 33(17), L17811,
41 doi:10.1029/2006GL026899, 2006.

1 Wang, Y., Munger, J. W., Xu, S., McElroy, M. B., Hao, J., Nielsen, C. P. and Ma, H.: CO₂ and its
2 correlation with CO at a rural site near Beijing: implications for combustion efficiency in China,
3 *Atmos. Chem. Phys.*, 10(18), 8881–8897, doi:10.5194/acp-10-8881-2010, 2010.

4 Weibring, P., Richter, D., Walega, J. G., Rippe, L. and Fried, A.: Difference frequency generation
5 spectrometer for simultaneous multispecies detection, *Opt. Express*, 18(26), 27670,
6 doi:10.1364/OE.18.027670, 2010.

7 Weinheimer, A. J., Walega, J. G., Ridley, B. A., Gary, B. L., Blake, D. R., Blake, N. J., Rowland,
8 F. S., Sachse, G. W., Anderson, B. E. and Collins, J. E.: Meridional distributions of NO_x, NO_y,
9 and other species in the lower stratosphere and upper troposphere during AASE II, *Geophys. Res.*
10 *Let.*, 21(23), 2583–2586, doi:10.1029/94GL01897, 1994.

11 WHO: Ambient air pollution: A global assessment of exposure and burden of disease, World
12 Health Organization., 2016.

13 Wisthaler, A., Hansel, A., Dickerson, R. R. and Crutzen, P. J.: Organic trace gas measurements by
14 PTR-MS during INDOEX 1999, *J. Geophys. Res.*, 107(D19), 8024, doi:10.1029/2001JD000576,
15 2002.

16 Wood, E. C., Canagaratna, M. R., Herndon, S. C., Onasch, T. B., Kolb, C. E., Worsnop, D. R.,
17 Kroll, J. H., Knighton, W. B., Seila, R., Zavala, M., Molina, L. T., DeCarlo, P. F., Jimenez, J. L.,
18 Weinheimer, A. J., Knapp, D. J., Jobson, B. T., Stutz, J., Kuster, W. C. and Williams, E. J.:
19 Investigation of the correlation between odd oxygen and secondary organic aerosol in Mexico City
20 and Houston, *Atmos. Chem. Phys.*, 10(18), 8947–8968, doi:DOI 10.5194/acp-10-8947-2010,
21 2010.

22 Woody, M. C., Baker, K. R., Hayes, P. L., Jimenez, J. L., Koo, B. and Pye, H. O. T.: Understanding
23 sources of organic aerosol during CalNex-2010 using the CMAQ-VBS, *Atmos. Chem. Phys.*,
24 16(6), 4081–4100, doi:10.5194/acp-16-4081-2016, 2016.

25 Wooldridge, P. J., Perring, A. E., Bertram, T. H., Flocke, F. M., Roberts, J. M., Singh, H. B., Huey,
26 L. G., Thornton, J. A., Wolfe, G. M., Murphy, J. G., Fry, J. L., Rollins, A. W., LaFranchi, B. W.
27 and Cohen, R. C.: Total Peroxy Nitrates (ΣPNs) in the atmosphere: the Thermal Dissociation-Laser
28 Induced Fluorescence (TD-LIF) technique and comparisons to speciated PAN measurements,
29 *Atmos. Meas. Tech.*, 3(3), 593–607, doi:DOI 10.5194/amt-3-593-2010, 2010.

30 Wu, W., Zhao, B., Wang, S. and Hao, J.: Ozone and secondary organic aerosol formation potential
31 from anthropogenic volatile organic compounds emissions in China, *J. Environ. Sci.*, 53,
32 doi:10.1016/j.jes.2016.03.025, 2016.

33 Xu, W., Croteau, P., Williams, L., Canagaratna, M., Onasch, T., Cross, E., Zhang, X., Robinson,
34 W., Worsnop, D. and Jayne, J.: Laboratory characterization of an aerosol chemical speciation
35 monitor with PM_{2.5} measurement capability, *Aerosol Sci. Technol.*, 51(1), 69–83,
36 doi:10.1080/02786826.2016.1241859, 2017.

37 Zhang, Q., Jimenez, J. L., Canagaratna, M. R., Allan, J. D., Coe, H., Ulbrich, I., Alfarra, M. R.,
38 Takami, A., Middlebrook, A. M., Sun, Y. L., Dzepina, K., Dunlea, E., Docherty, K., DeCarlo, P.
39 F., Salcedo, D., Onasch, T., Jayne, J. T., Miyoshi, T., Shimono, A., Hatakeyama, S., Takegawa,
40 N., Kondo, Y., Schneider, J., Drewnick, F., Borrmann, S., Weimer, S., Demerjian, K., Williams,
41 P., Bower, K., Bahreini, R., Cottrell, L., Griffin, R. J., Rautiainen, J., Sun, J. Y., Zhang, Y. M. and
42 Worsnop, D. R.: Ubiquity and dominance of oxygenated species in organic aerosols in

1 anthropogenically-influenced Northern Hemisphere midlatitudes, *Geophys. Res. Lett.*, 34(13),
2 L13801, doi:10.1029/2007gl029979, 2007.

3 Zhang, Q. J., Beekmann, M., Freney, E., Sellegri, K., Pichon, J. M., Schwarzenboeck, A., Colomb,
4 A., Bourrienne, T., Michoud, V. and Borbon, A.: Formation of secondary organic aerosol in the
5 Paris pollution plume and its impact on surrounding regions, *Atmos. Chem. Phys.*, 15(24), 13973–
6 13992, doi:10.5194/acp-15-13973-2015, 2015.

7 Zhang, X., Smith, K. A., Worsnop, D. R., Jimenez, J., Jayne, J. T. and Kolb, C. E.: A Numerical
8 Characterization of Particle Beam Collimation by an Aerodynamic Lens-Nozzle System: Part I.
9 An Individual Lens or Nozzle, *Aerosol Sci. Technol.*, 36, 617–631,
10 doi:10.1080/02786820252883856, 2002.

11 Zhang, X., Smith, K. A., Worsnop, D. R., Jimenez, J. L., Jayne, J. T., Kolb, C. E., Morris, J. and
12 Davidovits, P.: Numerical Characterization of Particle Beam Collimation: Part II Integrated
13 Aerodynamic-Lens–Nozzle System, *Aerosol Sci. Technol.*, 38, 619–638,
14 doi:10.1080/02786820490479833, 2004.

15 Zhang, X., Cappa, C. D., Jathar, S. H., McVay, R. C., Ensberg, J. J., Kleeman, M. J., Seinfeld, J.
16 H. and Christopher D. Cappa: Influence of vapor wall loss in laboratory chambers on yields of
17 secondary organic aerosol., *Proc. Natl. Acad. Sci. U. S. A.*, 111(16), 1–6,
18 doi:10.1073/pnas.1404727111, 2014.

19 Zhao, Y., Hennigan, C. J., May, A. A., Tkacik, D. S., de Gouw, J. A., Gilman, J. B., Kuster, W.
20 C., Borbon, A. and Robinson, A. L.: Intermediate-volatility organic compounds: a large source of
21 secondary organic aerosol, *Environ. Sci. Technol.*, 48(23), 13743–50, doi:10.1021/es5035188,
22 2014.

23 Zhao, Y., Nguyen, N. T., Presto, A. A., Hennigan, C. J., May, A. A. and Robinson, A. L.:
24 Intermediate Volatility Organic Compound Emissions from On-Road Gasoline Vehicles and Small
25 Off-Road Gasoline Engines, *Environ. Sci. Technol.*, 50(8), 4554–4563,
26 doi:10.1021/acs.est.5b06247, 2016.

27 Ziemba, L. D., Lee Thornhill, K., Ferrare, R., Barrick, J., Beyersdorf, A. J., Chen, G., Crumeyrolle,
28 S. N., Hair, J., Hostetler, C., Hudgins, C., Obland, M., Rogers, R., Scarino, A. J., Winstead, E. L.
29 and Anderson, B. E.: Airborne observations of aerosol extinction by in situ and remote-sensing
30 techniques: Evaluation of particle hygroscopicity, *Geophys. Res. Lett.*, 40(2), 417–422,
31 doi:10.1029/2012GL054428, 2013.

32